

BINDING OF HYDROLYSIS-PRONE TI(IV) IN MEDICINAL AND  
MINERAL FORM TO GLYCOPROTEIN HUMAN SERUM TRANSFERRIN

---

A Dissertation  
Submitted to  
the Temple University Graduate Board

---

In Partial Fulfillment  
of the Requirements for the Degree  
DOCTOR OF PHILOSOPHY

---

by  
Lauren A. Profitt  
May 2020

Examining Committee Members:

Professor Ann M. Valentine, Advisory Chair, TU Department of Chemistry  
Professor Michael J. Zdilla, TU Department of Chemistry  
Professor Robert J. Stanley, TU Department of Chemistry  
Professor Richard H.G. Baxter, External Member, TU School of Medicine

©  
Copyright  
2020

By

Lauren A. Profitt  
All Rights Reserved

## ABSTRACT

Human serum transferrin (Tf) is a bilobal glycoprotein responsible for the transport and metabolism of two ferric ions. However, at only 30% saturation in human serum, reports have found that Tf can bind a variety of other metals. Titanium, as it is similar ionic size and Lewis acidity to Fe, unsurprisingly is one of these metals that can coordinate to Tf. The hydrolysis prone nature of Ti allows us to visualize features of its binding that have otherwise been unseen in previously utilized spectroscopic methods used to detail the Ti-Tf interaction. This thesis explores the binding motifs of both titanocene dichloride and titanium oxide and reveals interesting binding profiles outside of the traditional binding lobes of Tf.

Titanocene dichloride (TDC) is a hydrolysis prone anticancer agent that has been shown to cause a ligand to metal charge transfer as it binds into the lobes of Tf. While UV/Vis proved the characteristic 2:1 metal to protein binding, ICP-OES detected spectroscopically mute interactions revealing higher binding equivalents were still prevalent in solution, up to approximately 50 equivalents of TDC to Tf, far past that seen in controls due to hydrolysis. Further studies showed an inability of TDC to cause a typical lobe closure of Tf as would have been seen with Fe. Lobe closure of Tf in the presence of TDC directly analyzed through protein volume SAXS measurements and denaturing urea-PAGE gels. Additionally, studies with Fe<sub>2</sub>Tf, or Fe(III) bound Tf, still showed solubilized TDC, which speaks further on the surface binding properties of Tf and possible new pathways of Ti cellular introduction.

In addition to being used as drug agents, titanium has many commercial applications in cosmetics, sunscreens, and medical devices such as implants. The introduction of  $\text{TiO}_2$  into human serum and complexation with Tf is highly probable and a previously untapped area. Exploring this interaction showed not only the dissolution of Ti seen spectroscopically in the binding pocket and a higher concentration of Ti found through ICP-OES, but interesting results through transmission electron microscopy (TEM) that show the changing morphology of the  $\text{TiO}_2$  particle as it reacts with Tf over time. TEM images showed the particle sizing degrading to smaller particles over the course of 168 h. TEM was also able to detect selective uptake of nanoparticles by Tf. An equilibrium of Ti-Tf uptake was found in ICP-OES and UV/Vis results, yet the ability of Tf to change the features of  $\text{TiO}_2$  particle's size could not have been understood fully without TEM. The formation of smaller particles and their introduction into human serum or transport with Tf could be the means of cellular accumulation of metal particles.

Finally, to analyze possible surface interactions on Tf, deglycosylation techniques were implemented. Tf has two glycan chains residing on the C-terminal lobe that can be cleaved off with an enzyme PNGase F. Preliminary experiments had varied results among the binding capabilities deglycosylated Tf has with  $\text{TiO}_2$  and TDC. The differences among these two could help reveal further information about the binding lobe capacity or the site directed binding on the surface of the protein in coordination complexes versus oxides. The superstoichiometric interaction of TDC with Tf was uninterrupted by deglycosylation of Tf. However, uptake of  $\text{TiO}_2$  by Tf was affected by the removal of the glycan chains on the surface of the protein. Experiments with  $\text{Fe}_2\text{Tf}$  could help decipher exact coordination

and complete the telling of this story of superstoichiometric Ti binding. In our results, deglycosylated Fe<sub>2</sub>Tf did not prevent TDC interacting with the protein surface, but ICP-OES results showed far less solubilized Ti from TiO<sub>2</sub>.

This thesis is dedicated to my parents,  
Frederick and Diana Profitt, and my grandfather, Louis Daluisio (Poppee)  
for their endless love and encouragement.

## ACKNOWLEDGMENTS

I am incredibly grateful to the supportive community that I had surrounding me during the completion of this thesis. I first and foremost must thank my advisor and mentor, Ann Valentine. I cannot fully express what your guidance and support has meant to me these past five years. You have shown me how to be a better scientist and person and have taught me so incredibly much. In times when I struggled the most or nearly quit, you have shown your unwavering encouragement and belief in me as a scientist. Thank you. I would like to thank my committee members, Professors Robert Stanley and Michael Zdilla, for their guidance and endless support. It has always been a pleasure to discuss research with you and gain insight from your perspectives. I'd also like to acknowledge my external committee member, Professor Richard Baxter, for his support during this thesis process and for joining with me in various fruitful collaborative projects.

Thank you to the Department of Chemistry and all those who keep it running, for their advice and guidance, especially Tanya Santiago, Lisa Lomax, Regina Shapiro, Bobbi Johnson, Kafi Chism, Samer Daher, Jennifer Walters, Carol Manhart, Elizabeth Cerkez, Farbod Alimohammadi, Nuwan Attanayake, Colin Fitzpatrick, Habib Sistani, Johanan Odhner, and David Plasket. Thank you to my teaching advisors, Drs. John Michael and Roy Keyer, for showing me by example how to be a great educator. I am also grateful to the other TAs who have worked alongside me, including Scott Witte, Rylee McBride, Megan Van Vliet, Matt Hurley, and Ravneet Bhullar.

To my friends and coworkers in the Earth and Environmental Science department, thank you for sharing instrumentation, knowledge, and lunch with me over the years. A

special thank you goes to Professor David Grandstaff for helping to maintain the ICP-OES and Professor Bojeong Kim for her DLS expertise. A big, huge, major thank you goes to Boyoung Song, my wonderful friend and my go-to when there are instrumentation issues or when I need ice cream.

I need to take a moment to thank Rachel Parise for being an invaluable friend throughout all these years in grad school, I am so appreciative of all our talks over pizza. I want to thank Andrew Mellinger, for being an incredible source of strength during this whole process. I cannot thank you enough for your encouragement and our loyal friendship. Let's have spaghetti and meatballs soon.

I have been incredibly blessed with an amazing family in the Valentine lab. Without them I would not be the scientist I am today. Kate Buettner, I have you to thank specifically for your insight and ideas that helped shape Chapter III of this thesis. You have been a wonderful mentor over the years. Thank you, Mark Zierden, for training me in lab and always being a scientific sounding board and source of weirdness. Kayleigh Jones, thank you for your brutal honesty, job advice, alcoholic pies, and fashion tips. To Corey Herbst-Gervasoni, thank you for answering my constant questioning about the thesis process and for being such a supportive friend. Although, I could have done without all the arguing (because whatever you're thinking is wrong). A major thank you goes to Anastassia Gallo for her encouragement and for believing in me. I can always count on you for a laugh or for caring advice. To Jodi Kraus, an honorary lab member and friend, thanks for all the shark and cat yoga! To our undergrads, Ethan Kimmett and Olivia Stepanic, I'm so excited to see what you become in graduate school. Thanks for all the baked goods along the way!

I am leaving the Valentine lab knowing it is in the good hands of Lori Cobani, Md. Imdadul Haque, and A.S.M. Saem. Thank you all for your support this past year and for throwing the best birthday celebrations. I look forward to seeing all the work you accomplish.

The community at Rosemont College, my undergraduate institution, has been most uplifting throughout my education. I'd especially like to thank my mentors, Dr. John Ullrich, Dr. Xiuni Wu, and Dr. Marilyn Moller for all that they have taught me throughout my career. I have the three best friends anyone could ask for in Dr. Hannah McGuigan, Dr. Lauren McGinnis, and Rossana Duffy. You are only as good as the people you surround yourself with, and I am so lucky to surround myself with smart, determined, thoughtful, encouraging friends who raise me up to become a better person. Thank you to David Parsons for your sweet encouragement during this time. I am continually thankful for having you as a bright light in my life.

My family has shown me their love and support my entire life, and for that I am eternally grateful. They deserve so much more than just this acknowledgment for supporting my education and encouraging my pursuits, along with everything else they have done for me. Thank you, Mom and Dad, for teaching me the value of education and rooting for me the entire way. I have the best siblings in Adam and Krista and my brother-in-law Andy, I'm truly thankful for your pep talks when I needed them most. I am grateful to my Aunt Sabrina, (Dr.) Uncle Steve, and Poppee for always asking about my progress in school and cheering me on, and to the family "therapy" dogs and cat, Watson, Kya, and Kermit, for their cuddles.

Finally, to quote Snoop Dogg, "I want to thank me for believing in me, I want to thank me for doing all this hard work." More seriously, I am very proud of the work I have accomplished and the person I have become, which is very much attributed to the support of my friends, family, peers, and mentors. You have all made a tremendous impact on my life and I am so grateful.

## TABLE OF CONTENTS

ABSTRACT.....	iii
DEDICATION.....	vi
ACKNOWLEDGMENTS .....	vii
LIST OF TABLES .....	xiv
LIST OF FIGURES .....	xv
CHAPTERS	
1. PERSPECTIVE ON METAL TRANSPORT AND TRAFFICKING BY PROTEINS AND GLYCANS IN HUMAN SERUM .....	1
1.1 Human Serum .....	1
1.2 Trace Metals in Human Serum .....	2
1.3 Metal-Albumin Binding.....	4
1.4 Metal-Transferrin Binding .....	5
1.5 Metal-Glycan Binding .....	11
1.6 Conclusion .....	12
1.7 References.....	13
2. SUPERSTOICHIOMETRIC BINDING OF THE ANTICANCER AGENT TITANOCENE DICHLORIDE BY HUMAN SERUM TRANSFERRIN AND THE EFFECTS ON LOBE CLOSURE.....	21
2.1 Introduction.....	21
2.2 Experimental .....	25
2.2.1 Materials .....	25
2.2.2 Methods.....	25
2.3 Results and Discussion .....	29

2.3.1 pH Deviation Among Varied Bicarbonate Concentrations .....	29
2.3.2 Human Serum Transferrin Supported TDC Resistance to Hydrolytic Precipitation .....	30
2.3.3 Fluorescence .....	32
2.3.4 Apparent Molar Absorptivity.....	34
2.3.5 Urea-PAGE Gel Analysis of TDC Lobe Closure .....	35
2.3.6 Small Angle X-ray Scattering Analysis (SAXS).....	39
2.3.7 Surface Interactions of TDC with Fe(III) Loaded Tf.....	41
2.4 Conclusion .....	43
2.5 References.....	45
3. THE UPTAKE OF TITANIUM OXIDE AND THE CHANGE IN PARTICLE SPECIATION BY HUMAN SERUM TRANSFERRIN .....	51
3.1 Introduction.....	51
3.2 Experimental.....	52
3.2.1 Materials .....	52
3.2.2 Methods.....	53
3.3 Results and Discussion .....	55
3.3.1 UV/Vis, Fluorescence, and Inductively Coupled Plasma Optical Emission Spectroscopy (ICP-OES) Titanium Detection .....	55
3.3.2 DLS and TEM.....	61
3.3.3 Fe <sub>2</sub> Tf and Rutile Dissolution .....	67
3.4 Conclusions.....	69

3.5 References.....	70
4. DEGLYCOSYLATION OF HUMAN SERUM TRANSFERRIN AFFECTS TITANOCENE DICHLORIDE AND TITANIUM OXIDE INTERACTION AT THE SURFACE OF THE PROTEIN .....	72
4.1 Introduction.....	72
4.2 Experimental .....	75
4.2.1 Materials .....	75
4.2.2 Methods.....	75
4.3 Results and Discussion .....	77
4.3.1 Deglycosylated transferrin .....	77
4.3.2 deTf Interactions with TDC .....	78
4.3.3 deTf Interaction with Titanium Oxide Surfaces .....	82
4.3.4 Ti(IV) Complexes Effects on deTf Lobe Closures .....	87
4.4 Conclusion .....	90
4.5 References.....	91
 APPENDICES	
A. ADDITIONAL FIGURES SHOWING SUPERSTOICHIOMETRIC BINDING OF TITANOCENE DICHLORIDE TO TRANSFERRIN.....	94
B. ADDITIONAL FIGURES FOR TITANIUM OXIDE AND TRANSFERRIN ASSOCIATION .....	104
C. ADDITIONAL FIGURES OF DEGLYCOSYLATED TRANSFERRIN.....	110
D. ASSAY OF TOPOISOMERASE I INHIBITION BY TITANOCENE DICHLORIDE.....	116

## LIST OF TABLES

Table 1.1: Average mass (g) of transition metals in a human body. Modified presentation from Kaim and Schwederski. <sup>17</sup> .....	4
Table 2.1: Fluorescence quenching relative to apoTf fluorescence. PTI. 168 h averaged of two samples.....	34
Table 2.2: Data values extracted from Guinier plot, P(r) distribution and Porod plots analysis of apoTf, Fe <sub>2</sub> Tf, Tf-Ti(citrate), Tf + TDC 2 equiv, and Tf +TDC 4 equiv.....	40
Table 2.3: First order rate constants for Tf preloaded with varied equivalents of TDC and 10 equiv additions of Fe(NTA) <sub>2</sub> . Ti:Tf ratios are the result of UV/Vis and ICP-OES analysis of Tf-TDC loaded prior to Fe(NTA) <sub>2</sub> additions.....	43
Table 4.1: Rate constants of kinetic exchange reaction of Tf + TDC varied equiv with 10 equiv of Fe(NTA) <sub>2</sub> . .....	81
Table A.1: Averaged UV/Vis absorbance at 321 nm and ICP-OES Ti concentration (μM) determined for 25 mM (pH 8.5) and 0.89 mM (pH 7.4) bicarbonate samples. ....	94

## LIST OF FIGURES

Figure 1.1: Structures of human serum transferrin. N-lobe is shown in blue, C-lobe in green: (A.) apo-transferrin (2HAU) <sup>46</sup> , (B.) diferric transferrin and (C.) the N-lobe Fe binding site in diferric transferrin (3V83) <sup>47</sup> . All figures were made using Pymol. Structures were positioned to highlight conformational change upon iron binding in the N-lobe. A similar change in the C-lobe is difficult to discern due to the position of the lobe. ....	7
Figure 1.2: Crystal structures of human serum transferrin with titanium. (A.) Structure from Tinoco et al (5DYH). <sup>73</sup> (B.) Structure from Curtin et al (5H52). <sup>72</sup> All figures were made using Pymol. ....	10
Figure 2.1: 20 $\mu\text{M}$ apoTf subtracted absorbance spectrum of Tf + TDC 2 equiv (solid), 4 equiv (dashed), 10 equiv (dotted) (40, 80, 200 $\mu\text{M}$ TDC).....	31
Figure 2.2: (A.) Ratio of Tf-TDC 2, 4, 10 equiv (40, 80, 200 $\mu\text{M}$ TDC) striped (ICP-OES), Solid (UV-Vis) [Tf] = 20 $\mu\text{M}$ ; (B.) Ratio of Tf-TDC 20, 50, 100 equiv striped (40, 100, 200 $\mu\text{M}$ TDC) (ICP-OES), Solid (UV-Vis) [Tf] = 2 $\mu\text{M}$ . ....	32
Figure 2.3: Apparent molar absorptivity; averaged of two trials; UV subtracted (apoTf and controls). ....	35
Figure 2.4: Urea-polyacrylamide gel electrophoresis of: 1) apo-Tf, 2) $\text{Fe}_2\text{Tf}$ (2 equiv binding) 3) partially loaded $\text{Fe}_1\text{Tf}$ (1 equiv binding), 4) Tf-TDC 2 equiv, 5) Tf-TDC 2 equiv (0.89 mM citrate), 6) Tf-Ti citrate 2 equiv, and 7) $\text{Fe}_2\text{Tf}$ (2 equiv binding) + TDC 2 equiv. ....	37
Figure 2.5: Urea-polyacrylamide gel electrophoresis of: 1) apo-Tf, 2) $\text{Fe}_2\text{Tf}$ (2 equiv binding) 3) Tf + TDC 2 equiv, 4) Tf + TDC 4 equiv, 5) Tf + TDC 10 equiv, 6) Tf + TDC 20 equiv, 7) Tf + TDC 50 equiv, 8) Tf + TDC 10 equiv (0.89 mM citrate), 9) $\text{Fe}_2\text{Tf}$ (2 equiv binding) + TDC 4 equiv, and 10) Tf + TDC 10 equiv (25 mM bicarbonate).....	38
Figure 2.6: ICP-OES results from $\text{Fe}_2\text{Tf}$ + TDC 4 equiv. Striped: Ratio Ti:Tf; Solid: Ratio Fe:Tf.....	41
Figure 3.1: ICP-OES results of 35 $\mu\text{M}$ Tf with varied concentration $\text{TiO}_2$ (A.) 168 h dissolution: apoTf (●), Tf + anatase 5 $\text{mg mL}^{-1}$ (●), Tf + rutile 5 $\text{mg mL}^{-1}$ (○); (B.) Dissolution over 2 h; (C.) Dissolution over 168 h: Tf + rutile 5 $\text{mg mL}^{-1}$ repeated (○), Tf + rutile 20 $\text{mg mL}^{-1}$ (■); (D.) Dissolution over 2 h. ....	57
Figure 3.2: Mineral loadings of anatase 5 $\text{mg mL}^{-1}$ (●) rutile 5 $\text{mg mL}^{-1}$ (●) and rutile 20 $\text{mg mL}^{-1}$ (○) with Tf.....	58

Figure 3.3: [Ti] as determined by LMCT UV/Vis absorbance using the molar absorptivity coefficient of $10,380 \text{ M}^{-1} \text{ cm}^{-1}$ at 321 nm with $35 \text{ }\mu\text{M}$ apoTf subtracted from UV/Vis absorbance. Tf + anatase $5 \text{ mg mL}^{-1}$ (●), Tf + rutile $5 \text{ mg mL}^{-1}$ (○), Tf + rutile $20 \text{ mg mL}^{-1}$ (■).....	60
Figure 3.4: 8 h DLS spectra apoTf (–), Tf + anatase $5 \text{ mg mL}^{-1}$ (–), Tf + rutile $5 \text{ mg mL}^{-1}$ (–), Tf + rutile $20 \text{ mg mL}^{-1}$ (–).....	62
Figure 3.5: TEM images of (A.) Tf + rutile $20 \text{ mg mL}^{-1}$ at 1 h; and (B.) rutile $20 \text{ mg mL}^{-1}$ 1 h unfiltered. ....	64
Figure 3.6: TEM images of Tf + rutile $5 \text{ mg mL}^{-1}$ at (A.) 0.5 h; (B.) 4 h; (C.) 8 h; and (D.) 168 h.....	65
Figure 3.7: TEM images of Tf + rutile $20 \text{ mg mL}^{-1}$ at (A.) 0.5 h; (B.) 4 h; (C.) 8 h; and (D.) 168 h.....	66
Figure 3.8: ICP-OES [Ti] results for $35 \text{ }\mu\text{M}$ $\text{Fe}_2\text{Tf}$ + rutile $5 \text{ mg mL}^{-1}$ (●) and $\text{Fe}_2\text{Tf}$ (○) over (A.)168 h and (B.) 8 h.....	68
Figure 4.1: Crystal structure of diferric human serum transferrin (3V83). <sup>9</sup> N-lobe is shown in blue, C-lobe in green. Inset depicts two asparagine residues, Asn 413 and Asn 610, on the C-lobe of transferrin, the site for N-linked glycosylation. Asn 413 and Asn 610 shown here as pink spheres. All figures were made using Pymol .....	73
Figure 4.2: UV/Vis results of Ti to Tf ratio from LMCT at 321 nm using $10,380 \text{ M}^{-1}\text{cm}^{-1}$ molar absorption coefficient and $20 \text{ }\mu\text{M}$ Tf for wild type transferrin and deTf with treatment of 4 and 10 equiv TDC. ....	79
Figure 4.3: ICP-OES results of TDC in solution with Tf and deTf after 24 h incubation periods.....	80
Figure 4.4: ICP-OES results from $\text{Fe}_2\text{Tf}$ of 0 and 4 equiv TDC and de $\text{Fe}_2\text{Tf}$ binding of 0, 4, and 10 equiv binding. Striped: Ratio Ti:Tf; Solid: Ratio Fe:Tf.....	82
Figure 4.5: UV/Vis results of Ti to Tf ratio from LMCT at 321 nm using $10,380 \text{ M}^{-1}\text{cm}^{-1}$ molar absorption coefficient and $20 \text{ }\mu\text{M}$ Tf for wild type transferrin and deTf after treatment with $20 \text{ mg mL}^{-1}$ rutile at 8 h and 24 h incubation. ....	85
Figure 4.6: ICP-OES results for $20 \text{ }\mu\text{M}$ Tf, deTf, and de $\text{Fe}_2\text{Tf}$ with $20 \text{ mg mL}^{-1}$ rutile at 8 h and 24 h.....	86
Figure 4.7: TEM of disperse nanoparticles in a sample of deTf with $20 \text{ mg mL}^{-1}$ rutile at 8 h.....	86

Figure 4.8: Fluorescence relative to apoTf of deTf and deFe <sub>2</sub> Tf treated with 0, 4, and 10 equiv of TDC or 20 mg mL <sup>-1</sup> rutile after 8 h and 24 h.....	88
Figure 4.9: (1) deTf + TDC 10 equiv; (2) deTf + TDC 4 equiv; (3) apoTf; (4) deTf; (5) deTf + R 20 mg mL <sup>-1</sup> 8 h; (6) deTf; (5) deTf + R 20 mg mL <sup>-1</sup> 24 h; (7) deFe <sub>2</sub> Tf + TDC 4 equiv; (8) deFe <sub>2</sub> Tf + TDC 10 equiv; (9) deFe <sub>2</sub> Tf; (10) Fe <sub>2</sub> Tf. ....	89
Figure A.1: 0, 40, 80, 200 μM TDC ICP-OES controls corresponding to Tf (20 μM) + TDC 0, 2, 4, 10 equiv.....	95
Figure A.2: 0, 40, 100, 200 μM TDC ICP-OES controls corresponding to Tf (2 μM) + TDC 0, 20, 50, 100 equiv.....	96
Figure A.3: (A.) 40 μM UV/Vis control corresponding to 2 and 20 equiv TDC. (B.) 80 μM UV/Vis control corresponding to 4 equiv TDC. (C.) 100 μM UV/Vis control corresponding to 50 equiv TDC. (D.) 200 μM UV/Vis control corresponding to 10 equiv TDC. 0 h (solid), 24 h (dashed), 96 h (dotted), 168 h (dash-dot).....	97
Figure A.4: 96 h fluorescence spectrum of (A.) 20 μM Tf + TDC 0 equiv (red), 2 equiv (dark blue), 4 equiv (light blue), 10 equiv (purple) and (B.) 2 μM Tf + TDC 0 equiv (red), 20 equiv (dark blue), 50 equiv (light blue), 100 equiv (purple). ....	98
Figure A.5: Concentration analysis of forwards scattering intensity (I <sub>0</sub> ) and the radius of gyration (R <sub>G</sub> ) versus each applied concentration ranging from 1 – 15 mg mL <sup>-1</sup> for (A.) apoTf, (B.) Fe <sub>2</sub> Tf, (C.) Tf-Ti(citrate), (D.) Tf + TDC 2 equiv, (E.) Tf + TDC 4 equiv. ....	100
Figure A.6: Guinier plot, P(r) distribution and Porod plots of each of the samples (A.) apoTf, (B.) Fe <sub>2</sub> Tf, (C.) Tf-Ti(citrate), (D.) Tf + TDC 2 equiv, (E.) Tf + TDC 4 equiv. ....	101
Figure A.7: Spin Dialysis UV/Vis Results with 0.89 mM bicarbonate (A.) and with 25 mM bicarbonate (B.). Striped – pre spin dialysis (ε <sub>321 nm</sub> =10,380 M <sup>-1</sup> cm <sup>-1</sup> ); light grey – Post spin dialysis (ε <sub>321 nm</sub> =10,380 M <sup>-1</sup> cm <sup>-1</sup> ); White – pre spin dialysis (ε <sub>321 nm</sub> =2415 M <sup>-1</sup> cm <sup>-1</sup> ); Dark grey – post spin dialysis (ε <sub>321 nm</sub> =2,415 M <sup>-1</sup> cm <sup>-1</sup> ). ....	102
Figure A.8: Kinetic exchange of 4 equiv of TDC loaded to Tf with 10 equivalent additions of Fe(NTA) <sub>2</sub> . Fit obtained through SPECFIT/32. (A.) Series of spectra scans over 260 minutes after initial addition of Fe(NTA) <sub>2</sub> at t=0 minutes. (B.) Concentration profile of the two species in respect to time. (C.) The molar extinction coefficients of each species. The red curve represents the Tf + TDC 4 equiv starting species and the blue curve represents the Fe <sub>2</sub> Tf (+ TDC 4 equiv) species. ....	103
Figure B.1: ICP-OES controls in buffer: apoTf (●), filtered anatase 5 mg mL <sup>-1</sup> (■), filtered rutile 5 mg mL <sup>-1</sup> (x), filtered rutile 20 mg mL <sup>-1</sup> (○).....	104
Figure B.2: UV/Vis spectrum of (A.) Tf + rutile 5 mg mL <sup>-1</sup> (apoTf subtracted); (B.) Tf +	

rutile 20 mg mL <sup>-1</sup> (apoTf subtracted); (C.) Tf + anatase 5 mg mL <sup>-1</sup> (apoTf subtracted).	105
Figure B.3: UV/Vis spectrum of (A.) rutile only 5 mg mL <sup>-1</sup> ; (B.) rutile only 20 mg mL <sup>-1</sup> ; (C.) anatase only 5 mg mL <sup>-1</sup> .	106
Figure B.4: DLS spectrum of (A.) anatase (-) and rutile (-) suspended in water control.	107
Figure B.5: DLS spectra of timepoints 0 h (-), 0.5 h (-), 1 h (-), 4 h (-), 8 h (-) (A.) apoTf; (B.) Tf + anatase 5 mg mL <sup>-1</sup> ; (C.) Tf + rutile 5 mg mL <sup>-1</sup> ; (D.) Tf + rutile 20 mg mL <sup>-1</sup> .	108
Figure B.6: ICP-OES [Fe] results for 35 μM Fe <sub>2</sub> Tf + rutile 5 mg mL <sup>-1</sup> (●) and Fe <sub>2</sub> Tf (○) over 168 h.	109
Figure C.1: SDS-PAGE gel result confirming deglycosylated transferrin. Lanes 1 and 4 containing low molecular weight ladder. Lane 2 contains apoTf. Lane 3 contains apoTf treated with PNGase F enzyme.	110
Figure C.2: MALDI-MS analysis results of apoTf in buffered solution.	111
Figure C.3: MALDI-MS analysis results of deTf in buffered solution. Sample set 1 of 2.	112
Figure C.4: MALDI-MS analysis results of deTf in buffered solution. Sample set 2 of 2.	113
Figure C.5: Kinetic exchange of 4 equiv of TDC loaded to deTf with 10 equivalent additions of Fe(NTA) <sub>2</sub> . Fit obtained through SPECFIT/32. (A.) Series of spectra scans over 260 minutes after initial addition of Fe(NTA) <sub>2</sub> at t=0 minutes. (B.) Concentration profile of the two species in respect to time. (C.) The molar extinction coefficients of each species. The red curve represents the deTf + TDC 4 equiv starting species and the blue curve represents the Fe <sub>2</sub> deTf (+ TDC 4 equiv) species.	114
Figure D.1: Topoisomerase I assay with varied equivalents of TDC. From left to right: 1 Kb ladder, substrate only, buffer control (topoI, plasmid, 10% DMSO), 1:1 topo I to TDC (ng:ng), blank, 1:2, 1:4, 1:6 topo I to TDC (ng:ng).	119
Figure D.2: Solvent control assay with topo I and plasmid relaxation with 10% DMSO and 10% DMSO/saline (1/9 v/v).	120

## CHAPTER 1

### PERSPECTIVE ON METAL TRANSPORT AND TRAFFICKING BY PROTEINS AND GLYCANS IN HUMAN SERUM

#### 1.1 Human Serum

Human serum is the soluble portion of clotted blood, excluding all blood cells. It is very similar to plasma, which is derived from blood that is uncoagulated, and therefore contains proteins and fibrinogens that are necessary in clotting procedures.<sup>1</sup> In order to prevent coagulation to collect plasma samples, an anticoagulant is used to chelate calcium. Common anticoagulants include EDTA, heparin, and sodium citrate.<sup>2</sup> Removal of fibrinogen proteins necessary in clotting leaves serum with a smaller difference in protein content than whole blood plasma.<sup>3</sup>

Human serum/plasma, used interchangeably, is diverse and ever changing and is believed to contain up to 5,000 proteins.<sup>4</sup> Current methods to characterize the serum proteome include mass spectrometry techniques, 2D gel electrophoresis, and chromatography techniques before using proteomic profiling.<sup>2,5,6</sup> While there is a very high number of different serum proteins, most are in very low abundance.<sup>1,7</sup> For example, human serum albumin makes up approximately 52% of serum proteins (40 – 45 g L<sup>-1</sup>) while human serum transferrin makes up a smaller fraction of serum proteins with 2.5 g L<sup>-1</sup> represented in serum.<sup>8</sup> Other key serum proteins include immunoglobulins, haptoglobin, lipoproteins, cytokines, receptor ligands, lysosomal proteins and other

temporary proteins transporting through serum, proteins of infectious organisms/parasites, and proteins released from cells as a result of cell death or diseased tissues/tumors.<sup>1,9-11</sup>

Besides proteins there are small molecules present in serum. Some of these include ligands, drugs, salts, lipids, and amino acids.<sup>11</sup> Sugars are also a significant part of human serum. Glycosylation of proteins is a very diversifying and abundant process and is essential in many roles of proteins and cellular functions.<sup>12</sup> Free glycans have also been noted to exist in human serum as a product of glycoproteins as well.<sup>13</sup>

Progress has been made to characterize the serum and plasma proteomes. Garnering more information about the human serum is essential to help improve diagnostic techniques, identifying disease biomarkers, and furthering the outlook on the physical condition of the human body. Blood glucose levels and lipoproteins have been a carefully monitored and researched biomarker for diabetes studies and transferrin levels are frequently used as a biomarker for iron quantitation in human serum.<sup>14,15</sup> Analyzing the components of human serum is another way to monitor metabolism of metals and their temporary transport through serum.

## **1.2 Trace Metals in Human Serum**

The amount of metal in human serum in particular is difficult to quantitate as the regulatory role of serum maintains relatively low metal concentration.<sup>16</sup> Regulatory and transport serum proteins and ligands are responsible for the trafficking and transport of metals throughout human serum to cells and then throughout the body. Three key serum proteins and ligands, human serum albumin, human serum transferrin, and glycans, all of

which play a role in metal binding and transport will be discussed in detail further in this chapter.

The elemental composition within the human body has been quantitated with transition metals with concentration ranges from 0.005 – 4.2 g, as displayed in Table 1.1<sup>17</sup> The emergence of transitory metal in serum can also be attributed to the largely growing use of metals in medicine. Medicinal metals became more popular since the use of cisplatin, the platinum-containing anticancer drug that binds to DNA and prevents replication and transcription.<sup>18–20</sup> A variety of other metals have been tested as anticancer drug compounds, including metallocenes. Inspired by the success of cisplatin, a variety of metallocenes were studied for their anticancer activity.<sup>21</sup> These metallocenes are metal centered compounds with two cyclopentadienyl anions. Metal ions studied have included ferrocene (Fe centered), vanadocene (V centered), and molybdocene (Mo centered). Titanium anticancer compounds include titanocene dichloride and budotitane, both of which were tested in human clinical trials.<sup>22–24</sup>

Besides the growing list of metal anticancer drugs, metals have been utilized in medicine as MRI contrast agents, radiopharmaceuticals, antimicrobials, selective photosensitizers for photodynamic therapies, and a variety of other inhibitors and chelation therapies.<sup>25</sup> The varied uses of metals for medicinal use are often introduced and transported through human serum, yet the exact metal-serum interaction is still unknown in many cases.

	Mass (g)
Fe	4.2
Zn	2.3
Zr	0.3
Cu	0.11
Mn	0.02
V	0.02
Ni	0.01
Cr	0.005
Co	0.003
Mo	0.005

Table 1.1: Average mass (g) of transition metals in a human body. Modified presentation from Kaim and Schwederski.<sup>17</sup>

### 1.3 Metal-Albumin Binding

As the most abundant protein in human serum, albumin carries out an important role in maintaining circulation in the bloodstream with the transport of hormones, vitamins, enzymes, metal ions, fatty acids, and drugs.<sup>26,27</sup> Albumin is a 66 kDa, 585 amino acid single chain protein with three main homologous domains, each with two subdomains.<sup>28</sup> Each domain typically has binding preference for the variety of ligands it is responsible for transporting. For example, primarily two binding sites have been found to have drug-binding capabilities and interactions.<sup>29</sup>

Albumin plays a major role in the transport of metal ions. Four metal binding sites have been identified in albumin, each with preferential binding to either Cd, Zn, Cu, Ni, Au, and Pt.<sup>30</sup> Much of the metal ion binding to human serum albumin can be attributed to a N-terminal Asp-Ala-His sequence, which strongly binds Cu(II) and Ni(II), preventing toxicity in physiological conditions.<sup>31-33</sup> These identified metals within albumin binding sites are mostly soft or intermediate metals, and binding of hard metals seems unlikely at

this site.<sup>34</sup> However, Al(III) binds to albumin and other metal complexes, like Mn(II) and Gd(III) contrast agents, bind to albumin as well, showing promise of hard metal sequestration in serum.<sup>35,36</sup> Studies with titanium showed complexation of anticancer compounds by albumin, weakly at the N-terminal sequence but more likely at sites along the surface.<sup>34</sup> By sequestering metal ions, albumin fulfills important antioxidant abilities for human serum.<sup>35</sup>

#### **1.4 Metal-Transferrin Binding**

The primary function of transferrin is iron (III) binding and transport, which affords solubility to insoluble iron and prevents oxidation by complexation. Human serum transferrin (Tf) is a bilobal glycoprotein that binds two iron ions, one in each lobe, in octahedral coordination to two tyrosines, one histidine, and one aspartic acid within its two binding lobes.<sup>37</sup> A synergistic anion, often a bicarbonate anion, is needed for this coordination of iron within the binding pocket. The two lobes of Tf have similar sequence, at approximately 30% homology, and the N-lobe and C-lobe are connected by a short linker to equal about 80 kDa in total.<sup>38</sup> As mentioned above, about 2.5 g L<sup>-1</sup> of Tf is present in serum, which equates to approximately 31 – 35 μM, a high serum concentration compared to other low abundance proteins.<sup>8</sup> This high concentration is significant since in order to meet bone marrow iron supply requirements alone, Tf is needed to turn over more than 10 times in a day.<sup>39</sup>

Once iron is bound, Tf undergoes a conformational change to a closed lobe as noted from a change in the radius of gyration as determined by small angle X-ray scattering (SAXS) techniques.<sup>40,41</sup> Crystallography has also been essential in defining the open and

closed lobe states of transferrin, as featured in the structures in Figure 1. This conformational change has often been cited as an essential step in recognition by the Tf receptor.<sup>42</sup> However, other reports state that while the N-lobe undergoes a conformational change, the C-lobe remains open upon Fe(III) binding, and the Tf receptor has capabilities to recognize sites on both lobes.<sup>43</sup> The transferrin receptor is an 97 kDa homodimer located on coated pits to mediate endocytosis from the cell surface.<sup>44,45</sup>

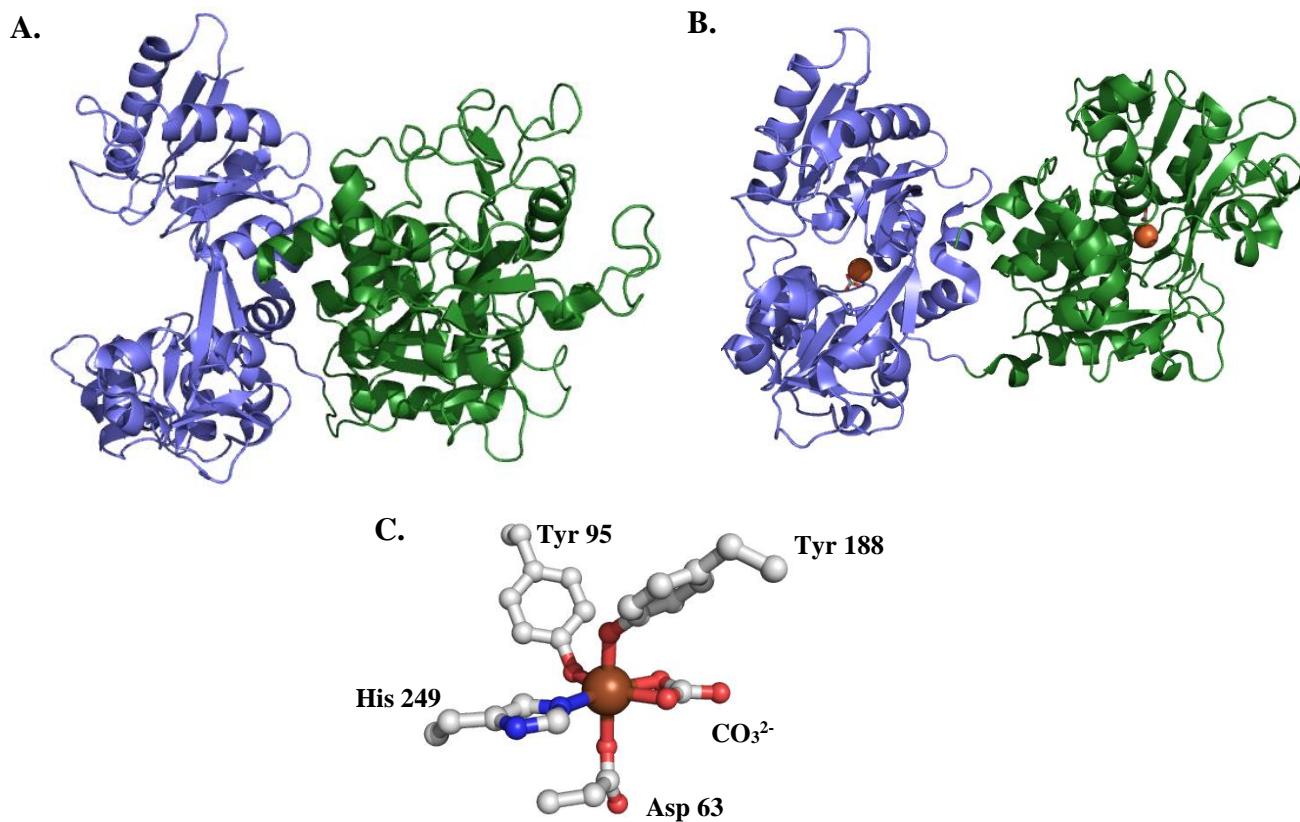


Figure 1.1: Structures of human serum transferrin. N-lobe is shown in blue, C-lobe in green: (A.) apo-transferrin (2HAU)<sup>46</sup>, (B.) diferric transferrin and (C.) the N-lobe Fe binding site in diferric transferrin (3V83)<sup>47</sup>. All figures were made using Pymol. Structures were positioned to highlight conformational change upon iron binding in the N-lobe. A similar change in the C-lobe is difficult to discern due to the position of the lobe.

The whole process of iron delivery via Tf endocytosis is pH dependent and leads to the recycling of the Tf protein back to human serum.<sup>48-50</sup> As Fe<sub>2</sub>Tf is bound to the receptor and brought into the cell, the pH drops to 5.6 and iron is reduced from Fe(III) to Fe(II) and released to a chelator yet to be identified.<sup>51</sup> ApoTf, still chelated to the receptor, is then returned to the cell surface where it is released at neutral serum pH of 7.4, all within 2 to 3 minutes from the start of the process.<sup>52</sup>

This quick and recyclable process of serum Tf is essential due to the high functional requirements of iron in the body. Also, at only 30% saturation of Tf with iron, quick turnover of the Tf cycle is needed.<sup>53,54</sup> With low site saturation and high turnover rate, other metals besides iron binding to Tf has been investigated. As various metals are being utilized for medicinal purposes and have high serum concentrations it has become commonplace to explore these interactions to determine mechanisms of metal incorporation into cells, and Tf is a logical target for metal trafficking.

Additions of transferrin to the medium of sarcoma cell tissue cultures saw a significant increase of gallium-67 uptake in tumors, which is applied as a clinical imaging tool.<sup>55,56</sup> Copper binding to Tf has been documented through pH titrations, fluorescence and UV absorption changes, as well as resonance Raman scattering.<sup>57-60</sup> Reports of Tf binding chromium, manganese, cobalt, bismuth, zinc and aluminum have been cited throughout literature as well.<sup>61-66</sup> There seems to be no correlation between ionic radius and binding strength for various metals binding to Tf compared to the 0.65 Å ionic radius of iron.<sup>66,67</sup> Correlation between Lewis acidity of metal ions and binding constants has been noted, as more Lewis acidic metals, similar to Fe(III), have tighter binding to Tf.<sup>68,69</sup>

Transferrin, despite its tight binding to Fe(III) complexes, is rather uninhibited in binding to other metals present in serum.

Several studies have shown titanium binding to the iron binding lobes of transferrin. Studies with the Ti containing anticancer drug titanocene dichloride analyzed transferrin as the mediator for Ti delivery to tumor cells.<sup>70</sup> The Fe(III) binding sites of transferrin were determined to be the location of Ti(IV) complexation to the protein.<sup>71</sup> Besides titanium metallocenes, titanium citrate can bind to transferrin in a similar fashion with formally higher affinity binding to Tf than Fe(III).<sup>69</sup> In fact, the only two Ti-Tf crystal structures to be solved both show citrate as a synergistic anion in the binding within the traditional Fe(III) lobe.<sup>72,73</sup> Additionally, both crystal structures show an opened lobe binding conformation, as seen in Figure 2. The addition of citrate to Ti-Tf binding was not only postulated to be important for Ti binding, but also for its cellular release. However, other studies reveal that Ti-Tf has too low a reduction potential under physiological conditions for Ti to be released in the same fashion as Fe(III) from transferrin.<sup>74,75</sup>

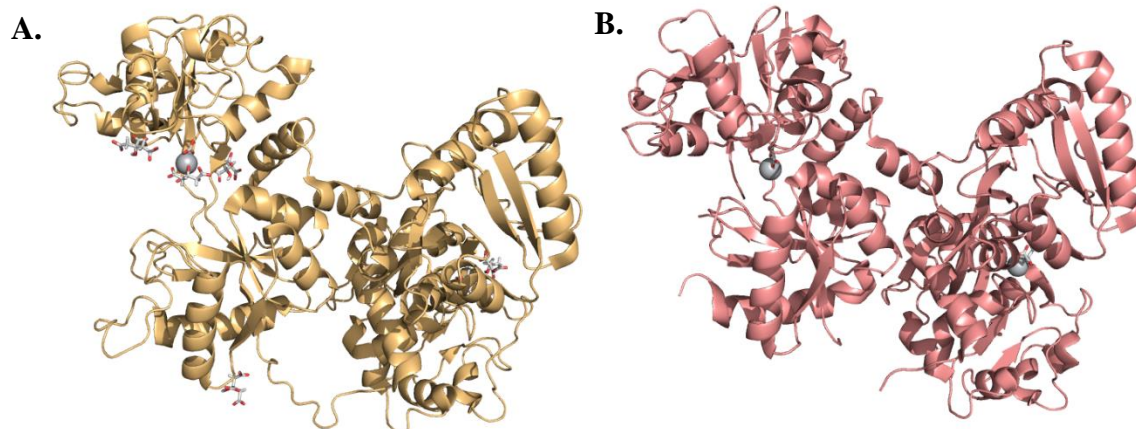


Figure 1.2: Crystal structures of human serum transferrin with titanium. (A.) Structure from Tinoco et al (5DYH).<sup>73</sup> (B.) Structure from Curtin et al (5H52).<sup>72</sup> All figures were made using Pymol.

## 1.5 Metal-Glycan Binding

Glycosylation is the most common and highly diverse protein modification process with nearly all proteins in human serum being glycosylated.<sup>76,77</sup> Glycan synthesis occurs in the Golgi apparatus, where nine monosaccharides precursors from the diet are assembled into diverse glycan chains and bound to cell surfaces.<sup>78</sup> The magnitude of the role of glycosylation in biological processes cannot be understated. One of the more important functions of glycosylation is increased solubility of proteins and prevention of protein aggregation.<sup>79</sup> Additionally, protein glycosylation helps the function of cell signaling and adhesion and with immune response, along with protein folding and overall structural integrity of proteins.<sup>80-83</sup> As noted earlier, free glycans exist in human serum. Disialo-biantennary glycans were the most abundant in serum, which are commonly derived from transferrin.<sup>13</sup>

A variety of instances in literature show glycan capabilities in metal coordination. For instance, carbohydrate microarrays are a great bioassay to quickly study diseases. Glycans are immobilized onto aluminum slides, showing the binding capabilities of glycan chains to the natural aluminum oxide coating on the slide, before they are utilized to scan for sugar-protein binding diagnostics.<sup>84</sup> An emerging term called metalloglycomics came from Codd's EPR study of sialic acid carbohydrates chelation to chromium compounds, relevant to Cr(V) metabolism.<sup>85</sup> Recent reports found Pt coordination complexes can bind to sulfated polysaccharide chains, which can alter the cytotoxicity of Pt anticancer agents and also determined a new cancer target, heparan sulfate proteoglycans (HSPGs).<sup>86-88</sup> Ion mobility spectrometry has been used to characterize and analyze the binding of an array of

metal ions, including Mn, Co, Ni, Cu, Fe, Mg, Ca, and Ba, to a glycan chain which revealed different structural conformations.<sup>89</sup>

The function of glycan chains has also been shown to moderate metal binding to proteins. Such as in the case of prion protein, Pr<sup>P</sup>, in which glycans occupied in the protein binds copper, preventing metal accessibility to the Pr<sup>P</sup> binding sites.<sup>90</sup> However, deglycosylated Pr<sup>P</sup> will bind metal to the protein domain and cause a conversion to prion disease related conformer, PrP<sup>Sc</sup>.<sup>90</sup>

## **1.6 Conclusion**

Human serum is a diverse and expansive regulatory system for trace metals. Biochemist simulate similar environments to serum through use of buffers mimicking physiological conditions in order to study interactions between metals and small molecules or proteins. This helps gain a greater understanding of individual interactions that could occur all within a controlled lab setting. Understanding the complexity of metal circulation through human serum can accelerate metal-based drug development by identifying possible targets in serum or improving metal toxicity screenings.

## 1.7 References

1. Anderson, N. L.; Anderson, N. G. The human plasma proteome: history, character, and diagnostic prospects. *Mol. Cell. Proteomics* **2002**, *1* (11), 845–867.
2. Issaq, H. J.; Xiao, Z.; Veenstra, T. D. Serum and plasma proteomics. *Chem. Rev.* **2007**, *107* (8), 3601–3620.
3. Han, Q.; Sun, X.; Xu, M.; Zhang, N.; Tang, L.; Tan, Y.; Hoffman, R. M. Comparison of serum and heparinized plasma samples for measurement of chemistry analytes. *Clin. Chem.* **2004**, *50* (9), 1704–1705.
4. Keshishian, H.; Burgess, M. W.; Gillette, M. A.; Mertins, P.; Clauser, K. R.; Mani, D. R.; Kuhn, E. W.; Farrell, L. A.; Gerszten, R. E.; Carr, S. A. Multiplexed, quantitative workflow for sensitive biomarker discovery in plasma yields novel candidates for early myocardial injury. *Mol. Cell. Proteomics* **2015**, *14* (9), 2375–2393.
5. Geyer, P. E.; Kulak, N. A.; Pichler, G.; Holdt, L. M.; Teupser, D.; Mann, M. Plasma proteome profiling to assess human health and disease. *Cell Syst.* **2016**, *2* (3), 185–195.
6. Strohkamp, S.; Gemoll, T.; Habermann, J. K. Possibilities and limitations of 2DE-based analyses for identifying low-abundant tumor markers in human serum and plasma. *Proteomics* **2016**, *16* (19), 2519–2532.
7. Lei, T.; He, Q. Y.; Wang, Y. L.; Si, L. S.; Chiu, J. F. Heparin chromatography to deplete high-abundance proteins for serum proteomics. *Clin. Chim. Acta* **2008**, *388* (1–2), 173–178.
8. Timerbaev, A. R.; Hartinger, C. G.; Aleksenko, S. S.; Keppler, B. K. Interactions of antitumor metallodrugs with serum proteins: Advances in characterization using modern analytical methodology. *Chem. Rev.* **2006**, *106* (6), 2224–2248.
9. Kennedy, S. Proteomic profiling from human samples: The body fluid alternative. *Toxicol. Lett.* **2001**, *120* (1–3), 379–384.
10. Schrader, M.; Schulz-Knappe, P. Peptidomics technologies for human body fluids. *Trends Biotechnol.* **2001**, *19* (10 Suppl), 55–60.
11. Adkins, J. N.; Varnum, S. M.; Auberry, K. J.; Moore, R. J.; Angell, N. H.; Smith, R. D.; Springer, D. L.; Pounds, J. G. Toward a human blood serum proteome: analysis by multidimensional separation coupled with mass spectrometry. *Mol. Cell. Proteomics* **2002**, *1* (12), 947–955.

12. Gebrehiwot, A. G.; Melka, D. S.; Kassaye, Y. M.; Rehan, I. F.; Rangappa, S.; Hinou, H.; Kamiyama, T.; Nishimura, S. I. Healthy human serum N-glycan profiling reveals the influence of ethnic variation on the identified cancer-relevant glycan biomarkers. *PLoS One* **2018**, *13* (12), 1–23.
13. Iwatsuka, K.; Watanabe, S.; Kinoshita, M.; Kamisue, K.; Yamada, K.; Hayakawa, T.; Suzuki, T.; Kakehi, K. Free glycans derived from glycoproteins present in human sera. *J. Chromatogr. B Anal. Technol. Biomed. Life Sci.* **2013**, *928*, 16–21.
14. Salek-Maghsoudi, A.; Vakhshiteh, F.; Torabi, R.; Hassani, S.; Ganjali, M. R.; Norouzi, P.; Hosseini, M.; Abdollahi, M. Recent advances in biosensor technology in assessment of early diabetes biomarkers. *Biosens. Bioelectron.* **2018**, *99* (May 2017), 122–135.
15. Cacoub, P.; Vandewalle, C.; Peoc'h, K. Using transferrin saturation as a diagnostic criterion for iron deficiency: A systematic review. *Crit. Rev. Clin. Lab. Sci.* **2019**, *56* (8), 526–532.
16. Versieck, J.; Cornelis, R. Normal levels of trace elements in human blood plasma or serum. *Anal. Chim. Acta* **1980**, *116* (2), 217–254.
17. Kaim, W.; Schwederski, B. *Bioinorganic Chemistry: Inorganic Elements in the Chemistry of Life*; John Wiley & Sons: West Sussex, 1994.
18. Apps, M. G.; Choi, E. H. Y.; Wheate, N. J. The state-of-play and future of platinum drugs. *Endocr. Relat. Cancer* **2015**, *22* (4), R219–R233.
19. Schwietert, C. W.; McCue, J. P. Coordination compounds in medicinal chemistry. *Coord. Chem. Rev.* **1999**, *184* (1), 67–89.
20. Shaloam, D.; Tchounwou, P. B. Cisplatin in cancer therapy: Molecular mechanisms of action. *Eur. J. Pharmacol.* **2014**, *740*, 364–378.
21. Kopf-Maier, P.; Kopf, H. *Metal Compounds in Cancer Therapy*; Chapman & Hall: London, 1994.
22. Schilling, T.; Keppler, K. B.; Heim, M. E.; Niebch, G.; Dietzfelbinger, H.; Rastetter, J.; Hanauske, A. R. Clinical phase I and pharmacokinetic trial of the new titanium complex budotitane. *Invest. New Drugs* **1995**, *13* (4), 327–332.
23. Kroger, N.; Kleeberg, U. R.; Mross, K.; Edler, L.; Sab, G.; Hossfeld, D. K. Phase II Clinical Trial of Titanocene dichloride in patients with metastatic breast cancer. *Onkologie* **2000**, *23*, 60–62.

24. Lummen, G.; Sperling, H.; Luboldt, H.; Otto, T.; Rubben, H. Phase II trial of titanocene dichloride in advanced renal-cell carcinoma. *Cancer Chemother Pharmacol* **1998**, *42*, 415–417.
25. Guo, Z.; Sadler, P. J. Metals in medicine: Metal-based drugs. *Angew. Chem. Int. Ed.* **1999**, *38*, 1512–1531.
26. He, X. M.; Carter, D. C. Atomic structure and chemistry of human serum albumin. *Nature* **1992**, *358* (6383), 209–215.
27. Peters, T. The Albumin Molecule: Its Structure and Chemical Properties. In *All about albumin: Biochemistry, genetics, and medical applications*; Academic Press, 1995; pp 9–11.
28. Carter, D. C.; He, X. Structure of human serum albumin. *Science (80-. )*. **1990**, *249*, 302–303.
29. Ghuman, J.; Zunszain, P. A.; Petitpas, I.; Bhattacharya, A. A.; Otagiri, M.; Curry, S. Structural basis of the drug-binding specificity of human serum albumin. *J. Mol. Biol.* **2005**, *353* (1), 38–52.
30. Mothes, E.; Faller, P. Evidence that the principal CoII-binding site in human serum albumin is not at the N-terminus: Implication on the albumin cobalt binding test for detecting myocardial ischemia. *Biochemistry* **2007**, *46* (8), 2267–2274.
31. Sadler, P. J.; Tucker, A.; Viles, J. H. Involvement of a lysine residue in the N-terminal Ni<sup>2+</sup> and Cu<sup>2+</sup> binding site of serum albumins. *Eur. J. Biochem.* **1994**, *200*, 193–200.
32. Glennon, J. D.; Sarkar, B. Nickel(II) transport in human blood serum. Studies of nickel(II) binding to human albumin and to native-sequence peptide, and ternary-complex formation with l-histidine. *Biochem. J.* **1982**, *203* (1), 15–23.
33. Bal, W.; Christodoulou, J.; Sadler, P. J.; Tucker, A. Multi-metal binding site of serum albumin. *J. Inorg. Biochem.* **1998**, *70* (1), 33–39.
34. Tinoco, A. D.; Eames, E. V.; Valentine, A. M.; V, Y. U.; Box, P. O.; V, N. H. Reconsideration of serum Ti (IV) transport: Albumin and transferrin trafficking of Ti (IV) and its complexes. *J. Am. Chem. Soc.* **2008**, *130*, 2262–2270.
35. Fasano, M.; Curry, S.; Terreno, E.; Galliano, M.; Fanali, G.; Narciso, P.; Notari, S.; Ascenzi, P. The extraordinary ligand binding properties of human serum albumin. *IUBMB Life* **2005**, *57* (12), 787–796.

36. Harris, W. R. Binding and transport of aluminum by serum proteins. *Coord. Chem. Rev.* **1996**, *149*, 347–365.
37. Thorstensen, K.; Romslo, I. The role of transferrin in the mechanism of cellular iron uptake. *Biochem. J.* **2015**, *271* (1), 1–9.
38. Lambert, L. A. Molecular evolution of the transferrin family and associated receptors. *Biochim. Biophys. Acta - Gen. Subj.* **2012**, *1820* (3), 244–255.
39. Gkouvatzos, K.; Papanikolaou, G.; Pantopoulos, K. Regulation of iron transport and the role of transferrin. *Biochim. Biophys. Acta - Gen. Subj.* **2012**, *1820* (3), 188–202.
40. Grossmann, J. G.; Crawley, J. B.; Strange, R. W.; Patel, K. J.; Murphy, L. M.; Neu, M.; Evans, R. W.; Hasnain, S. S. The nature of ligand-induced conformational change in transferrin in solution. An investigation using X-ray scattering, XAFS and site-directed mutants. *J. Mol. Biol.* **1998**, *279* (2), 461–472.
41. Grossmann, J. G.; Neu, M.; Pantos, E.; Schwab, F. J.; Evans, R. W.; Townes-Andrews, E.; Lindley, P. F.; Appel, H.; Thies, W. G.; Hasnain, S. S. X-ray solution scattering reveals conformational changes upon iron uptake in lactoferrin, serum and ovo-transferrins. *J. Mol. Biol.* **1992**, *225* (3), 811–819.
42. Sun, H.; Li, H.; Sadler, P. J. Transferrin as a metal ion mediator. *Chem. Rev.* **1999**, *99*, 2817–2842.
43. Mason, A. B.; Tam, B. M.; Woodworth, R. C.; Oliver, R. W. A.; Green, B. N.; Linr, L.-N.; Brandts, J. F.; Savage, K. J.; Lineback, J. A.; Macgillivray, R. T. A. Receptor recognition sites reside in both lobes of human serum transferrin. *Biochem. J* **1997**, *326*, 77–85.
44. Kawabata, H. Transferrin and transferrin receptors update. *Free Radic. Biol. Med.* **2019**, *133* (June 2018), 46–54.
45. Hopkins, C. R.; Trowbridge, I. S. Internalization and processing of transferrin and the transferrin receptor in human carcinoma A431 cells. *J. Cell Biol.* **1983**, *97* (2), 508–521.
46. Wally, J.; Halbrooks, P. J.; Vornrhein, C.; Rould, M. A.; Everse, S. J.; Mason, A. B.; Buchanan, S. K. The crystal structure of iron-free human serum transferrin provides insight into inter-lobe communication and receptor binding. *J. Biol. Chem.* **2006**, *281* (34), 24934–24944.
47. Noinaj, N.; Easley, N. C.; Oke, M.; Mizuno, N.; Gumbart, J.; Boura, E.; Steere, A. N.; Aisen, P.; Tajkhorshid, E.; Evans, R. W.; et al. Structural basis for iron piracy

- by pathogenic *Neisseria*. *Nature* **2012**, 483 (7387), 53–58.
48. Dautry-Varsat, A.; Ciechanover, A.; Lodish, H. F. . PH and the recycling of transferrin during receptor-mediated endocytosis. *PNAS* **2019**, 80 (8), 2258–2262.
  49. Mukherjee, S.; Ghosh, R. N.; Maxfield, F. R. Endocytosis. *Physiol. Rev.* **2019**, 77 (3), 759–803.
  50. Harding, C.; Heuser, J.; Stahl, P. Receptor-mediated endocytosis of transferrin and recycling of the transferrin receptor in rat reticulocytes. *J. Cell Biol.* **1983**, 97 (2), 329–339.
  51. Eckenroth, B. E.; Steere, A. N.; Chasteen, N. D.; Everse, S. J.; Mason, A. B. How the binding of human transferrin primes the transferrin receptor potentiating iron release at endosomal pH. *PNAS* **2011**, 108 (32), 13089–13094.
  52. Byrne, S. L.; Chasteen, N. D.; Steere, A. N.; Mason, A. B. The Unique Kinetics of Iron Release from Transferrin : The Role of Receptor , Lobe – Lobe Interactions , and Salt at Endosomal pH. *J. Mol. Biol.* **2010**, 396 (1), 130–140.
  53. Williams, J.; Moreton, K. The distribution of iron between the metal-binding sites of transferrin human serum. *Biochem. J.* **1980**, 185, 483–488.
  54. Eckenroth, B. E.; Steere, A. N.; Chasteen, N. D.; Everse, S. J.; Mason, A. B. How the binding of human transferrin primes the transferrin receptor potentiating iron release at endosomal pH. **2011**, 108 (32).
  55. Larson, S. M.; Rasey, J. S.; Allen, D. R.; Nelson, N. J. A transferrin-mediated uptake of gallium-67 by EMT-6 sarcoma. I. Studies in tissue culture. *J. Nucl. Med.* **1979**, 20 (8), 837–842.
  56. Harris, W. R.; Pecoraro, V. L. Thermodynamic binding constants for gallium transferrin. *Biochemistry* **1983**, No. 1974, 292–299.
  57. Hirose, J.; Fujiwara, H.; Magarifuchi, T.; Iguti, Y.; Iwamoto, H.; Kominami, S.; Hiromi, K. Copper binding selectivity of N- and C-sites in serum (human)- and ovo-transferrin. *Biochem. Biophys. Acta* **1996**, 1296, 103–111.
  58. Lehrer, S. Fluorescence and absorption studies of the binding of copper and iron to transferrin. *J. Biol. Chem.* **1969**, 244 (13), 3613–3617.
  59. Gaber, B. P.; Miskowski, V.; Spiro, T. G. Resonance raman scattering from iron(III)- and copper(II)-transferrin and an iron(III) model compound. A spectroscopic interpretation of the transferrin binding site. *J. Am. Chem. Soc.* **1974**,

96 (22), 6868–6873.

60. Aasa, R.; Malmström, B. G.; Saltman, P.; Vänngård, T. The specific binding of iron(III) and copper(II) to transferrin and conalbumin. *BBA - Biochim. Biophys. Acta* **1963**, 75 (C), 203–222.
61. Herrera, C.; Pettiglio, M. A.; Bartnikas, T. B. Investigating the role of transferrin in the distribution of iron, manganese, copper, and zinc. *J. Biol. Inorg. Chem.* **2014**, 19 (6), 869–877.
62. Qing-Yu, H. E.; Mason, A. B.; Woodworth, R. C. Spectrophotometric titration with cobalt(III) for the determination of accurate absorption coefficients of transferrins. *Biochem. J.* **1996**, 318 (1), 145–148.
63. Smith, T. A. D. Human serum transferrin cobalt complex: Stability and cellular uptake of cobalt. *Bioorganic Med. Chem.* **2005**, 13 (14), 4576–4579.
64. Aisen, P.; Aasa, R.; Redfield, A. G. The chromium, manganese, and cobalt complexes of transferrin. *J. Biol. Chemistry* **1969**, 244 (17), 4628–4633.
65. Moshtaghie, A. A.; Ani, M.; Bazrafshan, M. R. Comparative binding study of aluminum and chromium to human transferrin - effect of iron. *Biol. Trace Elem. Res.* **1992**, 32 (1–3), 39–46.
66. Li, H.; Sadler, P. J.; Sun, H. Unexpectedly strong binding of a large metal ion (Bi<sup>3+</sup>) to human serum transferrin. *J. Biol. Chem.* **1996**, 271 (16), 9483–9489.
67. Baker, E. N. Structure and Reactivity of Transferrins. *Adv. Inorg. Chem.* **1994**, 41, 3890463.
68. Li, H.; Sadler, P. J.; Sun, H. Rationalization of the strength of metal binding to human serum transferrin. *Eur. J. Biochem.* **1996**, 242 (2), 387–393.
69. Tinoco, A. D.; Valentine, A. M. Ti (IV) binds to human serum transferrin more tightly than does Fe (III). *J. Am. Chem. Soc.* **2005**, 127, 11218–11219.
70. Guo, M.; Sun, H.; Mcardle, H. J.; Gambling, L.; Sadler, P. J. Ti IV uptake and release by human serum transferrin and recognition of Ti IV -transferrin by cancer cells: Understanding the mechanism of action of the drug titanocene dichloride. *Biochemistry* **2000**, 39, 10023–10033.
71. Sun, H.; Li, H.; Weir, R. A.; Sadler, P. J. The first specific Ti IV ± protein complex: Potential relevance to anticancer activity of titanocenes. *Angew Chem Int Ed* **1998**, 37 (11), 1577–1579.

72. Curtin, J. P.; Wang, M.; Cheng, T.; Jin, L.; Sun, H. The role of citrate, lactate and transferrin in determining titanium release from surgical devices into human serum. *J. Biol. Inorg. Chem.* **2018**, *23* (3), 471–480.
73. Tinoco, A. D.; Saxena, M.; Sharma, S.; Noinaj, N.; Delgado, Y.; González, E. P. Q.; Conklin, S. E.; Zambrana, N.; Loza-Rosas, S. A.; Parks, T. B. Unusual synergism of transferrin and citrate in the regulation of Ti(IV) speciation, transport, and toxicity. *J. Am. Chem. Soc.* **2016**, *138* (17), 5659–5665.
74. Tinoco, A. D.; Incarvito, C. D.; Valentine, A. M.; V, Y. U.; Box, P. O. Calorimetric, spectroscopic, and model studies provide insight into the transport of Ti(IV) by human serum transferrin. *J. Am. Chem. Soc.* **2007**, *129*, 3444–3454.
75. Parker Siburt, C. J.; Lin, E. M.; Brandt, S. J.; Tinoco, A. D.; Valentine, A. M.; Crumbliss, A. L. Redox potentials of Ti(IV) and Fe(III) complexes provide insights into titanium biodistribution mechanisms. *J. Inorg. Biochem.* **2010**, *104* (9), 1006–1009.
76. Apweiler, R.; Hermjakob, H.; Sharon, N. On the frequency of protein glycosylation, as deduced from analysis of the SWISS-PROT database. *Biochim. Biophys. Acta* **1999**, *1473*, 4–8.
77. Sharon, N. *Complex Carbohydrates, Their Chemistry, Biosynthesis, and Functions*; Addison Wesley: Reading, MA, 1975.
78. Ohtsubo, K.; Marth, J. D. Glycosylation in Cellular Mechanisms of Health and Disease. *Cell* **2006**, *126* (5), 855–867.
79. Tams, J. W.; Vind, J.; Welinder, K. G. Adapting protein solubility by glycosylation. N-Glycosylation mutants of *Coprinus cinereus* peroxidase in salt and organic solutions. *Biochim. Biophys. Acta - Protein Struct. Mol. Enzymol.* **1999**, *1432* (2), 214–221.
80. Sperandio, M.; Gleissner, C. A.; Ley, K. Glycosylation in immune cell trafficking. *Immunol. Rev.* **2009**, *230* (1), 97–113.
81. Taniguchi, N.; Korekane, H. Branched N-glycans and their implications for cell adhesion, signaling and clinical applications for cancer biomarkers and in therapeutics. *BMB Rep.* **2011**, *44* (12), 772–781.
82. Lan, Y.; Hao, C.; Zeng, X.; He, Y.; Zeng, P.; Guo, Z.; Zhang, L. Serum glycoprotein-derived N- and O-linked glycans as cancer biomarkers. *Am. J. Cancer Res.* **2016**, *6* (11), 2390–2415.

83. Rudd, P. M.; Wormald, M. R.; Dwek, R. A. Glycosylation and the immune system. *J. Protein Chem.* **1998**, *17* (6), 519.
84. Tseng, S. Y.; Wang, C. C.; Lin, C. W.; Chen, G. L.; Yu, W. E.; Chen, C. H.; Wu, C. Y.; Wong, C. H. Glycan arrays on aluminum-coated glass slides. *Chem. - An Asian J.* **2008**, *3* (8–9), 1395–1405.
85. Codd, R. Metalloglycomics: A new perspective upon competitive metal-carbohydrate binding using EPR spectroscopy. *Chem. Commun.* **2004**, *08* (23), 2653–2655.
86. Peterson, E. J.; Daniel, A. G.; Katner, S. J.; Bohlmann, L.; Chang, C. W.; Bezos, A.; Parish, C. R.; Von Itzstein, M.; Berners-Price, S. J.; Farrell, N. P. Antiangiogenic platinum through glycan targeting. *Chem. Sci.* **2016**, *8* (1), 241–252.
87. Katner, S. J.; Johnson, W. E.; Peterson, E. J.; Page, P.; Farrell, N. P. Comparison of Metal – Ammine compounds binding to DNA and Heparin. Glycans as ligands in bioinorganic chemistry. *Inorg. Chem.* **2018**, *57*, 3116–3125.
88. Gorle, A. K.; Rajaratnam, P.; Chang, C.; Itzstein, M. Von; Berners-price, S. J.; Farrell, N. P. Glycans as ligands in bioinorganic chemistry. Probing the interaction of a trinuclear platinum anticancer complex with defined monosaccharide fragments of heparan sulfate. *Inorg. Chem.* **2019**, *58*, 7146–7155.
89. Zhu, F.; Glover, M. S.; Shi, H.; Trinidad, J. C.; Clemmer, D. E. Populations of metal-glycan structures influence MS fragmentation patterns. *J. Am. Soc. Mass Spectrom.* **2014**, *26* (1), 25–35.
90. Moudjou, M.; Bernard, J.; Sabuncu, E.; Langevin, C.; Laude, H. Glycan chains modulate prion protein binding to immobilized metal ions. *Neurochem. Int.* **2007**, *50* (5), 689–695.

## CHAPTER 2

### SUPERSTOICHIOMETRIC BINDING OF THE ANTICANCER AGENT TITANOCENE DICHLORIDE BY HUMAN SERUM TRANSFERRIN AND THE EFFECTS ON LOBE CLOSURE

#### 2.1 Introduction

Protein-metal coordination is one way nature has evolved to confer solubility to a biologically relevant but otherwise hydrolysis prone metal, such as Fe(III). Bilobal glycoprotein human serum transferrin (Tf) functions as a ferric ion transporter by coordinating Fe(III) in each lobe in octahedral binding motif to a histidine, aspartic acid, two tyrosines, and two oxygens from a synergistic anion.<sup>1-3</sup> Once Fe(III) is bound, 80 kDa Tf undergoes a conformational change, crystallographic structures of lactoferrin suggested a 54° rotation of the N lobe from an open to closed form to encompass iron in the binding site,<sup>4,5</sup> whereas later results by X-ray solution scattering noted both N- and C-lobe closures.<sup>6</sup>

There is approximately 35  $\mu\text{M}$  transferrin in human serum, but it is only about 30% saturated with Fe(III).<sup>1,7</sup> Tf may act as the transport vessel for other main group ( $\text{Bi}^{3+}$ ,  $\text{Ga}^{3+}$ ,  $\text{Al}^{3+}$ )<sup>8-10</sup> and transition metals ( $\text{Mn}^{2+}$ ,  $\text{Cu}^{2+}$ ,  $\text{Ru}^{3+}$ ).<sup>11-14</sup> Small-angle X-ray scattering and NMR studies, which have documented lobe closure upon  $\text{Fe}^{3+}$  binding, have been utilized to show  $\text{Cu}^{2+}$ ,  $\text{In}^{3+}$ ,  $\text{Al}^{3+}$ , and  $\text{Bi}^{3+}$  induced partial to full loadings and lobe closures as well.<sup>6,15-17</sup> Notably, interactions with Cu(II) has a similar lobe closure effect, but Al(III) only partially closes the lobes and Hf(IV) does not produce any change.<sup>18</sup> This lobe closure is widely thought as the recognition pathway for binding to the transferrin receptor to begin

endocytosis into the cells and release iron for cellular functions.<sup>19</sup> Ineffective metal-induced lobe closures can affect receptor recognition of the metal loaded protein, such as in the case with an incomplete conformational change with Al<sup>3+</sup>.<sup>20</sup>

In cancerous cells, Tf and the Tf receptor are upregulated.<sup>21</sup> Both Ga<sup>3+</sup> and Ru<sup>3+</sup> complexes are thought to utilize Tf as a drug delivery system. Imaging agent <sup>67</sup>Ga is transported across cell membranes of tumors by Tf,<sup>8,22</sup> while Ru(III) anticancer agents bind to Tf and still retain antitumor activity.<sup>13</sup> Titanium coordination compounds have been studied for their anticancer activity across a variety of cell lines in vitro,<sup>23</sup> with Tf as the main focus as a transport protein to shuttle Ti(IV) across cell membranes.<sup>24</sup> Titanocene dichloride (TDC) was one of these once-promising Ti drug candidates, but ultimately a soluble TDC formulation failed Phase II clinical trials due to ineffective responses and dose-limiting toxicity.<sup>25,26</sup> The water soluble TDC formulation known as MKT4 was used during all clinical trials due to the very hydrolysis prone nature of TDC, which is subject to rapid Cp ring loss at physiological pH.<sup>25-28</sup> MKT4 displayed different Ti binding motifs to Tf, which could explain why the formulation did not live up to the expectation of TDC activity in clinical trials.<sup>29</sup> Yet, the TDC formulation was seen through X-ray fluorescence imaging to accumulate near the nucleus of cells, showing cellular accumulation,<sup>30</sup> making TDC an interesting model for metal incorporation into the cell.

Studies with Ti(IV) found that it binds, in both hydrolyzed and unhydrolyzed forms, with formally higher affinity to Tf than Fe(III).<sup>11,24,31,32</sup> Complexation of TDC with Tf was consistent with two equivalent coordination in the Fe binding pockets of Tf, with characteristic UV/Vis ligand to metal charge transfer (LMCT) bands to tyrosine at 241,

295, and 321 nm.<sup>11,24</sup> In all previous UV/Vis experiments of Ti(IV) binding in Tf, the extracted information from UV/Vis, relying as it does on the tyrosine-to-Fe(III) charge transfer, only reports on binding in the Fe(III) site, but binding elsewhere on the protein is not detectable by this technique. The extinction coefficient of Ti binding in Fe's site was originally reported as  $\epsilon_{321 \text{ nm}} = 2,415 \text{ M}^{-1} \text{ cm}^{-1}$  per site for TDC to Tf binding.<sup>24</sup> Other reports describe higher extinction coefficients at  $\epsilon_{321 \text{ nm}} = 10,380 \text{ M}^{-1} \text{ cm}^{-1}$  per site for titanium citrate – Tf loading.<sup>31</sup> The discrepancies among extinction coefficients could be due to a number of factors such as conformational changes allowing more intense LMCT transitions, the hydrolyzed versus unhydrolyzed form of Ti in the binding site, or conditions supporting more complete Ti loadings.<sup>29,31</sup> Further evidence for lobe closure upon Ti(IV) binding to Tf was taken from the ability of the closed lobe selective Tf receptor to bind Ti-Tf.<sup>24,33,34</sup> Recent crystallographic work speculates transferrin lobe closure hinderance by Ti(IV), casting doubt on the Tf conformation and the likelihood of Tf receptor uptake.<sup>35</sup> Incorporation of citrate as the synergistic anions has been postulated as the ligand responsible for Ti(IV) binding to Tf and its cellular release.<sup>36</sup>

An unresolved problem is Ti(IV) release from Tf. Neither protonation nor reduction is likely to release the metal ion under physiological conditions. Surface binding on Tf with a species recognizable to the Tf receptor could also resolve a debated issue of how the Ti is removed out of the protein and into the cell. When cycled into the cell, release of Fe from Tf is in part by reduction from Fe(III) to Fe(II).<sup>37</sup> At endosomal pH, Fe<sub>2</sub>Tf reduction potential is too low for physiological agents to reduce Fe, but in complex with the Tf receptor, potential is raised 200 mV.<sup>38</sup> Model ligand for Tf *N,N'*-di(*o*-

hydroxybenzyl)ethylenediamine-*N,N'*-diacetic acid (HBED) complexation with Ti shows an even lower reduction potential than Fe<sub>2</sub>Tf, making it impossible for Ti(IV) to be reduced and released from Tf in endosomal conditions.<sup>32,39</sup> Surface site binding, however, could be an explanation for Ti endosomal release and possible higher reduction potentials of Ti(IV) at the surface of Tf.

The focus of TDC binding to transferrin has been on the Fe(III) binding sites leading to studies of how strongly Ti(IV) is bound and binding to transferrin receptor sites and release.<sup>24,31</sup> Recent studies into metallodrug binding to glycans offers insight to the potential of alternative binding to glycosaminoglycated protein surfaces.<sup>40</sup> Platinum coordination compounds and glycosaminoglycans showed competitive cellular binding affinities through electrostatic interactions.<sup>41</sup> Similarly, progress has been made in computational docking methods to identify passive and active binding of metal-protein stabilization in which secondary interactions that have been previously unseen through UV/Vis, ESI-MS, or other techniques now come to light.<sup>42,43</sup>

In this report we measure the resistance to hydrolysis of TDC and its aqueous products in Tf solutions at stoichiometry extending beyond two, comprising the Fe binding sites. Investigating additional binding potential and sites on glycoprotein transferrin would help to explain the incorporation of Ti in cells. The surface binding potential of Ti(IV) on transferrin led to investigations of protein lobe closures and conformational changes upon metal binding. Understanding TDC binding to Tf gives a broader scope of Ti(IV) transport through human serum and the role of human serum transferrin as the main ligand to warrant solubility. Potential stabilization of metal coordination compounds on the surface of

glycoprotein transferrin could explain cellular import pathways of metallodrugs, especially if stabilized to the receptor recognized closed lobe conformation of Fe<sub>2</sub>Tf.

## 2.2 Experimental

### 2.2.1 Materials

All solutions were prepared with nanopure water of 18.2 M $\Omega$ ·cm resistivity from a Barnstead model D11931 water purifier. All glassware was acid-washed using trace metal grade HCl (Fisher). Polyethersulfone (PES) 0.22  $\mu$ m Luer-Lok filters were 13 mm in diameter and were purchased from Tisch Scientific. Reagents were sourced from Acros Organics (nitrilotriacetic acid), Fisher Chemical (NaHCO<sub>3</sub>, FeCl<sub>3</sub>, and C<sub>13</sub>FeH<sub>12</sub>O<sub>6</sub>), J.T. Baker (KCl, NaH<sub>2</sub>PO<sub>4</sub>, NaCl, and Na<sub>3</sub>C<sub>6</sub>H<sub>5</sub>O<sub>7</sub>), Sigma Aldrich (Ti(IV) chloride, 99.9%), Fluka Chemical (Ti atomic absorption standard 1000 ppm) and Ricca Chemical (Fe atomic absorption standard 1000 ppm). Titanocene dichloride (TDC) was purchased from Acros Organics (97%) and prepared fresh in 1/9 v/v DMSO: 0.1 M saline solution at 4°C. The TDC solution was syringe filtered and ICP-OES was used to confirm the concentration. Human serum apotransferrin was obtained from Athens Research and its purity was checked by SDS-PAGE and was verified as iron-free by UV/Vis ( $\lambda_{\text{max}} = 465 \text{ nm}$ ;  $\epsilon_{465 \text{ nm}} = 2,500 \text{ M}^{-1} \text{ cm}^{-1}$ )<sup>24</sup>. All other chemicals were used as received.

### 2.2.2 Methods

Experiments were carried out at room temperature (22°C). A physiological buffer of 4 mM NaH<sub>2</sub>PO<sub>4</sub>, 100 mM NaCl, and 25 mM or 0.89 mM NaHCO<sub>3</sub> (pH=7.4)<sup>24</sup> was prepared to use for all UV/Vis and ICP-OES experiments. An apotransferrin (Tf) stock solution was prepared in buffer and its concentration was confirmed using UV/Vis with a

transferrin extinction coefficient of  $\epsilon_{280} = 93,000 \text{ M}^{-1} \text{ cm}^{-1}$ .<sup>44</sup> Titanocene dichloride additions to 6 mL Tf samples allowed for a final Tf concentration of 20  $\mu\text{M}$  (diluted from stock Tf) with 0, 2, 4, and 10 equiv of TDC and of 2  $\mu\text{M}$  for experimental equiv of 20, 50, and 100. The final concentration of DMSO in samples was  $< 0.5\%$ . Control samples were prepared without addition of Tf stock, to hold TDC in buffered solutions only. A Thermo Orion model 410 pH meter equipped with an Orion 8103BNUWP Ross Ultra semimicron pH electrode was used to measure and monitor pH. The pH of samples post addition of TDC to Tf were measured at  $\text{pH} = 7.31 \pm 0.01$ . All samples were kept in the dark and secured to a motor-rotating wheel and allowed to rotate gently. One milliliter aliquots of each sample were removed at 0, 2, 96, and 168 h, and syringe filtered with 0.22  $\mu\text{m}$  PES filters. Experiments were performed in duplicate and averaged between trials.

#### 2.2.2.1 UV/Vis

Experiments were performed by using a Varian Cary 50 Bio UV/Vis spectrophotometer. UV/Vis absorbance was measured from each sample and Ti(IV) binding to the iron binding site of Tf was monitored through absorbance at 321 nm using  $\epsilon_{321} = 10,380 \text{ M}^{-1} \text{ cm}^{-1} \text{ site}^{-1}$  extinction coefficient for Ti-Tf binding,<sup>31</sup> unless otherwise noted.

#### 2.2.2.2 Inductively Coupled Plasma Optical Emission Spectroscopy (ICP-OES)

Aliquots of each sample were analyzed by ICP-OES on a Thermo Scientific iCAP 7000 Series ICP-OES Spectrometer. Protein samples were filtered with 0.22  $\mu\text{m}$  syringe filters prior to 10 – 25X dilution with ultrapure water to obtain the final sample. All samples were run without digestion of protein.<sup>24</sup> A standard curve was matched to the matrix of the samples. Acid used in stock atomic absorption standards to preserve standards is  $< 0.015\%$ .

Standards were prepared and analyzed within 1 h of preparation. Reference power was set to 1150 W, auxiliary gas and nebulizer gas flow were both set to 0.5 L/min, with 50 rpm pump speed and functioned in axial mode. The detection wavelengths used to measure elemental emission included 336.121 nm for titanium and 259.940 nm for iron.

#### 2.2.2.3 Fe(III) Loading into Transferrin

A 10 mM iron(III) nitrilotriacetic acid ( $\text{Fe}(\text{NTA})_2$ ) stock was prepared from Fe(III) chloride and two equiv of nitrilotriacetic acid in water and the concentration of iron was confirmed by ICP-OES. Transferrin samples were loaded with 2 equiv diluted from  $\text{Fe}(\text{NTA})_2$  stock, dialyzed in Amicon Ultra 4 centrifugal filters by ultracentrifugation with buffer additions to remove unbound excess  $\text{Fe}(\text{NTA})_2$ , and characterized by UV-Vis to confirm Fe binding and molar ratios.

#### 2.2.2.4 Spin Dialysis for Excess Ti(IV) Removal

Aliquots of Tf at 20  $\mu\text{M}$  final protein concentration were equilibrated with 0, 2, 4, or 10 equiv of TDC for 30 min. Samples were added to Amicon Ultra 4 centrifugal filters, diluted with 1 mL physiological buffer and centrifuged at 3550 g for 10 min. Another buffer addition was then made, and the procedure repeated a total of 4 times. Duplicate trial runs using physiological buffer with both 25 mM  $\text{NaHCO}_3$  and 0.89 mM  $\text{NaHCO}_3$  were compared. UV/Vis confirmed Tf concentration before and after spin dialysis. Titanium concentration was determined by ICP-OES.

#### 2.2.2.5 Fluorescence

Readings were obtained by using a Photon Technology International (PTI) Fluorimeter with FeliX32 analysis software. Samples were excited at 280 nm and emission

was scanned from 200 – 650 nm. Fluorescence of proteins from 168 h timepoints was collected in duplicate and averaged among trials at a  $\lambda_{em, max} = 322$  nm.

#### 2.2.2.6 Small Angle X-Ray Scattering (SAXS) Analysis

Samples were prepared in 4 mM NaHPO<sub>4</sub>, 250 mM NaCl, 0.89 mM NaHCO<sub>3</sub> (pH = 7.4). To examine the effect of TDC binding on the solution state of transferrin, three separate preparations of human transferrin (Tf) were incubated with (i) buffer (apo), (ii) ferric [NTA] (Fe), (iii) titanium citrate (Ticit), (iv) two equivalents of TDC (TDC2), and (v) four equivalents of TDC (TDC4). The three preparations were used to prepare dilution series of 1–15 mg/ml Tf, all including the concentration 6 mg/ml Tf. Solution scattering data was collected in batch mode at the Soft Condensed Matter – Small Angle Scattering (B21) beamline at Diamond Light Source, UK.

#### 2.2.2.7 Urea-PAGE Gel Analysis of TDC Lobe Binding

Metal-protein binding was examined by urea-PAGE electrophoresis by using 10% TBE-urea gels.<sup>45</sup> Sample buffer (5X) was composed of 89 mM Tris, 89 mM boric acid, 12% Ficoll 400, 0.01% bromophenol blue, 0.02% xylene cyanole FF, and 7 M urea. A 1X Tris-borate buffer (89 mM Tris, 89 mM boric acid) was used as the running buffer. Both sample and running buffers were prepared without EDTA, as Ti(IV) may be sequestered in its presence,<sup>46–48</sup> but were otherwise equivalent to commercial and literature buffer protocols.<sup>49,50</sup> A 100 mM titanium citrate solution was prepared by additions of 1 M sodium citrate with titanium(IV) chloride, with 0.2 M KCl as counter ion. Titanium concentration of stock solution was confirmed by ICP-OES. Additions of sodium citrate in Tf-TDC

sample buffer were diluted to final concentration of 0.89 mM citrate. Gels were pre-run for 30 min at 125 V, loaded with 10 uL sample and run for 1.5 h at 125 V.

#### 2.2.2.8 Kinetic Studies of Ti(IV) Removal with Additions of Fe(III) to Tf Solution

Tf samples were loaded with TDC and analyzed by UV/Vis and ICP-OES as described above. Aliquots of sample were diluted to 5  $\mu\text{M}$ , and 50  $\mu\text{M}$  additions of  $\text{Fe(NTA)}_2$  were introduced just prior to sample scanning by UV/Vis. Samples were capped and parafilm. Spectrum scans (200-700 nm) were recorded. Scans were repeated in triplicate and averaged. Samples using physiological buffer containing either 25 mM or 0.89 mM bicarbonate were compared. Tf-  $\text{Fe(NTA)}_2$  samples were dialyzed and analyzed spectroscopically to confirm a 2:1 Fe to protein binding ratio prior to two equiv TDC additions.

## 2.3 Results and Discussion

### 2.3.1 pH Deviation Among Varied Bicarbonate Concentrations

Reactions of TDC with apo-Tf under physiological conditions were monitored first through changes in UV/Vis absorbance. The absorbance change at 321 nm was documented as an interaction between Ti(IV) and the two tyrosine residues in each of the two lobes of Tf.<sup>24</sup>

The physiological buffer in this study was adapted from the literature.<sup>24</sup> In our hands, at 25 mM  $\text{NaHCO}_3$ , the pH steadily rose from 7.4 to a pH of  $8.5 \pm 0.05$  over the course of a seven day study, even in a closed tube with minimal headspace. Although the concentration of bicarbonate in human serum is at higher levels (27 mM)<sup>8,51</sup>, pH is also maintained in serum by a system of regulatory functions. We hypothesize that for these in

vitro systems carbon dioxide escapes causing an upward drift in pH at physiological bicarbonate concentrations. We found that a lower bicarbonate concentration of 0.89 mM  $\text{NaHCO}_3$ , a value used in other experimental systems,<sup>52</sup> allows an excess of bicarbonate as a synergistic anion for maximum experimental concentrations of transferrin of 20  $\mu\text{M}$ , and allows us to keep constant pH buffers.<sup>53</sup>

Table A.1 shows the UV/Vis absorbance measured at 321 nm and the concentration determined by ICP-OES of Tf-TDC samples maintained at bicarbonate concentrations of 25 mM (pH 7.4 rising to 8.5) and 0.89 mM (pH 7.4). Increased bicarbonate concentrations have minimal effect on metal solubility comparatively to lower, pH maintainable concentrations. However, higher concentrations of bicarbonate showed a decrease in absorbance at 321 nm, most likely due to occupation of sites in the binding pocket by bicarbonate anions and a more accurate molar absorptivity factor of  $2,415 \text{ M}^{-1} \text{ cm}^{-1}$  when compared with ICP-OES concentrations. Figure 2.1 shows the apotransferrin subtracted UV spectrum of TDC binding. The apparent absorptivity coefficient used throughout these experiments at 0.89 mM to maintain a pH of 7.4 correlated more directly with  $10,380 \text{ M}^{-1} \text{ cm}^{-1}$  per site.

### 2.3.2 Human Serum Transferrin Supported TDC Resistance to Hydrolytic Precipitation

Results from ICP-OES studies describe what metal is measurable in solution. As higher equiv are introduced, the metal complex hydrolyzes as expected and is filtered out in ICP-OES controls (Figures A.1 and A.2) and is seen losing UV/Vis absorbance over time (Figure A.3). Titanocene dichloride remains soluble in solution with human serum

transferrin as equiv are increased beyond saturation in binding pockets while UV/Vis absorbance saturation at two equiv is reached. Several timepoints describe this interaction in the same manner, extending over the course of a seven-day period. Figure 2.2 shows averaged data of timepoints (0, 24, 96 and 168 h) for both ICP-OES and UV/Vis. Upwards of 50 equiv of Ti(IV) remains functionally soluble in the presence of transferrin. Error in results of 20, 50, or 100 equiv for both controls and protein-bound solutions are most likely due to variability in hydrolysis of TDC over the course of seven days as the upper limit of Ti(IV) solubility is reached.

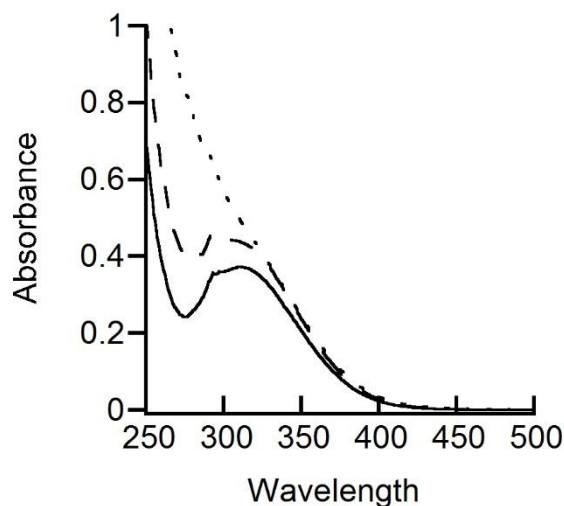


Figure 2.1: 20  $\mu\text{M}$  apoTf subtracted absorbance spectrum of Tf + TDC 2 equiv (solid), 4 equiv (dashed), 10 equiv (dotted) (40, 80, 200  $\mu\text{M}$  TDC).

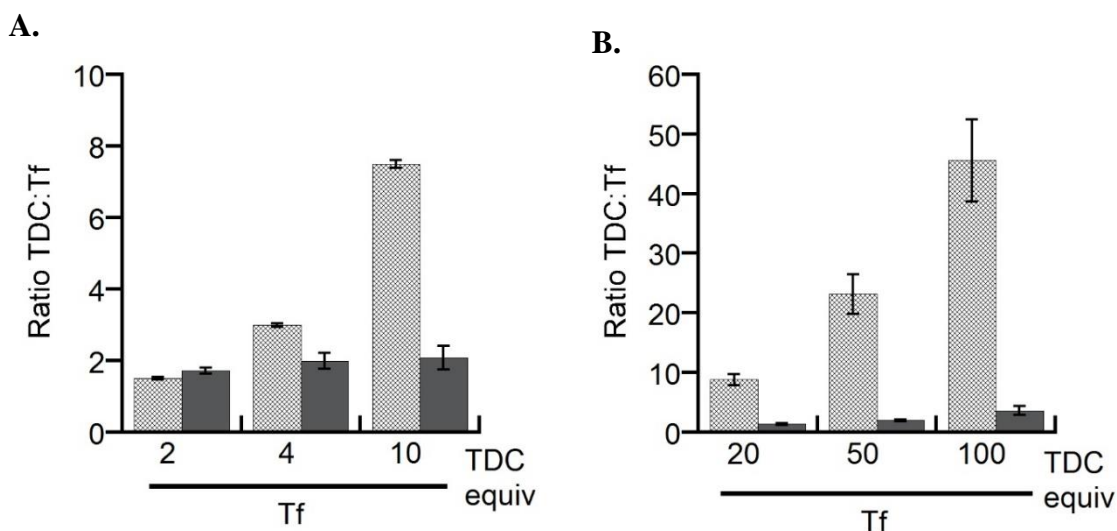


Figure 2.2: (A.) Ratio of Tf-TDC 2, 4, 10 equiv (40, 80, 200  $\mu\text{M}$  TDC) striped (ICP-OES), Solid (UV-Vis) [Tf] = 20  $\mu\text{M}$ ; (B.) Ratio of Tf-TDC 20, 50, 100 equiv striped (40, 100, 200  $\mu\text{M}$  TDC) (ICP-OES), Solid (UV-Vis) [Tf] = 2  $\mu\text{M}$ .

### 2.3.3 Fluorescence

Conformational changes and lobe closures upon Ti(IV) binding to both the surface of transferrin as well as in the binding pocket can be confirmed through fluorescence. Tryptophan fluorescence measurements are indicative of the conformational change that Tf undergoes. As a metal ion binds and causes a lobe closure fluorescence of Trp in the active site is quenched.<sup>54-57</sup> In the C-lobe, there are five tryptophan residues (Trp 344, 358, 441, 460, and 550) which contribute to the fluorescence of the lobe, with Trp460 located closest to iron bound to the lobe (Trp128 is the equivalent residue in the N-lobe) and is believed to be the main contributor of fluorescence for the protein.<sup>58</sup>

The standard of lobe closures and fluorescence quenching is seen in the model of Fe(III) binding to Tf, in which approximately 65% of total protein fluorescence is quenched as the lobe closes.<sup>55</sup> Fluorescence quenching of Tf with TDC binding was measured and is displayed in Table 2.1 (full spectrum represented in Figure A.4). For samples containing two to ten equiv of titanocene, quenching is comparable to control of Tf-Fe<sub>2</sub> and corresponding fluorescence values from literature. When Tf is exposed to higher equiv of TDC, exceeding a 20:1 mole ratio, fluorescence quenching is not as pronounced, yet the LMCT between metal and tyrosine residues within the binding pocket still correspond to a 2:1 binding ratio. Decrease in fluorescence and higher standard deviations in these instances could be due to variant exposure of Trp460 at higher equiv of Ti(IV). When Fe(III) is introduced first, lobe closures are unaffected by TDC introductions at the surface of Tf, with fluorescence quenching stable at Fe<sub>2</sub>-Tf literature standard values.

	% Fluorescence	% Quenching	Standard Deviation
Tf-Fe(NTA) <sub>2</sub> literature*	35	65	-
Tf-Fe(NTA) <sub>2</sub> 1 equiv	78.2	21.8	15.7
Tf-Fe(NTA) <sub>2</sub> 2 equiv	41.6	58.4	22.8
Tf-Fe(NTA) <sub>2</sub> +TDC 4 equiv	32.3	67.7	4.8
Tf + 2 equiv TDC	45.1	54.9	6.2
Tf + 4 equiv TDC	37.49	62.51	0.01
Tf+ 10 equiv TDC	37.4	62.6	10.5
Tf + 20 equiv TDC	73.5	26.5	10.1
Tf + 50 equiv TDC	75.0	25.0	3.4
Tf + 100 equiv TDC	77.8	22.2	10.7

\* He, Q., Mason, A. B., Lyons, B. A., Tam, B. M., Nguyen, V., Macgillivray, R. T. A., and Woodworth, R. C. (2001) Spectral and metal-binding properties of three single-point tryptophan mutants of the human transferrin N-lobe. *Biochem. J.* 354, 423–429.

Table 2.1: Fluorescence quenching relative to apoTf fluorescence. PTI. 168 h averaged of two samples.

#### 2.3.4 Apparent Molar Absorptivity

Analyzing the effects on molar absorptivity on these Tf-Ti species can be telling of the electronic transitions occurring near the tyrosines that are attributed to the absorbance at 321 nm. As equiv of TDC are increased, the apparent molar absorptivity reaches saturation around 3 equiv of metal to transferrin. Higher molar ratios cause a steady decrease in apparent absorptivity, or weaker electronic transitions per metal bound, as metal occupies sites in or around the binding site (Figure 2.3).

Less intense charge transfers could be telling of the lack of lobe closures of Tf when saturated with TDC, leading to fewer transitions between what would be a closed conformation and the metal center. Additionally, opened lobes could lead to solvent exposure of the coordinated metal, causing partial hydrolysis within the binding pocket.

Partial coordination through hydrolysis would have fewer charge transfers but could have binding within the lobes that is equivalent to or exceeding known capacity at the Fe binding sites.

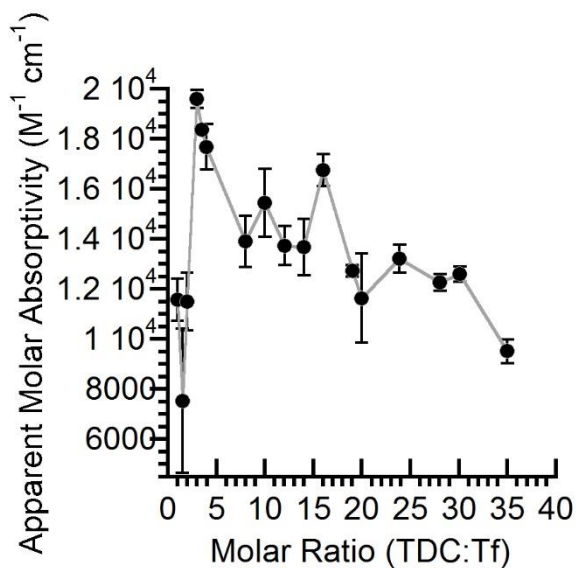


Figure 2.3: Apparent molar absorptivity; averaged of two trials; UV subtracted (apoTf and controls).

### 2.3.5 Urea-PAGE Gel Analysis of TDC Lobe Closure

To further assess conformational changes and binding to specific lobes of Tf, urea-PAGE gels were utilized. Urea-PAGE gels have been used to determine the effect of binding of metal ions to the two lobes of transferrin, as well as the conformation of the protein. Figure 2.4 reveals that even the lowest loading of Tf with TDC does not result in a conformational change comparable to that of Fe loaded Tf. Adjusting concentration of TDC to higher equivalents (Figure 2.5) shows no effect in lobe closures either, as no further

migrated bands can be seen compared to Fe<sub>2</sub>Tf controls. The mobility of the sample as it undergoes electrophoresis is influenced by the presence of urea. This method, first detailed by Makey and Seal in 1976 has been established in the transferrin literature to determine Fe(III) binding.<sup>45</sup> Due to the 40% homology among lobes, the mobility of the domains differ as they undergo electrophoresis.<sup>59</sup> Additionally, the closed conformation of transferrin has less exposure to the denaturing effects of urea and therefore can travel farther through the gel.<sup>60,61</sup> This discrepancy allows us to distinguish between apo-Tf, Fe<sub>2</sub>Tf, and partially loaded transferrin in either the C or N-lobe. Transferrin complexation with vanadium(IV) salts have been determined using urea electrophoresis, with results showing binding and a conformational change.<sup>49</sup>

While carbonate has long been established as the necessary synergistic anion in physiological octahedral metal coordination, other synergistic anions have been proposed. Citrate has been anticipated as a necessary synergistic anion specific for Ti(IV) binding to transferrin and crystallographic data points to citrate as the necessary anion in Ti(IV) binding.<sup>35</sup> Using both synthesized Ti(IV) citrate and additions of sodium citrate alongside TDC additions, conformations were determined via urea-PAGE gels. It can be seen that neither species caused a conformational change upon binding, yet UV/Vis and ICP-OES results indicate binding and the presence of soluble Ti(IV).

These results suggest that Ti(IV) does not induce a conformational change and does not discriminate against Ti(IV) source or synergistic anions. Additionally, Ti(IV) does not seem to affect the lobe closed conformation of Fe<sub>2</sub>Tf, which leads to a plausible mechanism of Ti(IV) uptake into cells.

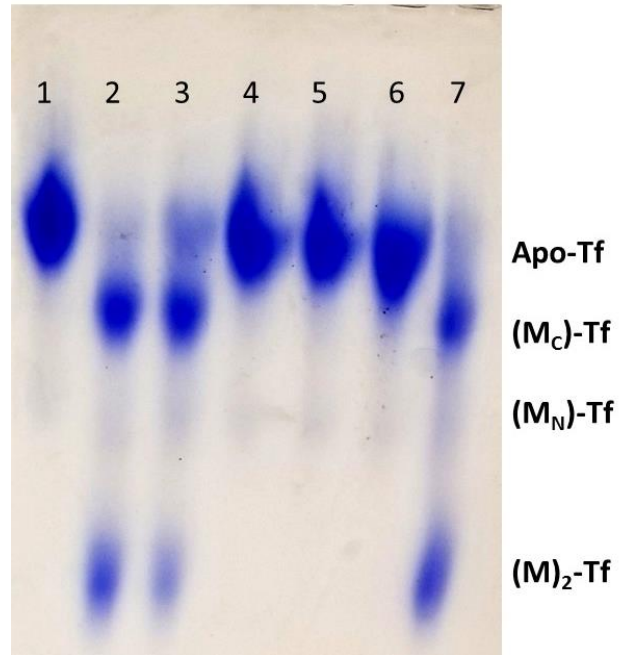


Figure 2.4: Urea-polyacrylamide gel electrophoresis of: 1) apo-Tf, 2) Fe<sub>2</sub>Tf (2 equiv binding) 3) partially loaded Fe<sub>1</sub>Tf (1 equiv binding), 4) Tf-TDC 2 equiv, 5) Tf-TDC 2 equiv (0.89 mM citrate), 6) Tf-Ti citrate 2 equiv, and 7) Fe<sub>2</sub>Tf (2 equiv binding) + TDC 2 equiv.

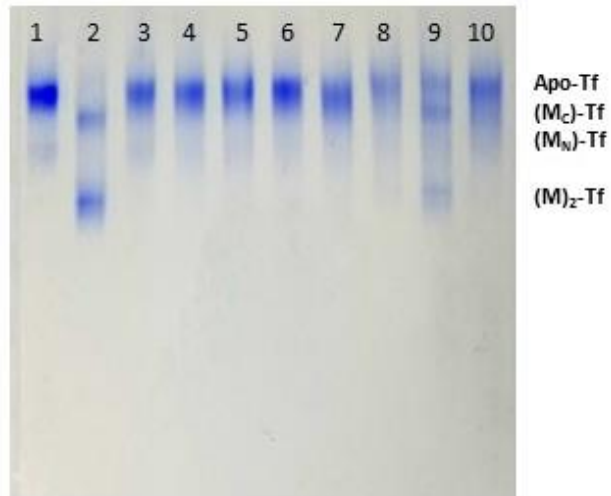


Figure 2.5: Urea-polyacrylamide gel electrophoresis of: 1) apo-Tf, 2) Fe<sub>2</sub>Tf (2 equiv binding) 3) Tf + TDC 2 equiv, 4) Tf + TDC 4 equiv, 5) Tf + TDC 10 equiv, 6) Tf + TDC 20 equiv, 7) Tf + TDC 50 equiv, 8) Tf + TDC 10 equiv (0.89 mM citrate), 9) Fe<sub>2</sub>Tf (2 equiv binding) + TDC 4 equiv, and 10) Tf + TDC 10 equiv (25 mM bicarbonate).

### 2.3.6 Small Angle X-ray Scattering Analysis (SAXS)

Primary data analysis indicated that all three preparations displayed near-ideal solution behavior (Figure A.5). A small negative trend in the radius of gyration ( $R_G$ ) vs. concentration was evident in all specimens, associated with decreasing molecular volume. Hence, to accurately compare the effect of all ligands data from the intermediate concentration  $6 \text{ mg mL}^{-1}$  was used, merging independent experiments where possible ( $n=3$  for apo, Fe and Ti citrate,  $n=2$  for TDC2,  $n=1$  for TDC4).

The Guinier approximation uses the lower region of the small angle scattering curve to give a calculation of the protein's size and shape by relating the forward scattering intensity,  $\ln(I_0)$ , versus the scattering vector,  $q^2$ .<sup>62,63</sup> The  $P(r)$  distribution measures the distribution distances of pairs within the molecule, whereas Porod plots give an estimation of particle volume from total and forward scattering data.<sup>62,63</sup> The resultant scattering curves were analyzed by Guinier plot,  $P(r)$  distribution and Porod plots, which produced consistent values of the radius of gyration ( $R_G$ ), and forward scattering intensity ( $I_0$ ) (Table 2.2 and Figure A.6).

Transferrin bound with Ti citrate or 2–4 equivalents of TDC had an equivalent molecular volume ( $V$ ) to the apo form, whereas the molecular volume of Fe-bound transferrin has a significantly reduced molecular volume. This result is consistent with solution analysis, shown in this paper, and previous crystallography results of Ti bound Tf.

	Apo	Fe	Ti citrate	TDC2	TDC4
<i>n</i>	3	3	3	2	1
<b>Guinier</b>					
$q, \text{\AA}^{-1}$	0.0053–0.041	0.0053–0.041	0.0053–0.041	0.0053–0.041	0.0053–0.041
( $sR_G$ )	(0.166–1.27)	(0.104–1.20)	(0.254–1.36)	(0.122–1.22)	(0.117–1.22)
$R_G, \text{\AA}$	31.0±0.05	30.9±0.04	31.1±0.04	31.1±0.05	31.2±0.07
$I_0$	0.4244±0.0004	0.4581±0.0003	0.4158±0.0004	0.4814±0.0004	0.4812±0.0006
<b><i>P(r)</i></b>					
$q, \text{\AA}^{-1}$	0.0053–0.36	0.0053–0.36	0.0053–0.36	0.0053–0.36	0.0053–0.36
$D_{\text{max}}, \text{\AA}$	93.0	91.0	94.0	94.0	92.5
$R_G, \text{\AA}$	31.02	30.93	31.05	31.01	31.08
$I_0$	0.4249	0.4588	0.4161	0.4812	0.4805
<b>Porod</b>					
$R_G, \text{\AA}$	31.16±0.04	30.74±0.04	31.15±0.15	31.14±0.05	31.19±0.17
$I_0$	0.424±0.01	0.459±0.01	0.414±0.01	0.480±0.01	0.479±0.02
$V, \text{nm}^3$	112.1±2.0	90.9±5.9	111.6±2.6	109.8±2.3	109.6±2.5

Table 2.2: Data values extracted from Guinier plot,  $P(r)$  distribution and Porod plots analysis of apoTf, Fe<sub>2</sub>Tf, Tf-Ti(citrate), Tf + TDC 2 equiv, and Tf +TDC 4 equiv.

### 2.3.7 Surface Interactions of TDC with Fe(III) Loaded Tf

When 4 equiv of TDC is incubated with Fe<sub>2</sub>Tf over 7 days, Ti remains in solution, presumably interacting with the Tf surface. Figure 2.6 details this interaction in which Fe(III) binding ratios stay constant at 2:1, while hydrolysis-prone TDC remains in solution. This further gives evidence to surface interactions of TDC, as Fe(III) is not removed from the binding site with the introduction of TDC over time, yet TDC remains soluble in the presence of the protein.

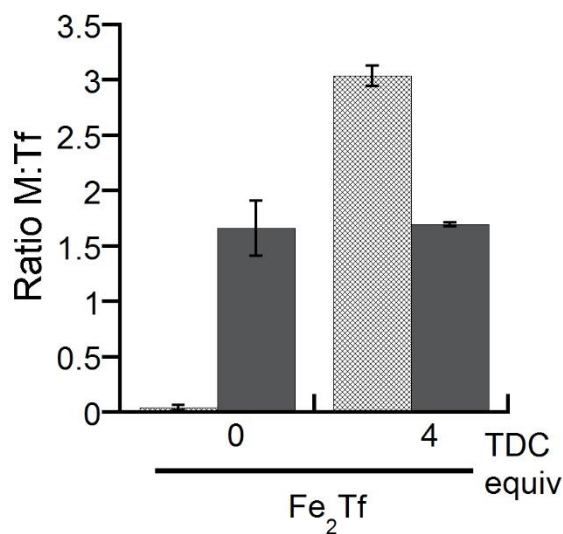


Figure 2.6: ICP-OES results from Fe<sub>2</sub>Tf + TDC 4 equiv. Striped: Ratio Ti:Tf; Solid: Ratio Fe:Tf.

Excess dialysis and buffer exchanges allow equilibration of protein and metal, presumably to binding sites of proteins. Equilibration of TDC loaded Tf at 0.89 mM sodium bicarbonate, still supported high molar ratios of TDC to Tf after dialysis (Figure A.7 A). However, at 25 mM sodium bicarbonate, equilibrated samples reached a minimum

molar ratio of 2:1 metal to protein, indicating weak binding at the surface of the protein (Figure A.7 B). The metal removal from surplus binding features of transferrin could be facilitated by excess bicarbonate when equilibrated in buffered solution or a change in pH over the course of the experiment. UV/Vis Ti:Tf ratio results are consistent, indicating minimal loss of Ti-Tyr transitions within the binding pocket.

Sadler et al. monitored the displacement of Ti(IV) in the binding site of Tf with the introduction of Fe(III) through methods of ICP-OES and  $^1\text{H}$  NMR.<sup>24</sup> This Ti(IV) displacement process is described as occurring in two phases, in which the first Ti(IV) is displaced after approximately 7 minutes and a second Ti(IV) is displaced after a week. However, as this exchange is monitored through methods that we have noted retain higher soluble concentrations of Ti(IV) in the presence of  $\text{Fe}_2\text{Tf}$ , and the slow disappearance of TDC over time can be attributed to excess dialysis to remove Ti(IV) surface interactions. When the spectroscopic kinetic reaction is monitored, the exchange of Ti and Fe is completed in a shorter timeframe overall (Figure A.8). Spectrophotometric analysis clearly details the disappearance of absorbance at 321 nm (associated with Tf-Ti) and the appearance of absorbance at 465 nm (the association of Tf-Fe). Table 2.2 describes the rate constants for the first order fit of each of these exchanges.

It is notable to mention that the exchange of Ti with iron loaded Tf does not result in ion exchange. Ti(IV) lack of exchange with Fe<sub>2</sub>Tf, is could likely be due to the exposure of coordination sites in the binding pocket, as Fe<sub>2</sub>Tf experiences a lobe closure upon binding. The reverse is true for Ti(IV) loaded Tf, in which exchange with Fe(III) is eased from possible forced lobe openings with Ti(IV) or varied hydrolytic states of Ti(IV) within the binding pocket.

	k1 (min <sup>-1</sup> )	Ratio Ti:Tf ( $\epsilon_{321} =$ 10,380 M <sup>-1</sup> cm <sup>-1</sup> )	Ratio Ti:M (ICP-OES)
ApoTf + Fe(NTA) <sub>2</sub>	0.13±0.05	-	-
Tf-TDC 2 equiv + Fe(NTA) <sub>2</sub>	0.024±0.005	2.3±0.2	3.2±0.2
Tf-TDC 4 equiv + Fe(NTA) <sub>2</sub>	0.029±0.006	2.2±0.2	4.7±1.3
Tf-TDC 10 equiv + Fe(NTA) <sub>2</sub>	0.024±0.004	3.2±0.9	12.1±2.9
Tf-TDC 2 equiv + Fe(NTA) <sub>2</sub> (25 mM bicarbonate)	0.2±0.2	0.7±0.2	1.6±0.2

Table 2.3: First order rate constants for Tf preloaded with varied equivalents of TDC and 10 equiv additions of Fe(NTA)<sub>2</sub>. Ti:Tf ratios are the result of UV/Vis and ICP-OES analysis of Tf-TDC loaded prior to Fe(NTA)<sub>2</sub> additions.

## 2.4 Conclusion

The hydrolytic nature of titanocene dichloride allowed us to see interactions with transferrin that otherwise would have been missed. Extra molar equivalent binding of titanium on the surface of transferrin leads to interesting ideas about surface interactions and possible transport of metal to protein, protein to receptor, receptor-protein to cell. Fluorescence quenching and LMCT results indicate binding of titanium in the established binding pockets, giving a 2:1 molar ratio with loading within each lobe of transferrin.

While fluorescence results alone would point to a conformational change upon Ti(IV) loading, Urea-PAGE gels and SAXS indicate that no such conformational change occurs with additions of TDC. Surface binding of Ti(IV) on Fe<sub>2</sub>Tf does not interfere with any conformational changes. Further investigation into receptor recognition of surface bound titanium-Fe<sub>2</sub>-transferrin could elucidate further the pathway of titanium from human serum to cells.

## 2.5 References

1. Sun, H.; Li, H.; Sadler, P. J. Transferrin as a metal ion mediator. *Chem. Rev.* **1999**, *99*, 2817–2842.
2. Thorstensen, K.; Romslo, I. The role of transferrin in the mechanism of cellular iron uptake. *Biochem. J.* **2015**, *271* (1), 1–9.
3. Wessling-Resnick, M. Crossing the iron gate: Why and how transferrin receptors mediate viral entry. *Annu. Rev. Nutr.* **2018**, *38* (1), 431–458.
4. Gerstein, M.; Anderson, B. F.; Norris, G. E.; E.N., B.; Lesk, A. M.; Chothia, C. Domain closure in Lactoferrin: Two hinges produce a see-saw motion between alternative close-packed interfaces. *J. Mol. Biol.* **1993**, *234* (2), 357–372.
5. B.F.Anderson; H.M.Baker; G.E.Norris; S.V.Rumball; E.N.Baker. Apolactoferrin structure demonstrates ligand-induced conformational change in transferrins. *Nature* **1990**, *344* (April), 784–787.
6. Grossmann, J. G.; Neu, M.; Pantos, E.; Schwab, F. J.; Evans, R. W.; Townes-Andrews, E.; Lindley, P. F.; Appel, H.; Thies, W. G.; Hasnain, S. S. X-ray solution scattering reveals conformational changes upon iron uptake in lactoferrin, serum and ovo-transferrins. *J. Mol. Biol.* **1992**, *225* (3), 811–819.
7. Williams, J.; Moreton, K. The distribution of iron between the metal-binding sites of transferrin human serum. *Biochem. J.* **1980**, *185*, 483–488.
8. Harris, W. R.; Pecoraro, V. L. Thermodynamic binding constants for gallium transferrin. *Biochemistry* **1983**, No. 1974, 292–299.
9. Li, H.; Sadler, P. J.; Sun, H. Unexpectedly strong binding of a large metal ion (Bi<sup>3+</sup>) to human serum transferrin. *J. Biol. Chem.* **1996**, *271* (16), 9483–9489.
10. Donovan, J. W.; Ross, D.; li, A.; li, A. Nonequivalence of the metal binding sites of conalbumin. *J. Biol. Chem.* **1975**, *250* (15), 6022–6025.
11. Sun, H.; Li, H.; Weir, R. A.; Sadler, P. J. The first specific Ti IV ± protein complex: Potential relevance to anticancer activity of titanocenes. *Angew Chem Int Ed* **1998**, *37* (11), 1577–1579.
12. Harris, W. R.; Chen, Y. Electron paramagnetic resonance and difference ultraviolet studies of Mn<sup>2+</sup> binding to serum transferrin. *J. Inorg. Biochem.* **1994**, *54*, 1–19.
13. Kratzs, F.; Hartmann, M.; Keppler, B.; Messori, L. The binding properties of two

- antitumor ruthenium (III) complexes to apotransferrin. *J. Biol. Chem.* **1993**, *269* (4), 2581–2588.
14. Hirose, J.; Fujiwara, H.; Magarifuchi, T.; Iguti, Y.; Iwamoto, H.; Kominami, S.; Hiromi, K. Copper binding selectivity of N- and C-sites in serum (human)- and ovo-transferrin. *Biochem. Biophys. Acta* **1996**, *1296*, 103–111.
  15. Grossmann, J. G.; Crawley, J. B.; Strange, R. W.; Patel, K. J.; Murphy, L. M.; Neu, M.; Evans, R. W.; Hasnain, S. S. The nature of ligand-induced conformational change in transferrin in solution. An investigation using X-ray scattering, XAFS and site-directed mutants. *J. Mol. Biol.* **1998**, *279* (2), 461–472.
  16. Sun, H.; Cox, M. C.; Li, H.; Mason, A. B.; Woodworth, R. C.; Sadler, P. J. [<sup>1</sup>H,<sup>13</sup>H] NMR determination of the order of lobe loading of human transferrin with iron: Comparison with other metal ions. *FEBS Lett.* **1998**, *422* (3), 315–320.
  17. Castellano, A. C.; Barteri, M.; Bianconi, A.; Borghi, E.; Cassiano, L.; Castagnola, M.; Della Longa, S.; La Monaca, A. X-ray small angle scattering of the human transferrin protein aggregates. A fractal study. *Biophys. J.* **1993**, *64* (2), 520–524.
  18. Grossmann, J. Gunter; Neu, Margarete; Evans, Robert W.; Lindley, Peter F.; Appel, Helmut; Hasnain, S. S. Metal-induced conformational changes in transferrins. *J. Mol. Biol.* **1993**, *229*, 585–590.
  19. Mason, A. B.; Tam, B. M.; Woodworth, R. C.; Oliver, R. W. A.; Green, B. N.; Linr, L.-N.; Brandts, J. F.; Savage, K. J.; Lineback, J. A.; Macgillivray, R. T. A. Receptor recognition sites reside in both lobes of human serum transferrin. *Biochem. J* **1997**, *326*, 77–85.
  20. Sakajiri, T.; Yamamura, T.; Kikuchi, T.; Ichimura, K.; Sawada, T.; Yajima, H. Absence of binding between the human transferrin receptor and the transferrin complex of biological toxic trace element, aluminum, because of an incomplete open/closed form of the complex. *Biol. Trace Elem. Res.* **2010**, *136* (3), 279–286.
  21. Faulk, W. P.; Hsi, B.-L.; Stevens, P. J. Transferrin and transferrin receptors in carcinoma of the breast. *Lancet* **1980**, *316*, 390–392.
  22. Larson, S. M.; Rasey, J. S.; Allen, D. R.; Nelson, N. J. A transferrin-mediated uptake of gallium-67 by EMT-6 sarcoma. I. Studies in tissue culture. *J. Nucl. Med.* **1979**, *20* (8), 837–842.
  23. Kopf, H.; Kopf-Maier, P. Titanocene dichloride - the first metallocene with cancerostatic activity. *Angew Chem Int Ed* **1979**, *18* (6), 477–478.

24. Guo, M.; Sun, H.; Mcardle, H. J.; Gambling, L.; Sadler, P. J. Ti IV uptake and release by human serum transferrin and recognition of Ti IV -transferrin by cancer cells: Understanding the mechanism of action of the drug titanocene dichloride. *Biochemistry* **2000**, *39*, 10023–10033.
25. Lummen, G.; Sperling, H.; Luboldt, H.; Otto, T.; Rubben, H. Phase II trial of titanocene dichloride in advanced renal-cell carcinoma. *Cancer Chemother Pharmacol* **1998**, *42*, 415–417.
26. Kroger, N.; Kleeberg, U. R.; Mross, K.; Edler, L.; Sab, G.; Hossfeld, D. K. Phase II Clinical Trial of Titanocene dichloride in patients with metastatic breast cancer. *Onkologie* **2000**, *23*, 60–62.
27. Korfel, A.; Scheulen, M. E.; Schmoll, H.-J.; Grundel, O.; Harstrick, A.; Knoche, M.; Fels, L. M.; Skorze, M.; Bach, F.; Baumgart, J.; et al. Phase I clinical and pharmacokinetic study of titanocene dichloride in adults with advanced solid tumors. *Clinical Cancer Res.* **1998**, *4*, 2701–2708.
28. Toney, J. H.; Marks, T. J. Hydrolysis chemistry of the metallocene dichlorides Ti, V, Zr. Aqueous kinetics, equilibria, and mechanistic implications for a new class of antitumor agents. *J. Am. Chem. Soc.* **1985**, *107*, 947–953.
29. Buettner, K. M.; Snoeberger, R. C.; Batista, V. S.; Valentine, A. M. Pharmaceutical formulation affects titanocene transferrin interactions. *Dalton Trans.* **2011**, *40* (37), 9580–9588.
30. Waern, J. B.; Harris, H. H.; Lai, B.; Cai, Z.; Harding, M. M.; Dillon, C. T. Intracellular mapping of the distribution of metals derived from the antitumor metallocenes. *J. Biol. Inorg. Chem.* **2006**, *10*, 443–452.
31. Tinoco, A. D.; Valentine, A. M. Ti (IV) binds to human serum transferrin more tightly than does Fe (III). *J. Am. Chem. Soc.* **2005**, *127*, 11218–11219.
32. Tinoco, A. D.; Incarvito, C. D.; Valentine, A. M. Calorimetric, spectroscopic, and model studies provide insight into the transport of Ti(IV) by human serum transferrin. *J. Am. Chem. Soc.* **2007**, *129* (11), 3444–3454.
33. Aisen, P. The transferrin receptor and the release of iron from transferrin. In *Progress in Iron Research*; 1994; pp 31–40.
34. Tinoco, A. D.; Eames, E. V.; Valentine, A. M.; V, Y. U.; Box, P. O.; V, N. H. Reconsideration of serum Ti(IV) transport: Albumin and transferrin trafficking of Ti(IV) and its complexes. *J. Am. Chem. Soc.* **2008**, *130*, 2262–2270.

35. Tinoco, A. D.; Saxena, M.; Sharma, S.; Noinaj, N.; Delgado, Y.; González, E. P. Q.; Conklin, S. E.; Zambrana, N.; Loza-Rosas, S. A.; Parks, T. B. Unusual synergism of transferrin and citrate in the regulation of Ti(IV) speciation, transport, and toxicity. *J. Am. Chem. Soc.* **2016**, *138* (17), 5659–5665.
36. Curtin, J. P.; Wang, M.; Cheng, T.; Jin, L.; Sun, H. The role of citrate, lactate and transferrin in determining titanium release from surgical devices into human serum. *J. Biol. Inorg. Chem.* **2018**, *23* (3), 471–480.
37. Kraiter, D. C.; Zak, O.; Aisen, P.; Crumbliss, A. L. A Determination of the Reduction Potentials for Diferric and C- and N-Lobe Monoferric Transferrins at Endosomal pH (5.8). *Inorg. Chem.* **1998**, *37* (5), 964–968.
38. Dhungana, S.; Taboy, C. H.; Zak, O.; Larvie, M.; Crumbliss, A. L.; Aisen, P. Redox Properties of Human Transferrin Bound to Its Receptor. *Biochemistry* **2004**, *43* (1), 205–209.
39. Parker Siburt, C. J.; Lin, E. M.; Brandt, S. J.; Tinoco, A. D.; Valentine, A. M.; Crumbliss, A. L. Redox potentials of Ti(IV) and Fe(III) complexes provide insights into titanium biodistribution mechanisms. *J. Inorg. Biochem.* **2010**, *104* (9), 1006–1009.
40. Gorle, A. K.; Rajaratnam, P.; Chang, C.; Itzstein, M. Von; Berners-price, S. J.; Farrell, N. P. Glycans as ligands in bioinorganic chemistry. Probing the interaction of a trinuclear platinum anticancer complex with defined monosaccharide fragments of heparan sulfate. *Inorg. Chem.* **2019**, *58*, 7146–7155.
41. Katner, S. J.; Johnson, W. E.; Peterson, E. J.; Page, P.; Farrell, N. P. Comparison of Metal – Ammine compounds binding to DNA and Heparin. Glycans as ligands in bioinorganic chemistry. *Inorg. Chem.* **2018**, *57*, 3116–3125.
42. Sciortino, G.; Garribba, E.; Marechal, J.-D. Validation and applications of protein – ligand docking approaches improved for metalloligands with multiple vacant sites. *Inorg. Chem.* **2019**, *58* (1), 294–306.
43. Ugone, V.; Sanna, D.; Sciortino, G.; Marechal, J.-D.; Garribba, E. Interaction of vanadium(IV) species with ubiquitin: A combined instrumental and computational approach. *Inorg. Chem.* **2019**, *58* (12), 8064–8078.
44. Chasteen, N. D. Human serotransferrin: Structure and function. *Coord. Chem. Rev.* **1977**, *22*, 1–36.
45. Makey, D. G.; Seal, U. S. The detection of four molecular forms of human transferrin during the iron binding process. *Biochem. Biophys. Acta* **1976**, *453* (1),

250–256.

46. Guinesi, L. S.; Ribeiro, C. A.; Crespi, M. S.; Santos, A. F.; Capela, M. V. Titanium(IV)-EDTA complex: Kinetics of thermal decomposition by non-isothermal procedures. *J. Therm. Anal. Calorim.* **2006**, *85* (2), 301–307.
47. Comba, P.; Merbach, A. The titanyl question revisited. *Inorg. Chem.* **1987**, *26* (8), 1315–1323.
48. Fackler, J. P.; Kristine, F. J.; Mazany, A. M.; Moyer, T. J.; Shepherd, R. E. The absence of a titanyl oxygen in the Ti(IV)-edta<sup>4-</sup> complex: [Ti(edta)(H<sub>2</sub>O)]. *Inorg. Chem.* **1985**, *24* (12), 1857–1860.
49. Mehtab, S.; Gonçalves, G.; Roy, S.; Tomaz, A. I.; Santos-Silva, T.; Santos, M. F. A.; Romão, M. J.; Jakusch, T.; Kiss, T.; Pessoa, J. C. Interaction of vanadium(IV) with human serum apo-transferrin. *J. Inorg. Biochem.* **2013**, *121*, 187–195.
50. BioRad. 2x TBE-urea sample buffer, 30 ml #1610768 <http://www.bio-rad.com/en-us/sku/1610768-2x-tbe-urea-sample-buffer-30-ml?ID=1610768>.
51. Lewis, A. E. *Principles in Hematology*; Appleton Century Crofts: New York City, 1970.
52. Vistica, D. T.; Skehan, P.; Boyd, M. R.; Bel, M. New carbon dioxide independent basal growth medium for culture of diverse tumor and nontumor cells of human and nonhuman origin. *J. Natl. Cancer Inst.* **1990**, *82*, 1055–1061.
53. Lelong, I. H.; Rebel, G. PH Drift of “physiological buffers” and culture media used for cell incubation during in vitro studies. *J. Pharmacol. Toxicol. Methods* **1998**, *39*, 203–210.
54. James, N. G.; Byrne, S. L.; Steere, A. N.; Smith, V. C.; MacGillivray, R. T. A.; Mason, A. B. Inequivalent contribution of the five tryptophan residues in the C-Lobe of human serum transferrin to the fluorescence increase when iron is released. *Biochemistry* **2009**, *48* (13), 2858–2867.
55. He, Q.; Mason, A. B.; Lyons, B. A.; Tam, B. M.; Nguyen, V.; Macgillivray, R. T. A.; Woodworth, R. C. Spectral and metal-binding properties of three single-point tryptophan mutants of the human transferrin N-lobe. *Biochem. J.* **2001**, *354*, 423–429.
56. Lehrer, S. Fluorescence and absorption studies of the binding of copper and iron to transferrin. *J. Biol. Chem.* **1969**, *244* (13), 3613–3617.

57. Evans, B. R. W.; Holbrook, J. J. Differences in the protein fluorescence of the two iron (III)-binding sites of ovotransferrin. *Biochem. J* **1975**, *145*, 201–207.
58. James, N. G.; Byrne, S. L.; Steere, A. N.; Smith, V. C.; MacGillivray, R. T. A.; Mason, A. B. Inequivalent contribution of the five tryptophan residues in the C-Lobe of human serum transferrin to the fluorescence increase when iron is released. *Biochemistry* **2009**, *48* (13), 2858–2867.
59. Aisen, P.; Listowsky, I. Iron Transport and Storage Proteins. *Annu. Rev. Biochem.* **1980**, *49* (1), 357–393.
60. Byrne, S. L.; Mason, A. B. Human serum transferrin: A tale of two lobes. Urea gel and steady state fluorescence analysis of recombinant transferrins as a function of pH, time, and the soluble portion of the transferrin receptor. *J. Biol. Inorg. Chem.* **2009**, *14* (5), 771–781.
61. Evans, R. W.; Williams, J. The electrophoresis of transferrins in urea/polyacrylamide gels. *Biochem. J.* **1980**, *189* (3), 541–546.
62. Doniach, S. Changes in biomolecular conformation seen by small angle X-ray scattering. *Chem. Rev.* **2001**, *101* (6), 1763–1778.
63. Meisburger, S. P.; Thomas, W. C.; Watkins, M. B.; Ando, N. X-ray Scattering Studies of Protein Structural Dynamics. *Chem. Rev.* **2017**, *117* (12), 7615–7672.

## CHAPTER 3

### THE UPTAKE OF TITANIUM OXIDE AND THE CHANGE IN PARTICLE SPECIATION BY HUMAN SERUM TRANSFERRIN

#### 3.1 Introduction

Titanium oxide is the most prevalent form of Ti and occurs naturally in high abundance in the environment. Crystalline anatase and rutile are the two most common morphologies of TiO<sub>2</sub>, of which rutile is more stable thermodynamically.<sup>1-3</sup> The low solubility of TiO<sub>2</sub> contributes to its overall low bioavailability and titanium is often regarded as a biologically inactive and inert species.<sup>4</sup> Due to its minimal demonstrated risk, TiO<sub>2</sub> and titanium alloys are commonly used in cosmetics, paints, sunscreens, and in pharmaceuticals and medical devices, such as medical and dental implants.<sup>1</sup> Titanium alloy implants are passivated with a TiO<sub>2</sub> layer which increases biocompatibility, and they are regarded as an inert and biosafe. However, elevated Ti levels have been observed in the serum of patients with implants.<sup>5</sup> Dissolution of Ti, even without initial signs of wear, can lead to implant corrosion and Ti accumulation in the serum, urine, spleen and lungs.<sup>6,7</sup> Additionally, implant failure and diagnosis has been correlated with increased serum Ti levels.<sup>8,9</sup>

The biological significance of the Ti release and its means of transport is under current question. To afford solubility to the otherwise insoluble Ti(IV), complexation with a ligand is often necessary. Analysis of Ti serum saturation in patients with implants revealed the molecular weight of Ti bound serum proteins to be very similar to that of serum albumin and serum transferrin (Tf).<sup>10</sup> Tf has been shown to have the advantage in

direct binding to solubilized Ti(IV) over albumin.<sup>11</sup> Furthermore, Tf was identified to work in conjunction with citrate to bind Ti from direct implant-serum measurements, but had a less pronounced effect when looking at serum containing Tf alone.<sup>12</sup>

Human serum transferrin is a bilobal glycoprotein capable of binding two ferric ions in octahedral coordination into binding pockets of the protein. Tf acts as the transport protein responsible for Fe(III) solubility and exchange in human serum to later participate in iron metabolism. At only 30% saturation with Fe(III), Tf is widely believed to bind other metals.<sup>13–16</sup> Ti(IV) binding to Tf has been formally shown to bind even stronger than iron in solution.<sup>17</sup> Additionally, stabilization by Tf has been noticed in other hydrolysis prone forms of Ti(IV), such as with anticancer agent titanocene dichloride.<sup>18</sup> In this study, the dissolution directly from TiO<sub>2</sub> by Tf is of interest to explain the phenomenon of cellular Ti accumulation from commercialized sources. While previous research studied the stabilization of Ti ions in serum by Tf, the direct dissolution of TiO<sub>2</sub> to Tf has potential to reveal foundational information about the passivating inert coating on Ti implants and the distribution of Ti in human serum.

## **3.2 Experimental**

### **3.2.1 Materials**

All solutions were prepared with nanopure water of 18.2 M $\Omega$ ·cm resistivity from a Barnstead model D11931 water purifier. Glassware was acid-washed with trace metal grade HCl (Fisher). Titanium oxide (anatase and rutile) was purchased from Aldrich. Particle size was confirmed by dynamic light scattering (DLS) to be 342 and 615 nm for anatase and rutile respectively. Brunauer–Emmett–Teller (BET) analysis confirmed

particle surface areas to be 16.1 and 5.7 m<sup>2</sup> g<sup>-1</sup> for anatase and rutile respectively. Human serum apotransferrin was obtained from Athens Research and its purity was confirmed by SDS-PAGE and was verified as iron-free by UV/Vis at  $\lambda_{\text{max}}$  465 nm and a molar absorptivity constant of 2,500 M<sup>-1</sup> cm<sup>-1</sup>.<sup>18</sup> All other chemicals were used as received. Reagents were sourced from Acros Organics (nitrilotriacetic acid), Fisher Chemical (NaHCO<sub>3</sub>, FeCl<sub>3</sub>, and C<sub>13</sub>FeH<sub>12</sub>O<sub>6</sub>), J.T. Baker (NaH<sub>2</sub>PO<sub>4</sub>, and NaCl), and Sigma Aldrich (Ti (IV), 99.9%).

### 3.2.2 Methods

A physiological buffer of 4 mM NaH<sub>2</sub>PO<sub>4</sub>, 100 mM NaCl, 0.89 mM NaHCO<sub>3</sub> (pH=7.4) was prepared to use for all experiments. A Thermo Orion model 410 pH meter equipped with an Orion 8103BNUWP Ross Ultra semimicro pH electrode was used to measure buffer pH. An apotransferrin (Tf) stock solution of 35  $\mu$ M was prepared in buffer and its concentration was confirmed using UV/Vis with the transferrin extinction coefficient at  $\epsilon_{280} = 93,000 \text{ M}^{-1} \text{ cm}^{-1}$ .<sup>19</sup> Tf solutions was added to prepared vials of measured anatase (5 mg mL<sup>-1</sup>) or rutile (5 or 20 mg mL<sup>-1</sup>). Buffer was added to anatase or rutile samples in the absence of Tf as controls. All samples were kept in darkened incubator at 37°C, added to a motor-rotating wheel to be gently agitated. Aliquots of each sample were removed, and syringe filtered with 0.22  $\mu$ m PES filters. Polyethersulfone (PES) 0.22  $\mu$ m Luer-Lok filters were 13 mm in diameter and were purchased from Tisch Scientific. Experiments were performed in triplicate.

### 3.2.2.1 Inductively Coupled Plasma Optical Emission Spectroscopy (ICP-OES)

An iCAP 7000 Series ICP-OES Spectrometer was used to conduct all measurements. Aliquots of the filtered samples were diluted with ultrapure water to obtain the final sample. All samples were run without digestion of protein.<sup>18</sup> A standard curve was utilized without addition of acid to match the matrix of the samples. Standards were sourced from Fluka Chemical (Ti atomic absorption standard 1000 ppm) and Ricca Chemical (Fe atomic absorption standard 1000 ppm). Nitric acid used in stock atomic absorption standards to preserve standards is negligible post dilution. Standards were prepared and analyzed within 1 hour of preparation to allow for accuracy due to stability of standards. Reference power was set to 1150 W, auxiliary gas and nebulizer gas flow were both set to 0.5 L/min, with 50 rpm pump speed and functioned in axial mode. Detection wavelengths used to measure elemental emission included 336.1 nm for titanium and 259.9 nm for iron.

### 3.2.2.2 UV/Vis

Experiments were performed using a Varian Cary 50 Bio UV/Vis spectrophotometer. UV/Vis absorbance was measured from each sample, and Ti(IV) binding to Tf was monitored at 321 nm using  $\epsilon_{321} = 10,380 \text{ M}^{-1} \text{ cm}^{-1}$  for Ti-Tf binding.<sup>17</sup>

### 3.2.2.3 Fluorescence

Readings were obtained on 96 well plates using the SpectraMax Gemini EM Microplate Reader (Molecular Devices). Samples were excited at 280 nm and emission was recorded with a 1 nm step from 200 – 600 nm. Samples were analyzed in triplicate and trials averaged at  $\lambda_{\text{em, max}} = 322 \text{ nm}$ .

#### 3.2.2.4 Transmission Electron Microscopy (TEM)

Images were obtained using a JEOL JEM1400 microscope operating at 120 kV. Samples were deposited directly onto a carbon mesh grid (Ted Pella) and allowed to dry.

#### 3.2.2.5 Dynamic Light Scattering

A Zetasizer Nano ZS (Malvern) was used for dynamic light scattering (DLS) analyses. All samples were run at 25°C using 0.8954 viscosity and 1.330 refractive index for the physiological buffer dispersant. Individual samples were analyzed with an absorbance of 0.000 and individualized refractive indexes based on sample type (i.e. protein RI 1.450, anatase RI 2.561, rutile RI 2.616).<sup>3</sup>

#### 3.2.2.6 Fe(III) loading into transferrin

A 10 mM iron (III) nitrilotriacetic acid ( $\text{Fe}(\text{NTA})_2$ ) stock was prepared from Fe(III) chloride and two equiv of nitrilotriacetic acid in water. The concentration of iron was confirmed by ICP-OES. Transferrin samples were loaded with 2 equiv diluted from  $\text{Fe}(\text{NTA})_2$  stock, dialyzed in Amicon Ultra 4 centrifugal filters by ultracentrifugation with buffer additions to remove unbound excess  $\text{Fe}(\text{NTA})_2$ , and characterized by UV-Vis and ICP-OES to confirm Fe binding and molar ratios.

### 3.3 Results and Discussion

#### 3.3.1 UV/Vis, Fluorescence, and Inductively Coupled Plasma Optical Emission Spectroscopy (ICP-OES) Titanium Detection

Minimum dissolution of titanium ions was observed, as expected, in any of the controls of  $\text{TiO}_2$  particles in buffered solutions (Figure B.1). ICP-OES results of transferrin samples ranging from 5 – 20 mg mL<sup>-1</sup> of rutile displayed a dissolution increase in the

presence of Tf. Figure 3.1 A shows dissolution at 5 mg mL<sup>-1</sup> rutile at concentrations exceeding samples not treated with Tf protein additions as well as anatase – Tf additions within the same concentration range. Tf reactions with lower rutile loadings (5 mg mL<sup>-1</sup>) displayed Ti uptake levels up to 10 μM with trends in saturation at the 2 h mark (Figure 3.1 B). Dissolution increases with more concentrated TiO<sub>2</sub> additions, reaching upwards of 30 μM Ti in human serum transferrin solutions reacting with 20 mg mL<sup>-1</sup> TiO<sub>2</sub> (Figure 3.1 C). Varied timepoints track the dissolution process up to 168 h of incubation. Substrate saturation is seen rather quickly for all samples at two hours with particle scattering at later timepoints (Figure 3.1 B and D).

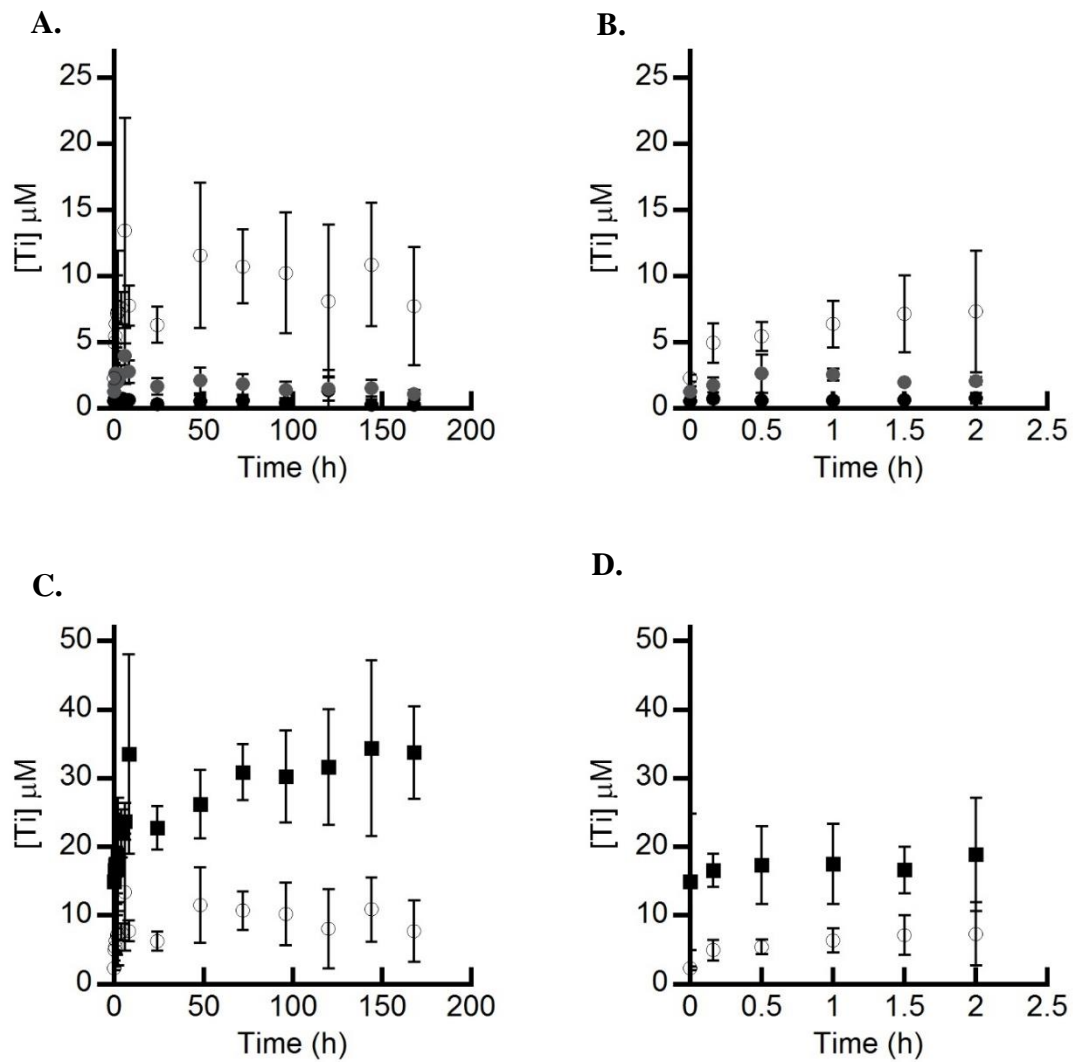


Figure 3.1: ICP-OES results of 35  $\mu\text{M}$  Tf with varied concentration  $\text{TiO}_2$  (A.) 168 h dissolution: apoTf (●), Tf + anatase 5  $\text{mg mL}^{-1}$  (●), Tf + rutile 5  $\text{mg mL}^{-1}$  (○); (B.) Dissolution over 2 h; (C.) Dissolution over 168 h: Tf + rutile 5  $\text{mg mL}^{-1}$  repeated (○), Tf + rutile 20  $\text{mg mL}^{-1}$  (■); (D.) Dissolution over 2 h.

Anatase at 5 mg mL<sup>-1</sup> was analyzed concurrently but was far less actively solubilized in solution with transferrin. Comparing the crystalline structure of anatase and rutile, the crystal packing of rutile makes it far more susceptible to ligand complexation and is naturally more abundant. This trend is apparent in analyzing the mineral loadings of anatase compared to rutile in Figure 3.2, in which rutile at 5 and 20 mg mL<sup>-1</sup> both see higher loadings to Tf compared to anatase. Interestingly, lower mineral exposure (5 mg mL<sup>-1</sup> rutile) saw slightly increased loadings to Tf compared to exposure to more bulk material.

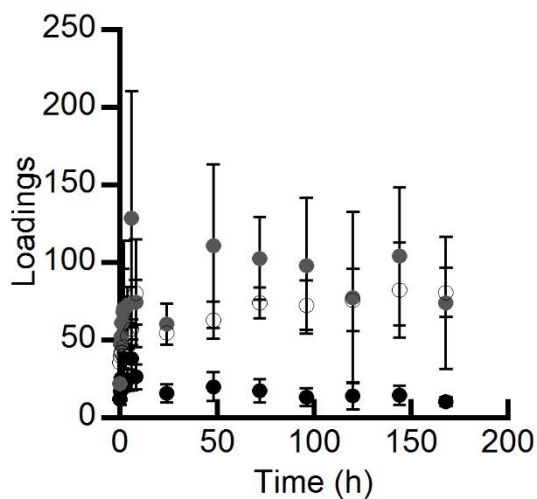


Figure 3.2: Mineral loadings of anatase 5 mg mL<sup>-1</sup> (●) rutile 5 mg mL<sup>-1</sup> (●) and rutile 20 mg mL<sup>-1</sup> (○) with Tf.

The resulting concentration of titanium as calculated by the LMCT at  $\lambda_{321 \text{ nm}}$  with an apparent molar absorptivity of  $10,380 \text{ M}^{-1} \text{ cm}^{-1}$  is detailed in Figure 3.3.<sup>17</sup> UV/Vis results do not point to full 2:1 binding in the traditional lobes as has been seen with other Ti forms.<sup>18</sup> UV/Vis characterization of these Ti-Tf complexes revealed minimal electronic transitions between  $\text{TiO}_2$  and the tyrosine residues in the Fe-binding pocket of transferrin that typically confirm metal binding in the lobes of Tf. Protein subtracted spectrum can be seen in Figure B.2. The high deviation in concentrations derived from ICP-OES and UV/Vis is telling of the reactivity of  $\text{TiO}_2$  with Tf and even pointing to possible surface interactions, which could hinder full 2:1 Ti(IV) binding in the Fe binding pocket of Tf. UV/Vis controls of particles in buffered solution in the absence of protein displayed minimal scattering (Figure B.3).

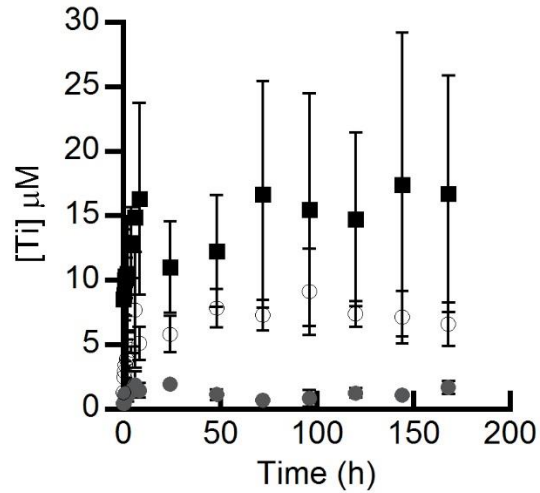


Figure 3.3: [Ti] as determined by LMCT UV/Vis absorbance using the molar absorptivity coefficient of  $10,380 \text{ M}^{-1} \text{ cm}^{-1}$  at 321 nm with  $35 \text{ } \mu\text{M}$  apoTf subtracted from UV/Vis absorbance. Tf + anatase  $5 \text{ mg mL}^{-1}$  (●), Tf + rutile  $5 \text{ mg mL}^{-1}$  (○), Tf + rutile  $20 \text{ mg mL}^{-1}$  (■).

For both anatase and rutile forms, the ICP-OES detection of Ti had high variability compared to UV/Vis. This could be due to the capability of the Tf surface to adhere Ti(IV) ions. It is important to note that ICP-OES detects not only soluble metal ions, but all metal in solution. The use of the term dissolution here is therefore loosely used to describe all functionally solubilized Ti(IV) ions and Ti particles adhered to the surface of Tf as detected by ICP-OES.

Conformational changes of the protein, corresponding to lobe closures upon metal binding at the Fe-binding sites of transferrin, can be monitored via fluorescence quenching of the tryptophan residues residing in the C-lobe of Tf. Fe(III) binding to Tf results in a 65% quenching of fluorescence.<sup>20</sup> For anatase 5 mg mL<sup>-1</sup>, rutile 5 mg mL<sup>-1</sup>, and rutile 20 mg mL<sup>-1</sup> fluorescence quenching was insignificant for all Ti loading variables. Ti(IV) interactions occurring within the binding pocket, observed in UV/Vis, either does not result in a protein conformational change upon binding or unobstructed the tryptophan residues within the lobe.

### 3.3.2 DLS and TEM

In addition to aqueous analysis, the TiO<sub>2</sub> particles were analyzed after reaction with Tf. Dynamic light scattering (DLS) tracked two different sized species over 0.5 h, 4 h, 8 h, and 168 h monitored timepoints within filtered samples. The small diameter of Tf protein (approximately 8 nm)<sup>21</sup> was detected in all treated samples and controls. A larger particle species developed a scattering intensity in the presence of anatase and rutile 5 – 20 mg mL<sup>-1</sup> (Figure 3.4). The size range of this secondary particle species is smaller than or near the size of the particle cutoff of the syringe filters used (at 0.22 μm). Controls of anatase and rutile suspended in water were used to confirm that original particle sizes were larger than the cutoff of the selected 0.22 μm filters (Figure B.4). Particle sizes larger than the filter in samples reacted with Tf could be the result of particle aggregation post filtration.

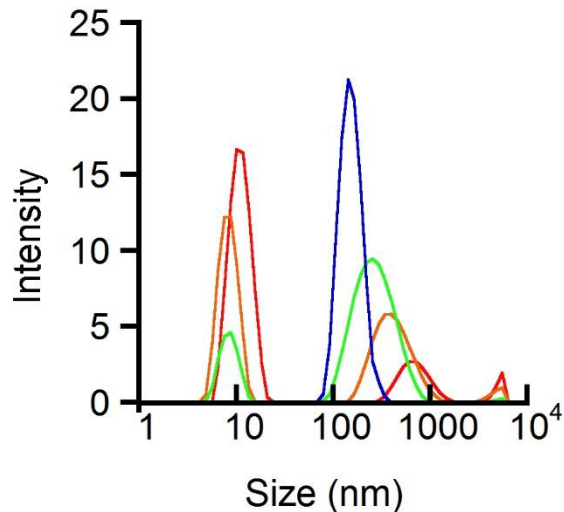


Figure 3.4: 8 h DLS spectra apoTf (—), Tf + anatase 5 mg mL<sup>-1</sup> (—), Tf + rutile 5 mg mL<sup>-1</sup> (—), Tf + rutile 20 mg mL<sup>-1</sup> (—).

Imaged timepoints of Tf with anatase and rutile from 0.5 h, 4 h, 8 h, and 168 h were obtained by transmission electron microscopy (TEM). The electronic character of the metal oxide was visualized, but inherent nature of TEM limits the visualization of the presence of the protein. Unfiltered Tf – rutile samples show a smoother particle surface in the presence of protein compared to unfiltered controls without protein (Figure 3.5). While rutile and anatase particles were confirmed by dynamic light scattering (DLS) to be homogeneous in size, it is plausible that particle aggregation occurred, or the smaller nanoparticles seen in TEM were masked in DLS by larger particle scattering. Particle surface smoothing observed in the presence of protein would speak of selective nanoparticle uptake by Tf. Additionally, nanoparticles were visualized in TEM images of

rutile at  $5 \text{ mg mL}^{-1}$  loading with Tf over all imaged timepoints filtered post reaction (Figure 3.6). These nanoparticles indicate the potential breaking down of larger particle species, which can be tracked over the Tf reaction time course. The presence of two species in DLS, that of Tf and of a larger particle, is consistent with what is seen and theorized in TEM imaging, that Tf surface adhesion to initial large  $\text{TiO}_2$  particles induces degradation. However, DLS data did not reveal a trend in particle size reduction as the time course continued for any of the Ti particle loadings or morphologies (Figure B.5). Aggregation of particles or the interaction with Tf could still be a factor while collecting DLS data which can be seen in TEM interpretations despite the appearance of smaller particles at increased timepoints.

When larger quantities of rutile were introduced,  $20 \text{ mg mL}^{-1}$ , crystalline features were observed in earlier timepoints in the TEM (Figure 3.7). The degradation of larger quantities of rutile particles occurs at a much slower rate as visualized through TEM, which is consistent with ICP-OES findings of mineral loading of Ti to Tf (Figure 3.2) which shows a lower bulk loading of material over time than rutile  $5 \text{ mg mL}^{-1}$ .

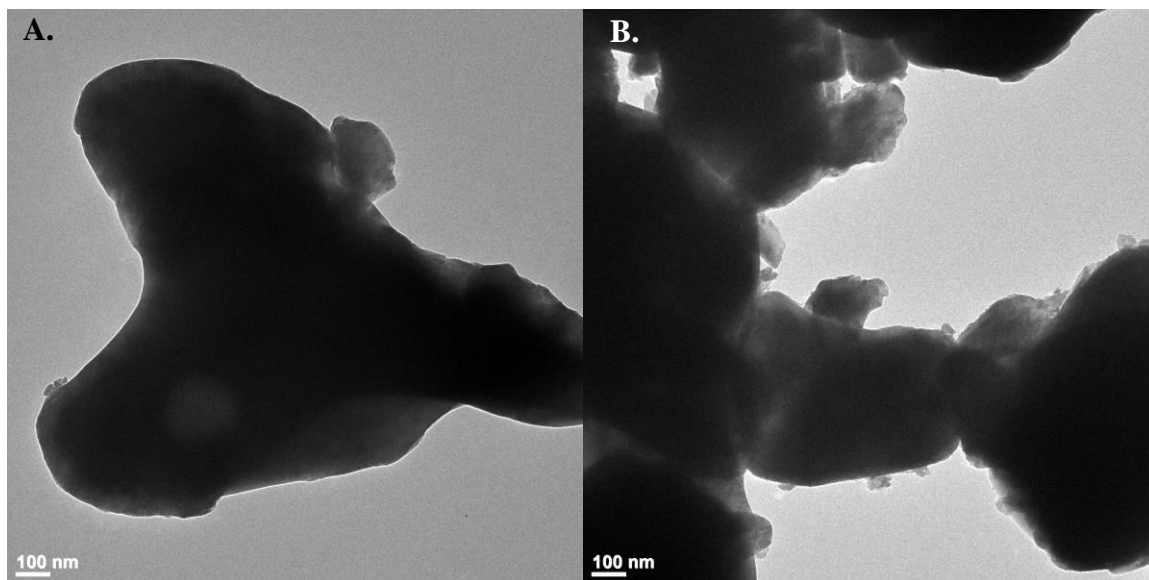


Figure 3.5: TEM images of (A.) Tf + rutile  $20 \text{ mg mL}^{-1}$  at 1 h; and (B.) rutile  $20 \text{ mg mL}^{-1}$  1 h unfiltered.

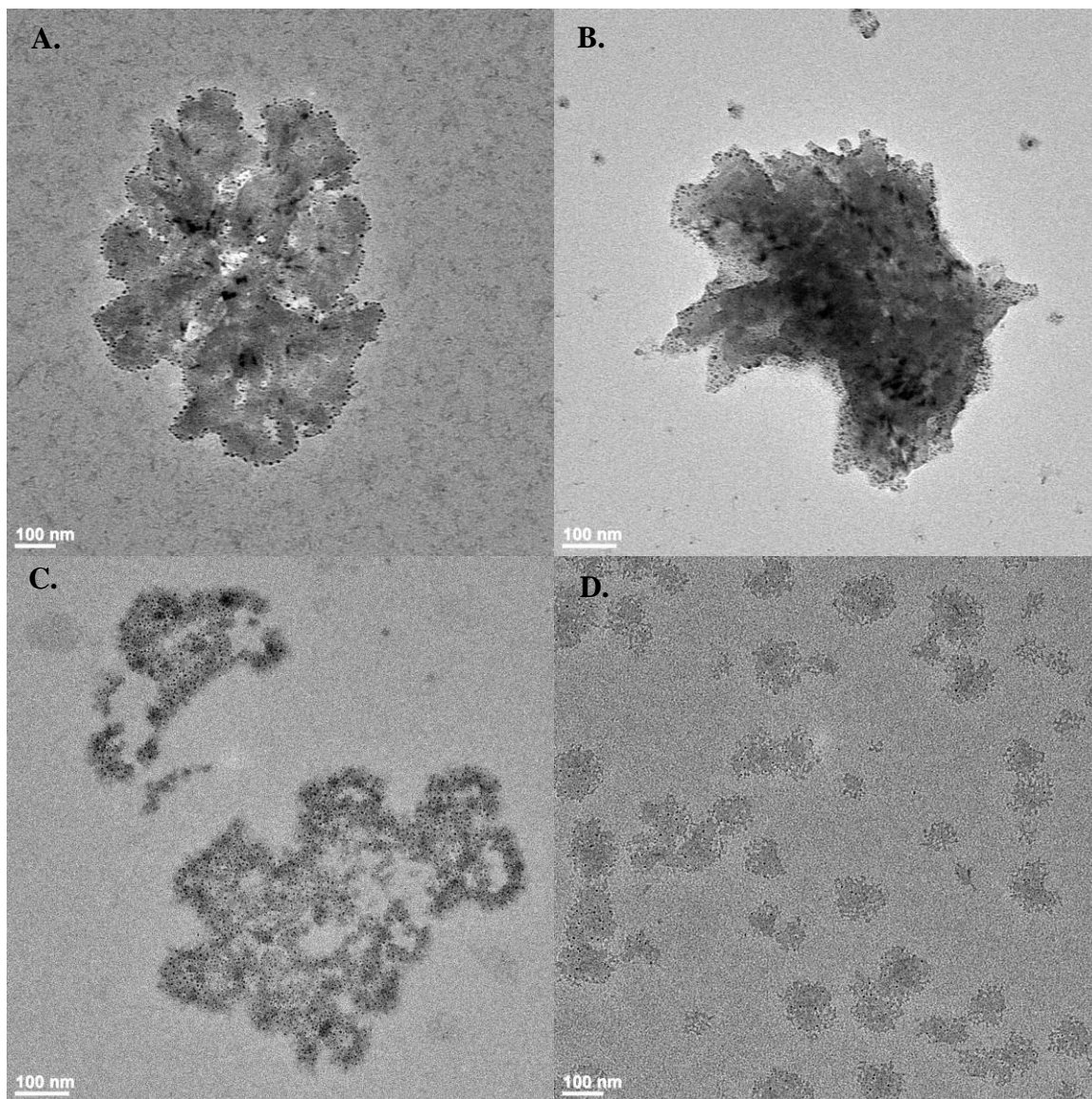


Figure 3.6: TEM images of Tf + rutile  $5 \text{ mg mL}^{-1}$  at (A.) 0.5 h; (B.) 4 h; (C.) 8 h; and (D.) 168 h.

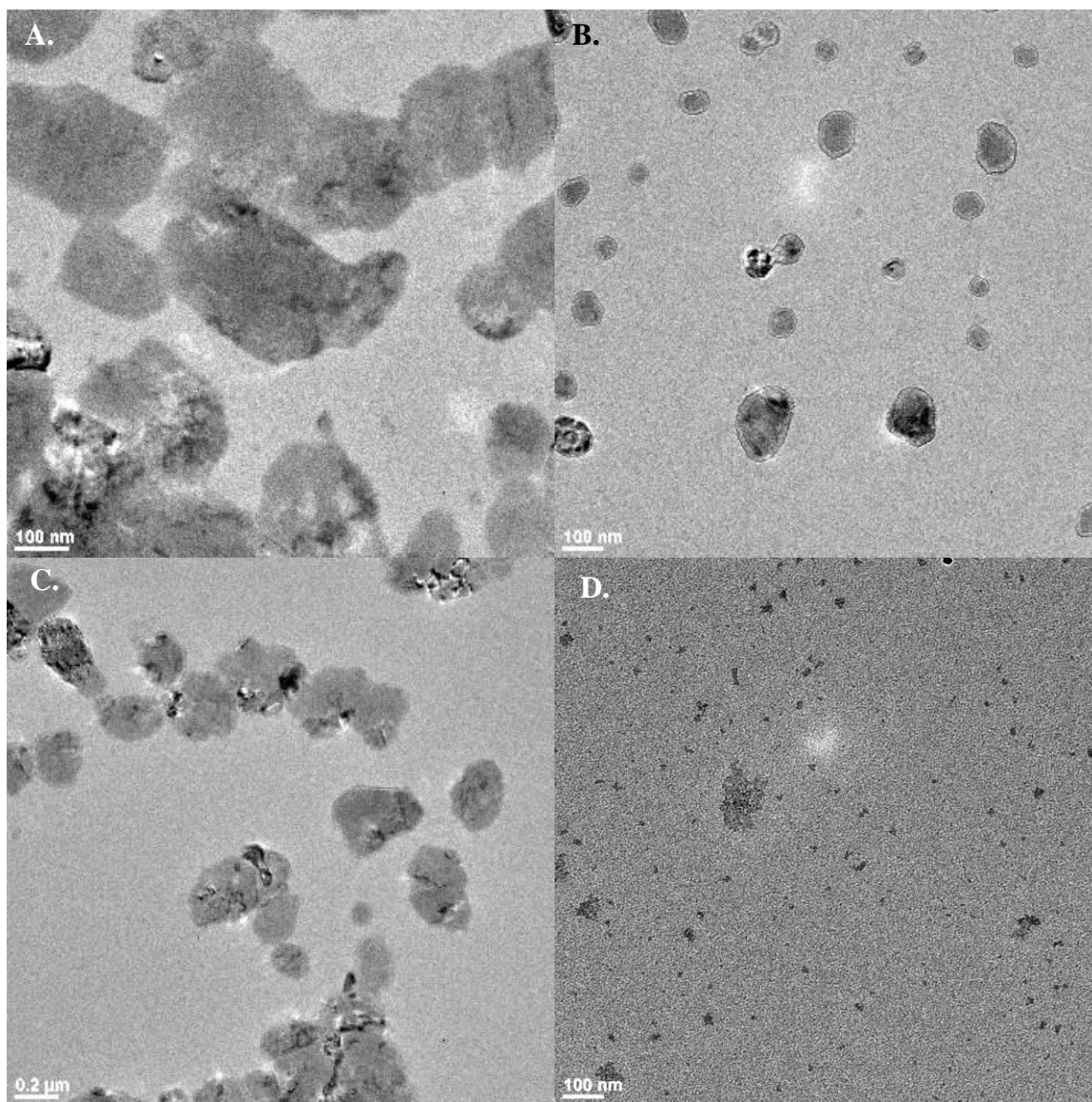


Figure 3.7: TEM images of Tf + rutile  $20 \text{ mg mL}^{-1}$  at (A.) 0.5 h; (B.) 4 h; (C.) 8 h; and (D.) 168 h.

Regardless of original mineral loadings, the changing morphology of rutile to smaller nanoparticles (NPs) in the presence of Tf in human serum could cause health implications that otherwise were overlooked due to the initial size of the manufactured particle. TiO<sub>2</sub> NPs pose their own health concerns and are still under review for their toxicological consequences in the human body. The engineering of NPs in human serum by Tf from TiO<sub>2</sub> sources increases potential risk of accumulation and organ lesions induced from NPs.<sup>22</sup>

### 3.3.3 Fe<sub>2</sub>Tf and Rutile Dissolution

Fe<sub>2</sub>Tf, used here to refer to dually loaded Fe(III) to Tf, is the intermediate Tf complex of Fe(III) regulation. A conformational change is initiated with the binding of Fe(III) in the Tf lobes, this closed conformation is important for receptor recognition and endocytosis. Dissolution studies with rutile and Fe<sub>2</sub>Tf were especially important in order to demonstrate possible surface binding effects on Fe<sub>2</sub>Tf. The effects on Fe(III) binding and the lobe conformation with the reaction with TiO<sub>2</sub> could disturb the metabolic functions of Tf if Ti binding is not site directed to the surface of Tf as suspected.

Interestingly, Fe<sub>2</sub>Tf displays similar dissolution of rutile at 5 mg mL<sup>-1</sup> at a similar rate and concentration as the same reaction with apo-Tf (Figure 3.8). ICP-OES and UV/Vis were used to monitor the concentration of Fe in Fe<sub>2</sub>Tf. ICP-OES maintained a 1.68 ± 0.13 Fe:Tf ratio (Figure B.6). The molar ratio as determined by UV/Vis is more telling of the inability to exchange Fe and Ti ions within the binding pocket of Tf, as was calculated by a LMCT at λ<sub>465 nm</sub> with ε = 2,500 M<sup>-1</sup>cm<sup>-1</sup> to be near full binding with a 1.95 ± 0.13 Fe:Tf ratio. Surface adhesion of TiO<sub>2</sub> particles does not disturb the electronic characteristics of Fe(III) binding within the Tf lobes. Absorbance of Fe-Tf binding at λ<sub>465 nm</sub> distorts measurement of Ti-Tf characteristic binding at λ<sub>321 nm</sub>.

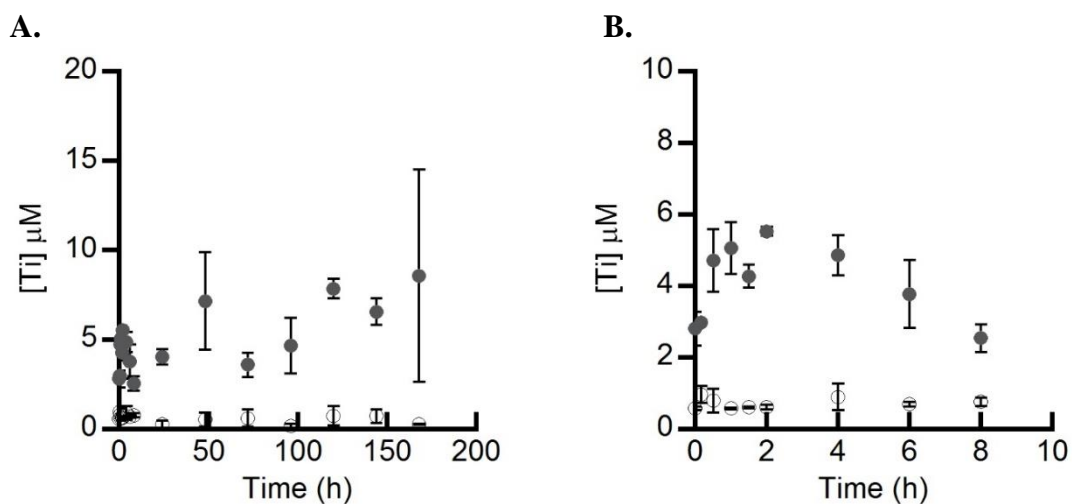


Figure 3.8: ICP-OES [Ti] results for 35 μM Fe<sub>2</sub>Tf + rutile 5 mg mL<sup>-1</sup> (●) and Fe<sub>2</sub>Tf (○) over (A.) 168 h and (B.) 8 h.

Rapid metal oxide surface adhesion of Tf is a distinct pathway of titanium transport through human serum. As results indicate an open lobe conformation of Tf after dissolution of titanium oxides and only partial Ti ion interaction in the binding pocket as calculated by LMCTs in UV/Vis, thus, Fe(III) could have accessibility to Tf binding lobes and subsequently to the Tf receptor to incite endocytosis.

### **3.4 Conclusions**

Uptake of titanium ions from titanium oxides by Tf in the traditional binding lobes was visualized through UV/Vis spectroscopy but does not give a complete understanding of the full reaction. The higher concentrations detected by ICP-OES points to an interaction of the protein with the metal oxide that is otherwise unseen spectroscopically. The open lobe conformation of the protein after reactions with TiO<sub>2</sub> are indicated by fluorescence results and could be suggestive of additional incorporation of Fe(III) within the binding lobes. TiO<sub>2</sub> reactions with Fe<sub>2</sub>Tf further support surface binding as a plausible means of Ti transport. While ICP-OES and UV/Vis data find saturation of Ti uptake, TEM results show changes to the particle over time at an equilibrium point of the particle-protein interaction. The selective uptake of particles as well as the changes to the particle size from adhering to Tf causes a wearing down of particle speciation over the course of 168 h. It is now not so much the uptake or dissolution of particles from oxide passivated implants, but the affected morphology of those particles in human serum that calls into question the inertness of TiO<sub>2</sub> in biological environments.

### 3.5 References

1. Buettner, K. M.; Valentine, A. M. Bioinorganic chemistry of titanium. *Chem. Rev.* **2012**, *112* (3), 1863–1881.
2. Bourikas, K.; Kordulis, C.; Lycourghiotis, A. Titanium dioxide (anatase and rutile): Surface chemistry, liquid–solid interface chemistry, and scientific synthesis of supported catalysts. *Chem. Rev.* **2014**, *114* (19), 9754–9823.
3. Diebold, U. The surface science of titanium dioxide. *Surf. Sci. Rep.* **2003**, *48*, 53–229.
4. Iavicoli, I.; Leso, V.; Bergamaschi, A. Toxicological Effects of Titanium Dioxide Nanoparticles: A Review of In Vivo Studies . *J. Nanomater.* **2012**, *2012*, 1–36.
5. Nuevo-Ordonez, Y.; Montes-Bayon, M.; Blanco-Gonzalez, E.; Paz-Aparicio, J.; Raimundez, J. D.; Tejerina, J. M.; Pena, M. A.; Sanz-Medel, A. Titanium release in serum of patients with different bone fixation implants and its interaction with serum biomolecules at physiological levels. *Anal. Bioanal. Chem.* **2011**, *401* (9), 2747–2754.
6. Sarmiento-González, A.; Encinar, J. R.; Marchante-Gayón, J. M.; Sanz-Medel, A. Titanium levels in the organs and blood of rats with a titanium implant, in the absence of wear, as determined by double-focusing ICP-MS. *Anal. Bioanal. Chem.* **2009**, *393* (1), 335–343.
7. Addison, O.; A.J., D.; R.J., N.; S., K.; M., M.; J.F.W., M.; D., P.; R.A., M. Do “passive” medical titanium surfaces deteriorate in service in the absence of wear? *J. R. Soc. Interface* **2012**, *9* (76), 3161–3164.
8. Jacobs, J. J.; Skipor, A. K.; Campbell, P. A.; Hallab, N. J.; Urban, R. M.; Amstutz, H. C. Can metal levels be used to monitor metal-on-metal hip arthroplasties? *J. Arthroplasty* **2004**, *19* (8 SUPPL.), 59–65.
9. Leopold, S. S.; Berger, R. A.; Patterson, L.; Skipor, A. K.; Urban, R. M.; Jacobs, J. J. Serum titanium level for diagnosis of a failed, metal-backed patellar component. *J. Arthroplasty* **2000**, *15* (7), 938–943.
10. Hallab, N. J.; Jacobs, J. J.; Skipor, A.; Black, J.; Mikecz, K.; Galante, J. O. Systemic metal-protein binding associated with total joint replacement arthroplasty. *J. Biomed. Mater. Res.* **2000**, *49* (3), 353–361.
11. Tinoco, A. D.; Eames, E. V; Valentine, A. M.; V, Y. U.; Box, P. O.; V, N. H. Reconsideration of serum Ti (IV) transport: Albumin and transferrin trafficking of

- Ti (IV) and its complexes. *J. Am. Chem. Soc.* **2008**, *130*, 2262–2270.
12. Curtin, J. P.; Wang, M.; Cheng, T.; Jin, L.; Sun, H. The role of citrate, lactate and transferrin in determining titanium release from surgical devices into human serum. *J. Biol. Inorg. Chem.* **2018**, *23* (3), 471–480.
  13. Sun, H.; Li, H.; Sadler, P. J. Transferrin as a metal ion mediator. *Chem. Rev.* **1999**, *99*, 2817–2842.
  14. Harris, W. R.; Chen, Y. Electron paramagnetic resonance and difference ultraviolet studies of Mn<sup>2+</sup> binding to serum transferrin. *J. Inorg. Biochem.* **1994**, *54*, 1–19.
  15. Kratzs, F.; Hartmann, M.; Keppler, B.; Messori, L. The binding properties of two antitumor ruthenium (III) complexes to apotransferrin. *J. Biol. Chem.* **1993**, *269* (4), 2581–2588.
  16. Hirose, J.; Fujiwara, H.; Magarifuchi, T.; Iguti, Y.; Iwamoto, H.; Kominami, S.; Hiromi, K. Copper binding selectivity of N- and C-sites in serum (human)- and ovo-transferrin. *Biochem. Biophys. Acta* **1996**, *1296*, 103–111.
  17. Tinoco, A. D.; Valentine, A. M. Ti (IV) binds to human serum transferrin more tightly than does Fe (III). *J. Am. Chem. Soc.* **2005**, *127*, 11218–11219.
  18. Guo, M.; Sun, H.; Mcardle, H. J.; Gambling, L.; Sadler, P. J. Ti IV uptake and release by human serum transferrin and recognition of Ti IV -transferrin by cancer cells: Understanding the mechanism of action of the drug titanocene dichloride. *Biochemistry* **2000**, *39*, 10023–10033.
  19. Chasteen, N. D. Human serotransferrin: Structure and function. *Coord. Chem. Rev.* **1977**, *22*, 1–36.
  20. He, Q.; Mason, A. B.; Lyons, B. A.; Tam, B. M.; Nguyen, V.; Macgillivray, R. T. A.; Woodworth, R. C. Spectral and metal-binding properties of three single-point tryptophan mutants of the human transferrin N-lobe. *Biochem. J.* **2001**, *354*, 423–429.
  21. Kilár, F.; Simon, I. The effect of iron binding on the conformation of transferrin. A small angle x-ray scattering study. *Biophys. J.* **1985**, *48* (5), 799–802.
  22. Shi, H.; Magaye, R.; Castranova, V.; Zhao, J. Titanium dioxide nanoparticles: a review of current toxicological data. *Part. Fibre Toxicol.* **2013**, *10* (15), 1–33.

## CHAPTER 4

### DEGLYCOSYLATION OF HUMAN SERUM TRANSFERRIN AFFECTS TITANOCENE DICHLORIDE AND TITANIUM OXIDE INTERACTION AT THE SURFACE OF THE PROTEIN

#### 4.1 Introduction

Sugars are a very diverse, complex, and abundant class of biomolecules that are essential in cellular adhesion, cellular migration, progression of diseases, and a variety of other biological functions.<sup>1,2</sup> However, much has been left unexplored in the field of glycobiology, mostly due to the diversity of biomolecules. An emerging study of metal-oligosaccharide coordination and effects, termed metalloglycomics, looks at the sialic acid carbohydrate family and the bio-metallic interactions that could occur.<sup>3</sup>

Transferrin is a glycoprotein whose main role is ligation and transport of essential iron to cells. The role of glycan chains on the C-terminal lobe of transferrin has been of interest for some time. The two glycan chains of transferrin are N-linked to Asn-413 and Asn-610 residues very near to the Fe(III) binding pocket on that same lobe (Figure 4.1).<sup>4</sup> The oligosaccharides of transferrin are typically identified as sialylated biantennary structures.<sup>5</sup> Deglycosylation of Tf (deTf) does not hinder receptor binding and endocytosis of Fe(III) bound Tf into the cell.<sup>6</sup> While the deglycosylated protein has been studied for interactions with Fe(III) in terms of its involvement in Fe(III) binding and receptor binding, deTf studies have not included interactions with other metal complexes.<sup>6-8</sup>

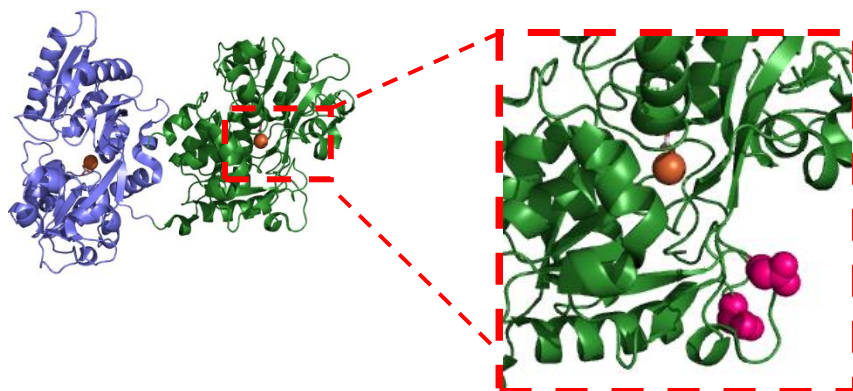


Figure 4.1: Crystal structure of diferric human serum transferrin (3V83).<sup>9</sup> N-lobe is shown in blue, C-lobe in green. Inset depicts two asparagine residues, Asn 413 and Asn 610, on the C-lobe of transferrin, the site for N-linked glycosylation. Asn 413 and Asn 610 shown here as pink spheres. All figures were made using Pymol

Titanocene dichloride (TDC) is Ti(IV) anticancer compound well-studied for its interactions with Tf as a possible means of cellular import. TDC faltered in phase II of clinical trials, but still remains a valuable model for drug interactions with transport proteins and the study of Ti(IV) cellular accumulation.<sup>10</sup> Previous research found a unique superstoichiometric binding motif with TDC bound in excess to transferrin with possible surface interactions.<sup>11</sup> Modifying the glycation sites on transferrin is an easy tool to determine site specific binding on the transport protein. Glycan chains have recently been noted for their ability to bind metal-ammine coordination complexes, such as Pt anticancer agents, which could change the cytotoxic effects of these compounds due to these glycan interactions.<sup>12-14</sup>

Titanium oxide is abundant in nature, but hardly bioavailable due to its limited solubility. Because of this, it is often believed that TiO<sub>2</sub> is an inert compound and is often featured in many manufactured products and medical devices.<sup>15,16</sup> However, the accumulation of TiO<sub>2</sub> in patients with titanium implants as well as the findings on toxicity of TiO<sub>2</sub> nanoparticles, is a cause for concern for titanium oxide in consumer products.<sup>17,18</sup> A possible route for cellular uptake, similarly to TDC, is through transferrin binding and endocytosis. A previous study has found from rutile and anatase TiO<sub>2</sub> particles, that a selective interaction is seen for smaller sized particles and the exposure to Tf of the surface of the oxide particle can cause the decrease in particle size over the course of a 168 h study.<sup>19</sup> Glycan chains on transferrin could possibly be responsible for this outcome. Interactions between glycans and TiO<sub>2</sub> nanoparticles, especially with sialic acid containing glycans like those in transferrin, have already been explored. Chromatography techniques have been established by utilizing the affinity of sialic acids for TiO<sub>2</sub> to identify glycosylation sites on glycoproteins and peptides.<sup>20,21</sup>

By removing the glycan chains from Tf and reacting the deglycosylated transferrin (deTf) with both TDC and TiO<sub>2</sub>, we will be able to elicit further information about the binding phenomenon seen in both Ti complexes. Additionally, understanding the role of glycan chains in the cellular metal circulation will be very crucial, not just in terms of transferrin, but for metal distribution by this large class of sugars in general.

## 4.2 Experimental

### 4.2.1 Materials

All solutions were prepared with nanopure water of 18.2 M $\Omega$ ·cm resistivity from a Barnstead model D11931 water purifier. All glassware was acid-washed using trace metal grade HCl (Fisher). Polyethersulfone (PES) 0.22  $\mu$ m Luer-Lok filters were 13 mm in diameter and were purchased from Tisch Scientific. Reagents were sourced from Acros Organics (nitrilotriacetic acid), Fisher Chemical (NaHCO<sub>3</sub>, FeCl<sub>3</sub>, and C<sub>13</sub>FeH<sub>12</sub>O<sub>6</sub>), J.T. Baker (NaH<sub>2</sub>PO<sub>4</sub> and NaCl), Fluka Chemical (Ti atomic absorption standard 1000 ppm) and Ricca Chemical (Fe atomic absorption standard 1000 ppm). PNGase F enzyme (P0704S) was used as received from New England Biolabs. Titanocene dichloride (TDC) was purchased from Acros Organics (97%) and prepared fresh in 1/9 v/v DMSO: 0.1 M saline solution at 4°C. The TDC solution was syringe filtered and ICP-OES was used to confirm the concentration. Human serum apotransferrin (apoTf) was obtained from Athens Research and its purity was checked by SDS-PAGE and was verified as iron-free by UV/Vis ( $\lambda_{\text{max}} = 465 \text{ nm}$ ;  $\epsilon_{465 \text{ nm}} = 2,500 \text{ M}^{-1} \text{ cm}^{-1}$ )<sup>10</sup>. All other chemicals were used as received.

### 4.2.2 Methods

A physiological buffer of 4 mM NaH<sub>2</sub>PO<sub>4</sub>, 100 mM NaCl, 0.89 mM NaHCO<sub>3</sub> (pH=7.4<sup>10</sup> and pH=8.3) was prepared to use for all UV/Vis and ICP experiments. A Thermo Orion model 410 pH meter equipped with an Orion 8103BNUWP Ross Ultra semi-micron pH electrode was used to measure and monitor pH. Deglycosylation procedures from New England Biolabs were carried out accordingly with slight modifications. An apotransferrin

(Tf) stock solution at 125  $\mu\text{M}$  was prepared in pH 8.3 buffer and its concentration was confirmed using UV/Vis with a transferrin extinction coefficient of  $\epsilon_{280} = 93,000 \text{ M}^{-1} \text{ cm}^{-1}$ .<sup>22</sup> A higher pH was more compatible with enzymatic processes. PNGase F enzyme (10  $\mu\text{L}$ ) was added to apoTf and incubated for 48 h at 37°C. Following incubation, an aliquot of the mixture was analyzed by 10% SDS-PAGE gel and by MALDI-MS (dialyzed into 10 mM  $\text{NH}_4\text{HCO}_3$ ) to determine whether reaction was complete. The reaction mixture was used as is to complete experimental analysis. Titanocene dichloride additions to deTf samples allowed for a final deTf concentration of 20  $\mu\text{M}$  (diluted from stock Tf with pH 7.4 buffer) with 4 and 10 equiv of TDC. All samples were kept in the dark and added to a motor-rotating wheel and allowed to rotate gently. One milliliter aliquots of each sample were removed at specified time intervals, and syringe filtered with 0.22  $\mu\text{m}$  PES filters.

#### 4.2.2.1 Timepoints

Experimental data are averaged from collected timepoints at 8 and 24 h for all rutile 20 mg  $\text{mL}^{-1}$  experiments. Protein samples treated with TDC were incubated at room temperature for 24 h prior to filtration. Experiments were performed in triplicate and averaged among trials.

#### 4.2.2.2 UV/Vis, Inductively Coupled Plasma Optical Emission Spectroscopy (ICP-OES), Fe(III) Loading into Transferrin, Fluorescence, Urea-PAGE Gels Analysis of TDC Lobe Binding, and Kinetic Studies of Ti(IV) Removal with Additions of Fe(III) to deTf Solution

All protein sample preparation, treatment and analysis is equivalent to description in Chapter II with the exception of using transferrin protein samples pretreated with PNGase F for deglycosylation.

### 4.3 Results and Discussion

#### 4.3.1 Deglycosylated transferrin

The easiest method for cleaving the N-linked oligosaccharides on Tf is by enzymatic digestion with Peptide-*N*- Glycosidase F (PNGase F). Following the incubation period with the enzyme, the protein was analyzed by 10% SDS PAGE gels to determine a shift to lower molecular weight. Figure C.1 shows a representation of the molecular weight shift in this characterization.

MALDI-MS was further utilized to characterize the shift in molecular weight as a determinant of successful deglycosylation. A decrease in molecular weight from 78.8 kDa (wild type transferrin) to 76.9 kDa after PNGase F treatment (Figure C.2 – 4) was seen in deglycosylation results. When comparing this to ES-MS results of the removal of sialylated oligosaccharides on transferrin from 79.5 kDa deglycosylated to 75.1 kDa,<sup>5</sup> most likely we have achieved a partial deglycosylation of transferrin with only a 2.4% decrease in molecular weight from the glycan chains compared to a typical 5% mass decrease. Partial deglycosylation may have been due to experimental constraints that required the

deglycosylation procedure to be scaled up. However, we are analyzing the overall change in binding effects from the fully glycosylated to deglycosylated transferrin, in which even partial deglycosylated transferrin would represent this change.

#### 4.3.2 deTf Interactions with TDC

The superstoichiometric trend that was seen in surface glycosylated transferrin was originally postulated to be due to the binding effects of the glycan chains with the hydrolysis prone titanocene dichloride (TDC). However, in the surface modified protein, we see very similar superstoichiometric trends as what was previously noted in wild type transferrin. Absorbances in the UV/Vis correlated to a 2:1 TDC to deTf binding ratio using the molar absorptivity of the tyrosine residues in the binding lobes of transferrin. As predicted, truncation of the glycan chains offers no interference with the TDC binding into the lobes of transferrin (Figure 4.2). Spectroscopic analysis alone offers a parallel comparison to Fe(III) binding in the traditional lobes; however, inductively coupled plasma optical emission spectroscopy (ICP-OES) tells of all metal in solution, and can be very telling of extraneous interactions, especially for hydrolysis prone TDC.

In the case of TDC with deTf, the concentration of Ti metal in solution determined by ICP-OES was nearly equivalent to the dosed concentration of TDC. This is very telling of the minimal role that glycan chains play on the surface of transferrin in the superstoichiometric binding phenomenon previously seen. Comparison of the deglycosylated and wild type transferrin can be seen in Figure 4.3. The interaction of TDC with transferrin in superfluous amounts therefore are either site directed at another surface location on transferrin or are accumulated and possibly hydrolyzed within the binding pocket of

transferrin, exceeding the documented 2:1 metal to protein ratio. Either case is probable given that excess TDC would be silent in the UV/Vis outside of the binding pockets.

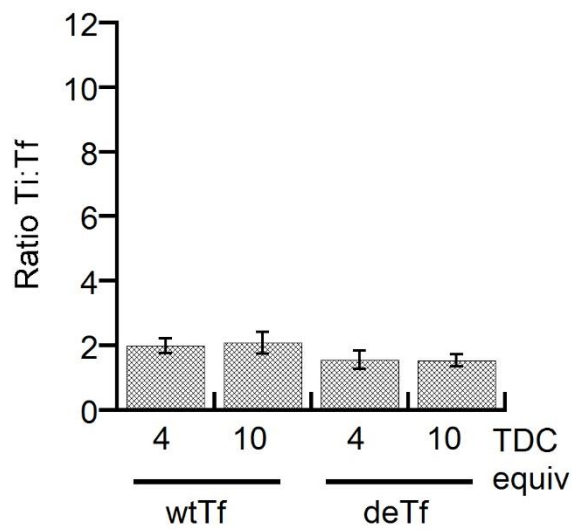


Figure 4.2: UV/Vis results of Ti to Tf ratio from LMCT at 321 nm using  $10,380 \text{ M}^{-1}\text{cm}^{-1}$  molar absorption coefficient and  $20 \mu\text{M}$  Tf for wild type transferrin and deTf with treatment of 4 and 10 equiv TDC.

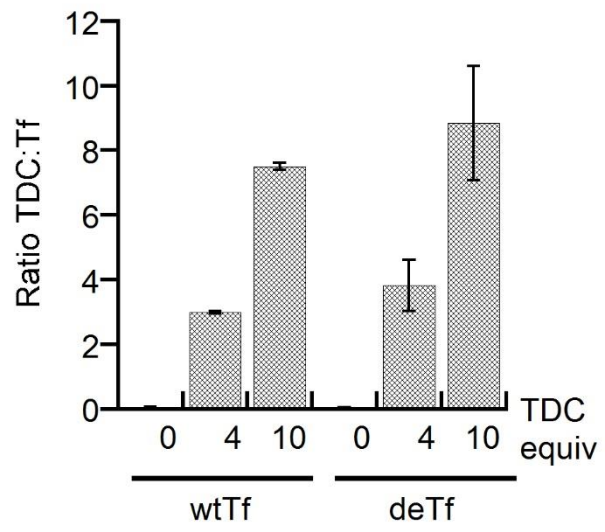


Figure 4.3: ICP-OES results of TDC in solution with Tf and deTf after 24 h incubation periods.

In order to understand more about the glycation binding effects on TDC, kinetic exchange experiments with Fe(III) were compared to wild type protein. The exchange of TDC for Fe(III) within the binding lobes of deTf involves a decrease in absorbance at 321 nm (corresponding to a LMCT for tyrosine to Ti(IV)) and a corresponding increase in absorbance at 465 nm (corresponding to tyrosine – Fe(III)’s LMCT). Figure C.5 details the exchange of 4 equiv TDC with 10 equiv Fe(III) on deTf. The appearance of the Fe<sub>2</sub>Tf species is defined around 50 min of equilibration. Comparison of rate constants between deTf and Tf are detailed in Table 4.1. While 10 equiv TDC reactions were along the same order, 4 equiv TDC were noticeably slower, speaking towards the possibility of a tighter and more site directed binding in the binding lobe of deTf. It is speculated that lower equivalents of TDC allow for more traditional, tighter binding in the lobe, compared to what may be metal hydrolysis in the pocket with higher equivalents.

	k1 (min <sup>-1</sup> )
Tf + TDC 4 equiv	0.029 ± 0.006
Tf + TDC 10 equiv	0.024 ± 0.004
deTf + TDC 4 equiv	0.042 ± 0.002
deTf + TDC 10 equiv	0.029 ± 0.004

Table 4.1: Rate constants of kinetic exchange reaction of Tf + TDC varied equiv with 10 equiv of Fe(NTA)<sub>2</sub>.

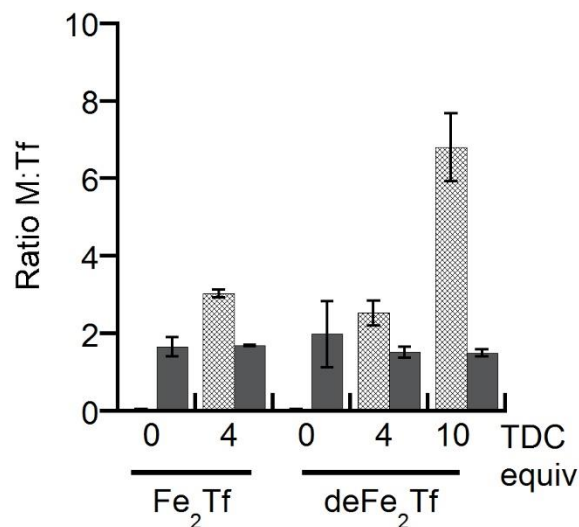


Figure 4.4: ICP-OES results from Fe<sub>2</sub>Tf of 0 and 4 equiv TDC and deFe<sub>2</sub>Tf binding of 0, 4, and 10 equiv binding. Striped: Ratio Ti:Tf; Solid: Ratio Fe:Tf.

The reverse analysis was also conducted in analyzing TDC surface interactions on a closed lobe deglycosylated Fe<sub>2</sub>Tf species. By titrating TDC in deTf post equilibration of Fe, the effect of glycan chains can be visualized more clearly. By eliminating access to the binding pocket with Fe(III) additions and by modifying the surface of the protein by enzymatically removing the glycan chains, the surface binding of TDC to Tf is evident. Figure 4.4 shows that there is still clear binding of TDC to an unseen interaction on the deTf surface. This evidence enhances the theory of surface bound transport of TDC by Fe<sub>2</sub>Tf for the future use of Ti anticancer drugs and for understanding of Ti(IV) transport.

#### 4.3.3 deTf Interaction with Titanium Oxide Surfaces

The ligand to metal charge transfer of Ti from TiO<sub>2</sub> in the binding lobe of Tf never fully reached a 2:1 binding ratio, even with unmodified protein (Chapter 3). Enzymatically

deglycosylated deTf still follows this trend in the UV/Vis absorbance results, where the LMCT of Ti-tyrosine (seen in Figure 4.5) reaches less than one eighth saturation of deTf within the binding lobes. Full potential binding in the traditional lobes of transferrin was not fully understood in wild type TiO<sub>2</sub> experiments, and the decreased lobe binding in deglycosylated transferrin tracks with the newly gained information from ICP-OES. A significant decrease in Ti concentration as determined by ICP-OES over 8 and 24 h incubation period of deTf with 20 mg mL<sup>-1</sup> rutile is noticeable from wild type transferrin results (Figure 4.6). There was a 96% decrease in functionally soluble TiO<sub>2</sub> at 24 h by deTf, a result that speaks on the significant role of glycan chains in TiO<sub>2</sub> interactions. Minimal soluble Ti can be detected in controls of anatase and rutile in filtered buffer solutions in the absence of protein (Figure B.1).

Another interesting comparison has been with analysis of transmission electron microscopy (TEM) imaging. Filtered samples of Tf reacted with 20 mg mL<sup>-1</sup> additions of rutile at earlier timepoints in TEM images showed crystalline features, evident of larger TiO<sub>2</sub> particles capable of passing through the filter. Over time these crystals were broken down into smaller particles by later timepoints (Chapter 3). Additionally, it was postulated that nanoparticulate interactions were prevalent and then led to the degradation of micron-sized particles. However, in the filtered deglycosylated Tf case, 8 h TEM time points of exposure of 20 mg mL<sup>-1</sup> rutile did not feature crystalline features, but only displayed dispersed nanoparticles (Figure 4.7). Without the glycan chains on Tf, minimal interaction between the TiO<sub>2</sub> particle and Tf seems to occur. Coupled with the lower solution concentrations in ICP-OES, it is logical that only the few nanoparticles in the micron-

characterized commercialized rutile had an interaction with deTf. It is undetermined if this interaction is site-directed to the binding lobes of transferrin, as it is near the natural solubility of titanium oxides or a factor of the relative sizes of the particle and lobe opening. Regardless, a fraction of Ti in solution is accounted for by the UV/Vis LMCT for binding lobe interactions.

Further evidence of the role of glycan chains is noticeable in the interaction of TiO<sub>2</sub> with deglycosylated Fe<sub>2</sub>Tf. With the preloaded Fe<sub>2</sub>Tf lobes already undergoing a conformational change and the modified deglycosylated surface, ICP-OES results show that about half of the TiO<sub>2</sub> is detectable in solution compared to deTf without Fe(III) (Figure 4.6). This is near control levels of how much Ti is naturally solubilized in buffered solutions at this pH. The result is very telling of the primary role of the glycan chains in the functional solubility of Ti, where the secondary interaction would be in the binding lobe.

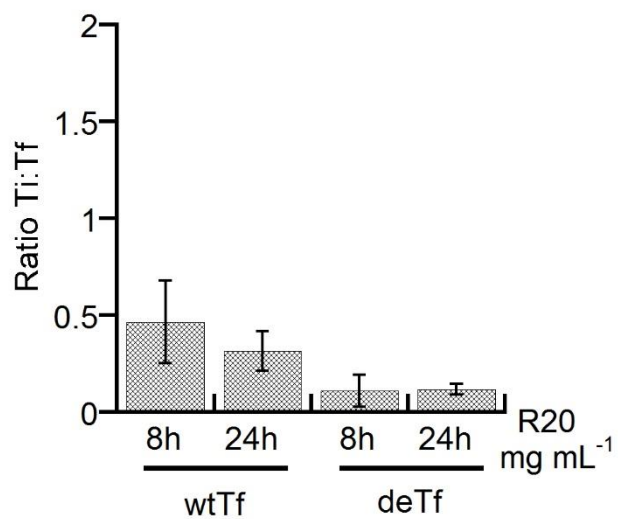


Figure 4.5: UV/Vis results of Ti to Tf ratio from LMCT at 321 nm using  $10,380 \text{ M}^{-1}\text{cm}^{-1}$  molar absorption coefficient and  $20 \text{ }\mu\text{M}$  Tf for wild type transferrin and deTf after treatment with  $20 \text{ mg mL}^{-1}$  rutile at 8 h and 24 h incubation.

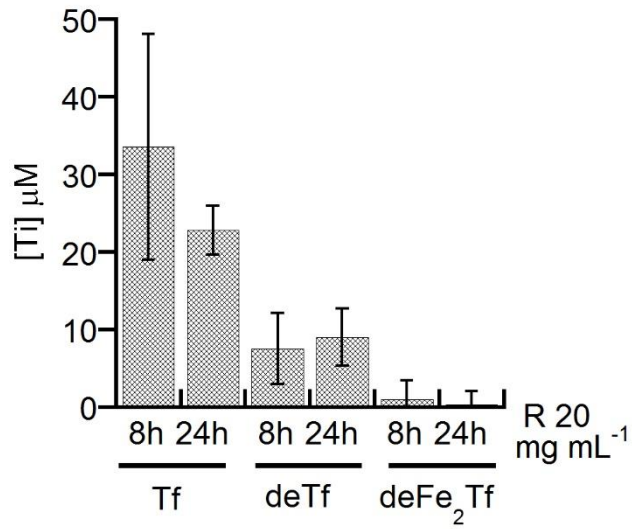


Figure 4.6: ICP-OES results for 20  $\mu\text{M}$  Tf, deTf, and deFe<sub>2</sub>Tf with 20  $\text{mg mL}^{-1}$  rutile at 8 h and 24 h.

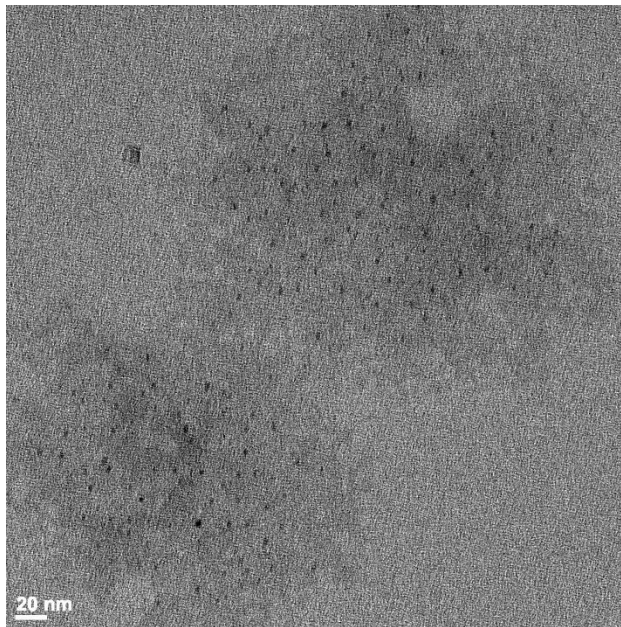


Figure 4.7: TEM of disperse nanoparticles in a sample of deTf with 20  $\text{mg mL}^{-1}$  rutile at 8 h.

#### 4.3.4 Ti(IV) Complexes Effects on deTf Lobe Closures

##### 4.3.4.1 Fluorescence

Fluorescence of the tryptophan residues near the metal-binding pocket of Tf can help detail the conformational position of the protein before and after Ti(IV) complex introduction. Relative fluorescence of deglycosylated Tf compared to apoTf in Figure 4.8 shows minimal fluorescence quenching, telling of the fluorescent influence of the glycan chains in this method. Deglycosylated Fe<sub>2</sub>Tf behaved similarly to fluorescence quenching studies of glycosylated Fe<sub>2</sub>Tf from literature. Analysis of TDC 4 equiv and 10 equiv loaded deTf, on average, had slightly higher fluorescence compared to trials with glycosylated Tf. Yet, both deglycosylated and glycosylated TDC-Tf samples typically had higher standard deviation in fluorescence quenching studies, due to what we believe is varied tryptophan residue exposure from hydrolysis of TDC within the binding lobe, making it difficult to draw a conclusion based on glycosylation alone.

Fluorescence studies were remarkably similar in the glycosylated and deglycosylated states for samples with TiO<sub>2</sub> additions. TiO<sub>2</sub>, while seen in UV/Vis studies to be partially lobe directed, is not affecting tryptophan fluorescence, which is often interpreted as sign of a conformational change of the protein. When looking at Fe<sub>2</sub>Tf with either Ti(IV) complex, TDC or TiO<sub>2</sub>, Fe(III) site directed bilobal binding and assumed conformational change is prevalent over the presence of titanium. The prevalent Fe<sub>2</sub>Tf form causes fluorescence quenching consistent in the wildtype Tf form of tryptophan saturated protein.

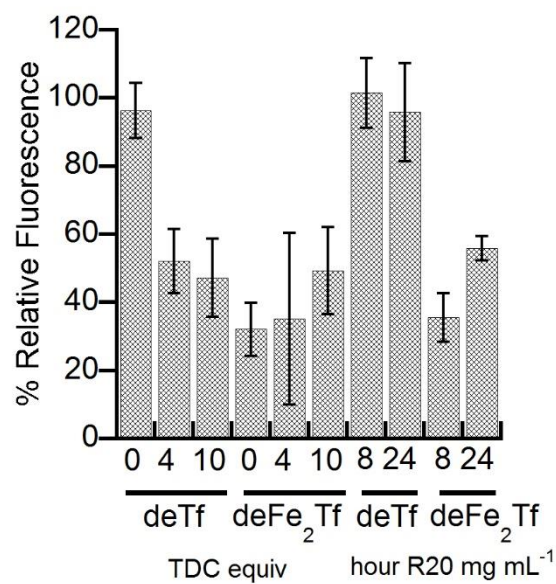


Figure 4.8: Fluorescence relative to apoTf of deTf and deFe<sub>2</sub>Tf treated with 0, 4, and 10 equiv of TDC or 20 mg mL<sup>-1</sup> rutile after 8 h and 24 h.

#### 4.3.4.2 Urea-PAGE Gel Analysis of TDC Lobe Binding

Previous studies have shown that a conformational change can be characterized with fluorescence quenching, but a decrease in fluorescence is not necessarily a sure sign of a conformational change. Urea-PAGE gels have been utilized by Makey and Seal to determine a closed conformation of transferrin when bound to a metal ion migrates farther down the gel due to less exposure to the denaturing urea.<sup>23</sup> Small angle X-ray scattering (SAXS) techniques previously has shown consistent results with Urea-PAGE gels to determine transferrin conformation in solution and the accuracy of denaturing gels compared to fluorescence quenching studies. Figure 4.9 shows the early denaturing effects in the Urea-PAGE gel on deTf samples containing varied equivalents of TDC and with rutilite 20 mg mL<sup>-1</sup> at 8 and 24 h timepoints. Glycosylation has no effect on lobe closure of Fe<sub>2</sub>Tf samples, even with incorporation of Ti(IV) complexes. This is a consistent result with the work of Mason et al. who noted that surface glycation of transferrin is not necessary for receptor recognition, only the conformational lobe closure which would in turn initiate endocytosis.<sup>6,8,24</sup>

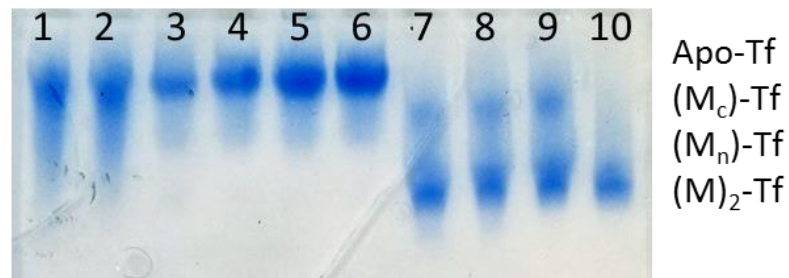


Figure 4.9: (1) deTf + TDC 10 equiv; (2) deTf + TDC 4 equiv; (3) apoTf; (4) deTf; (5) deTf + R 20 mg mL<sup>-1</sup> 8 h; (6) deTf; (5) deTf + R 20 mg mL<sup>-1</sup> 24 h; (7) deFe<sub>2</sub>Tf + TDC 4 equiv; (8) deFe<sub>2</sub>Tf + TDC 10 equiv; (9) deFe<sub>2</sub>Tf; (10) Fe<sub>2</sub>Tf.

#### 4.4 Conclusion

The removal of glycan chain residues on the surface of transferrin plays a variable role for its interaction with different Ti(IV) complexes. The distribution of TiO<sub>2</sub> particles is greatly affected by the presence of glycosylated transferrin surfaces, with a primary binding being on glycan chains. Secondary binding in the traditional binding pockets is completely inhibited when TiO<sub>2</sub> is incubated with Fe<sub>2</sub>Tf, due to a conformational change of the modified protein. As glycosylation plays a major role in the functions of proteins, interaction of TiO<sub>2</sub> in human serum seems unavoidable.

On the other hand, glycation played no major role in TDC binding, in either the Fe(III) inhibited lobes or on the surface of the protein. It seems clear that even if there is hydrolysis of TDC within the binding lobe of Tf, that there is still a mechanism of surface adhesion regardless of the presence of glycans. This study reaffirms our hypothesis of receptor recognition of surface bound Ti(IV) to Fe<sub>2</sub>Tf as a possible means of transport and Ti metal accumulation in cells. The shuttling of anticancer drug model TDC on surface sites of diferric transferrin sees unique binding interactions to the surface landscape of Tf, making Tf an interesting target for drug design.

## 4.5 References

1. Hudak, J. E.; Bertozzi, C. R. Glycotherapy: New advances inspire a reemergence of glycans in medicine. *Chem. Biol.* **2014**, *21* (1), 16–37.
2. Cummings, R. D.; Pierce, J. M. The challenge and promise of glycomics. *Chem. Biol.* **2014**, *21* (1), 1–15.
3. Codd, R. Metalloglycomics: A new perspective upon competitive metal-carbohydrate binding using EPR spectroscopy. *Chem. Commun.* **2004**, *08* (23), 2653–2655.
4. Macgillivray, R. T. A.; Mendezt, E.; Sinha, S. K.; Michael, R.; Lineback-zins, J.; Brew, K. The complete amino acid sequence of human serum transferrin. *Proc. Natl. Acad. Sci.* **1982**, *79* (April), 2504–2508.
5. Dell, A.; Morris, H. R. Glycoprotein structure determination by mass spectrometry. *Science (80-. )*. **2001**, *291*, 2351–2357.
6. Mason, A. B.; Miller, M. K.; Funk, W. D.; Banfield, D. K.; Savage, K. J.; Oliver, R. W. A.; Green, B. N.; MacGillivray, R. T. A.; Woodworth, R. C. Expression of glycosylated and nonglycosylated human transferrin in mammalian cells. Characterization of the recombinant proteins with comparison to three commercially available transferrins. *Biochemistry* **1993**, *32* (20), 5472–5479.
7. Hoefkens, P.; Huijskes-Heins, M. I. E.; De Jeu-Jaspars, C. M. H.; Van Noort, W. L.; Van Eijk, H. G. Influence of transferrin glycans on receptor binding and iron-donation. *Glycoconj. J.* **1997**, *14* (2), 289–295.
8. Luck, A. N.; Mason, A. B. *Transferrin-Mediated Cellular Iron Delivery*; Elsevier, 2012; Vol. 69.
9. Noinaj, N.; Easley, N. C.; Oke, M.; Mizuno, N.; Gumbart, J.; Boura, E.; Steere, A. N.; Aisen, P.; Tajkhorshid, E.; Evans, R. W.; et al. Structural basis for iron piracy by pathogenic Neisseria. *Nature* **2012**, *483* (7387), 53–58.
10. Guo, M.; Sun, H.; Mcardle, H. J.; Gambling, L.; Sadler, P. J. Ti IV uptake and release by human serum transferrin and recognition of Ti IV -transferrin by cancer cells: Understanding the mechanism of action of the drug titanocene dichloride. *Biochemistry* **2000**, *39*, 10023–10033.
11. Profitt, L. A.; Baxter, R. H. G.; Valentine, A. M. Superstoichiometric binding of the anticancer agent titanocene dichloride by human serum transferrin and the effects on lobe closure. **2020**.

12. Katner, S. J.; Johnson, W. E.; Peterson, E. J.; Page, P.; Farrell, N. P. Comparison of Metal – Ammine compounds binding to DNA and Heparin. Glycans as ligands in bioinorganic chemistry. *Inorg. Chem.* **2018**, *57*, 3116–3125.
13. Peterson, E. J.; Daniel, A. G.; Katner, S. J.; Bohlmann, L.; Chang, C. W.; Bezos, A.; Parish, C. R.; Von Itzstein, M.; Berners-Price, S. J.; Farrell, N. P. Antiangiogenic platinum through glycan targeting. *Chem. Sci.* **2016**, *8* (1), 241–252.
14. Gorle, A. K.; Rajaratnam, P.; Chang, C.; Itzstein, M. Von; Berners-price, S. J.; Farrell, N. P. Glycans as ligands in bioinorganic chemistry. Probing the interaction of a trinuclear platinum anticancer complex with defined monosaccharide fragments of heparan sulfate. *Inorg. Chem.* **2019**, *58*, 7146–7155.
15. Buettner, K. M.; Valentine, A. M. Bioinorganic chemistry of titanium. *Chem. Rev.* **2012**, *112* (3), 1863–1881.
16. Iavicoli, I.; Leso, V.; Bergamaschi, A. Toxicological Effects of Titanium Dioxide Nanoparticles: A Review of In Vivo Studies . *J. Nanomater.* **2012**, *2012*, 1–36.
17. Sarmiento-González, A.; Encinar, J. R.; Marchante-Gayón, J. M.; Sanz-Medel, A. Titanium levels in the organs and blood of rats with a titanium implant, in the absence of wear, as determined by double-focusing ICP-MS. *Anal. Bioanal. Chem.* **2009**, *393* (1), 335–343.
18. Nuevo-Ordóñez, Y.; Montes-Bayon, M.; Blanco-Gonzalez, E.; Paz-Aparicio, J.; Raimundez, J. D.; Tejerina, J. M.; Pena, M. A.; Sanz-Medel, A. Titanium release in serum of patients with different bone fixation implants and its interaction with serum biomolecules at physiological levels. *Anal. Bioanal. Chem.* **2011**, *401* (9), 2747–2754.
19. Profitt, L. A.; Cerkez, E. B.; Alimonhamadi, F.; Valentine, A. M. The uptake of titanium oxide and the change in particle speciation by human serum transferrin. **2020**.
20. Palmisano, G.; Lendal, S. E.; Engholm-keller, K.; Leth-larsen, R.; Parker, B. L.; Larsen, M. R. Selective enrichment of sialic acid – containing glycopeptides using titanium dioxide chromatography with analysis by HILIC and mass spectrometry. *Nat. Protoc.* **2010**, *5* (12), 1974–1982.
21. Larsen, M. R.; Jensen, S. S.; Jakobsen, L. A.; Heegaard, N. H. H. Exploring the sialome using titanium dioxide chromatography and mass spectrometry. *Mol. Cell. Proteomics* **2007**, *6* (10), 1778–1787.
22. Chasteen, N. D. Human serotransferrin: Structure and function. *Coord. Chem. Rev.*

**1977**, 22, 1–36.

23. Makey, D. G.; Seal, U. S. The detection of four molecular forms of human transferrin during the iron binding process. *Biochem. Biophys. Acta* **1976**, 453 (1), 250–256.
24. Hershberger, C. L.; Larson, J. L.; Arnold, B.; Rosteck, P. R.; Williams, P.; DeHoff, B.; Dunn, P.; O’Neal, K. L.; Riemen, M. W.; Tice, P. A.; et al. A cloned gene for human transferrin. *Ann. N. Y. Acad. Sci.* **1991**, 646 (1), 140–154.

## APPENDIX A

### ADDITIONAL FIGURES SHOWING SUPERSTOICHIOMETRIC BINDING OF TITANOCENE DICHLORIDE TO TRANSFERRIN

	<i>25 mM NaHCO<sub>3</sub></i>		<i>0.89 mM NaHCO<sub>3</sub></i>	
	Absorbance	ICP-OES (mM)	Absorbance	ICP-OES (mM)
<i>Tf + TDC 2 equiv</i>	0.19 ± 0.001	1.86 ± 0.029	0.36 ± 0.017	1.51 ± 0.035
<i>Tf + TDC 4 equiv</i>	0.19 ± 0.008	3.42 ± 0.316	0.41 ± 0.046	2.99 ± 0.046
<i>Tf + TDC 10 equiv</i>	0.22 ± 0.009	8.65 ± 1.261	0.43 ± 0.069	7.49 ± 0.108

Table A.1: Averaged UV/Vis absorbance at 321 nm and ICP-OES Ti concentration ( $\mu\text{M}$ ) determined for 25 mM (pH 8.5) and 0.89 mM (pH 7.4) bicarbonate samples.

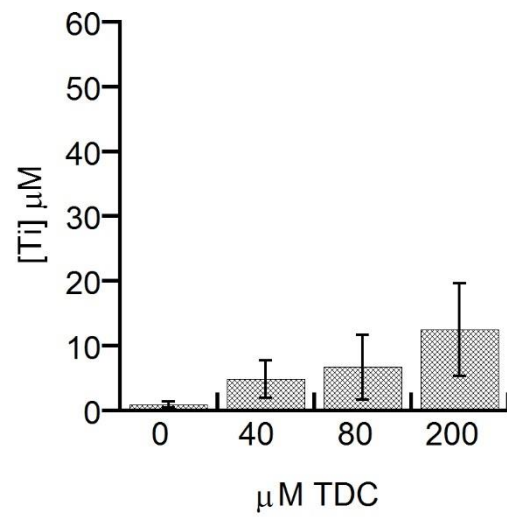


Figure A.1: 0, 40, 80, 200 μM TDC ICP-OES controls corresponding to Tf (20 μM) + TDC 0, 2, 4, 10 equiv.

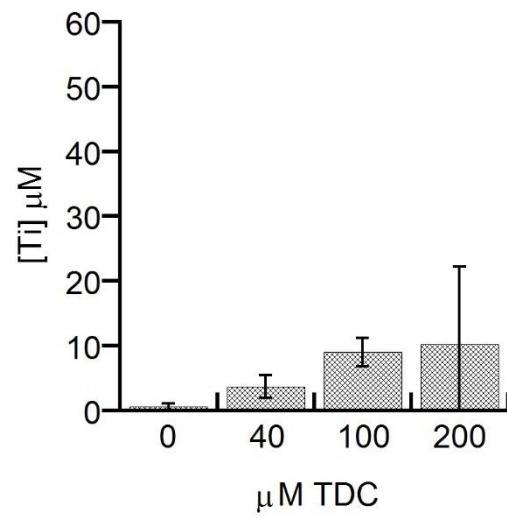


Figure A.2: 0, 40, 100, 200  $\mu\text{M}$  TDC ICP-OES controls corresponding to Tf (2  $\mu\text{M}$ ) + TDC 0, 20, 50, 100 equiv.

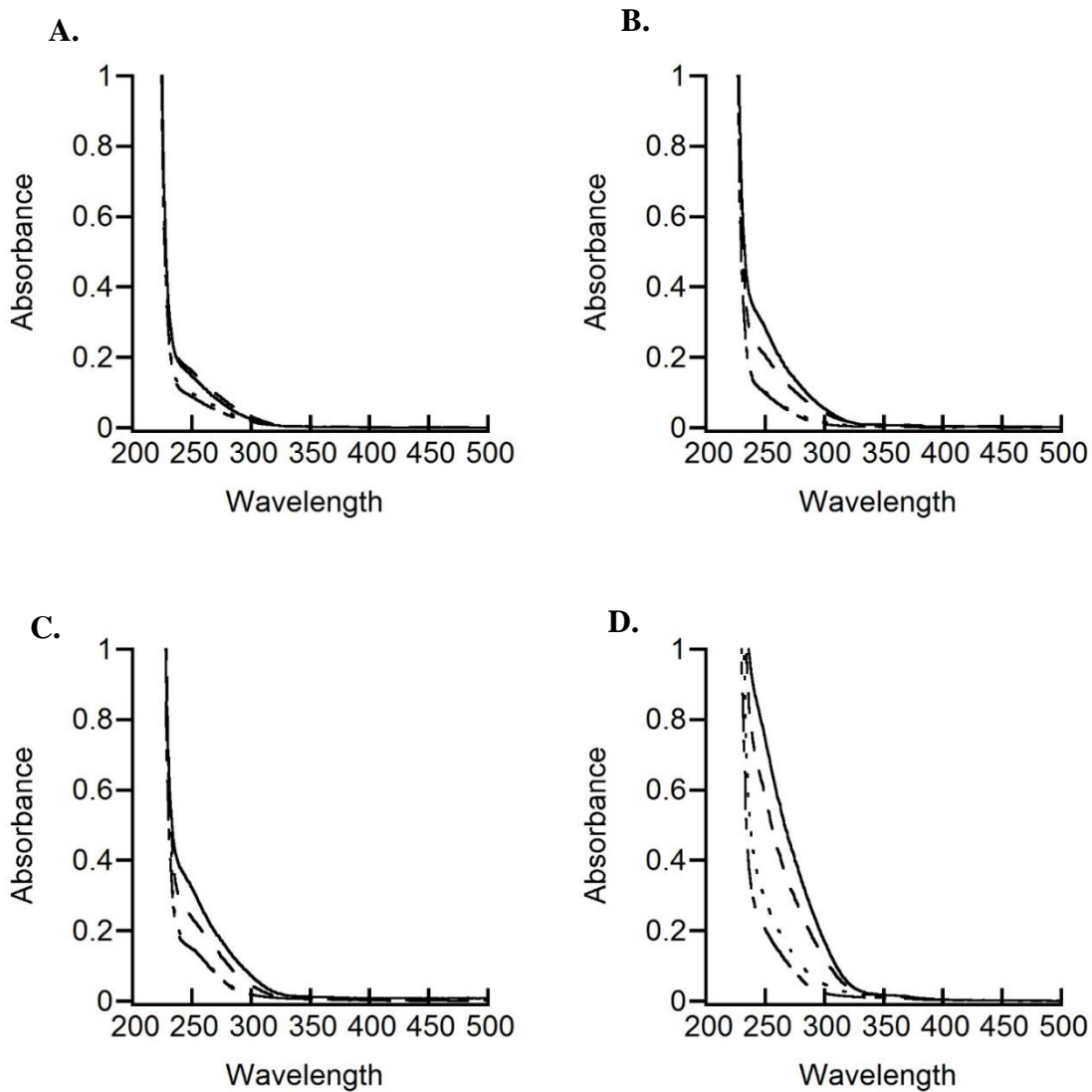


Figure A.3: (A.) 40  $\mu\text{M}$  UV/Vis control corresponding to 2 and 20 equiv TDC. (B.) 80  $\mu\text{M}$  UV/Vis control corresponding to 4 equiv TDC. (C.) 100  $\mu\text{M}$  UV/Vis control corresponding to 50 equiv TDC. (D.) 200  $\mu\text{M}$  UV/Vis control corresponding to 10 equiv TDC. 0 h (solid), 24 h (dashed), 96 h (dotted), 168 h (dash-dot).

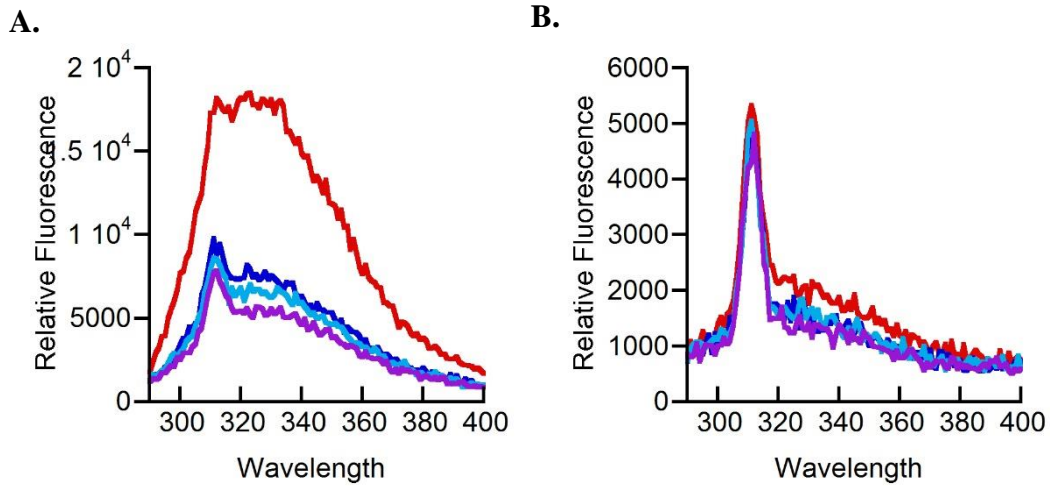
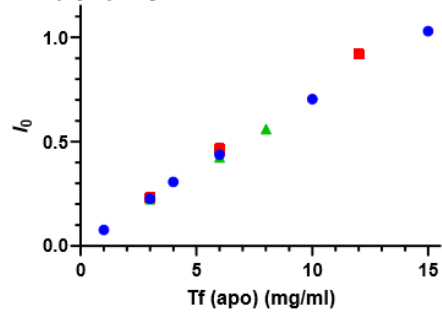
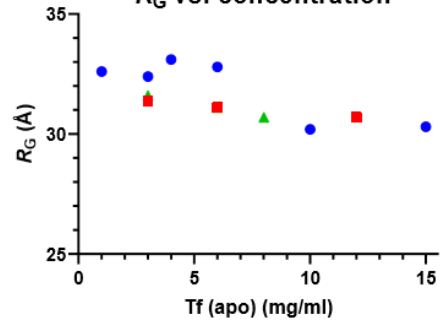


Figure A.4: 96 h fluorescence spectrum of (A.) 20  $\mu\text{M}$  Tf + TDC 0 equiv (red), 2 equiv (dark blue), 4 equiv (light blue), 10 equiv (purple) and (B.) 2  $\mu\text{M}$  Tf + TDC 0 equiv (red), 20 equiv (dark blue), 50 equiv (light blue), 100 equiv (purple).

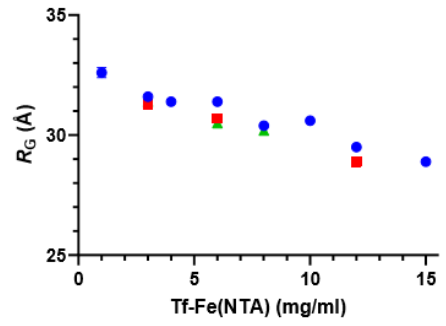
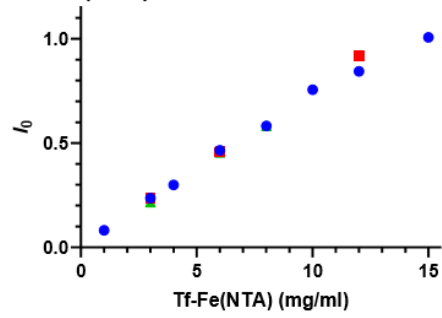
**A Tf (apo)  $I_0$  vs. concentration**



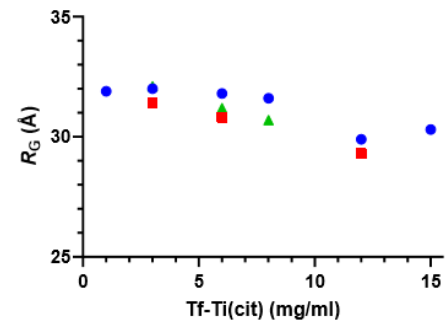
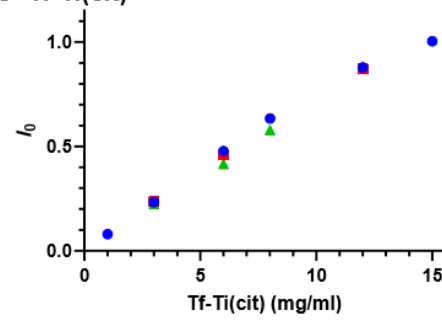
**$R_G$  vs. concentration**



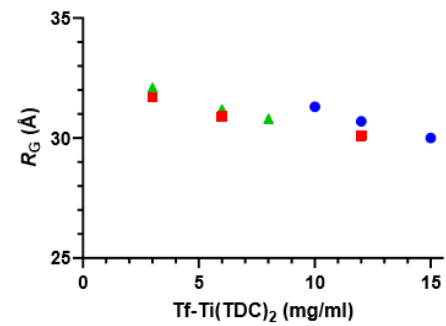
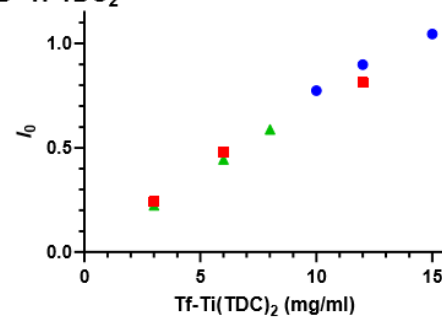
**B Tf-Fe(NTA)**



**C Tf-Ti(cit)**



**D Tf-Ti(TDC)<sub>2</sub>**



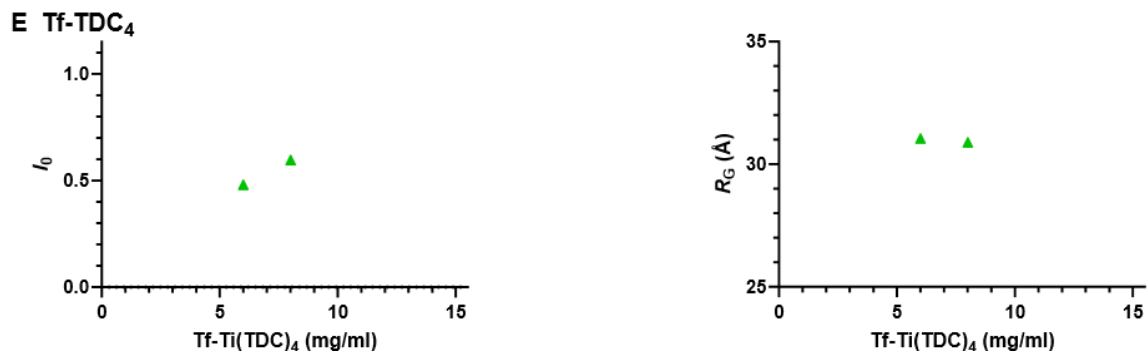


Figure A.5: Concentration analysis of forwards scattering intensity ( $I_0$ ) and the radius of gyration ( $R_G$ ) versus each applied concentration ranging from 1 – 15 mg mL<sup>-1</sup> for (A.) apoTf, (B.) Fe<sub>2</sub>Tf, (C.) Tf-Ti(citrate), (D.) Tf + TDC 2 equiv, (E.) Tf + TDC 4 equiv.

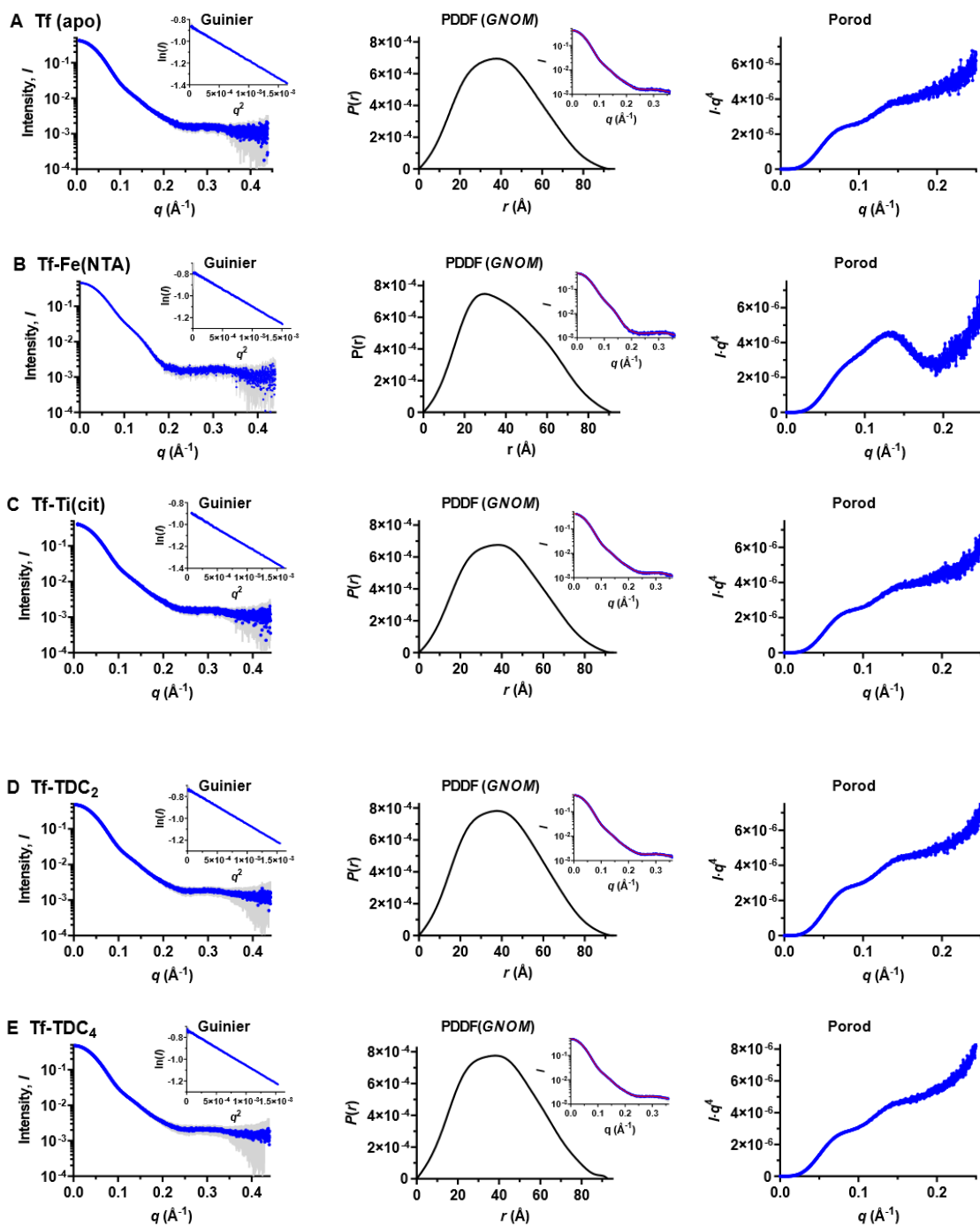


Figure A.6: Guinier plot,  $P(r)$  distribution and Porod plots of each of the samples (A.) apoTf, (B.)  $\text{Fe}_2\text{Tf}$ , (C.) Tf-Ti(citrate), (D.) Tf + TDC 2 equiv, (E.) Tf + TDC 4 equiv.

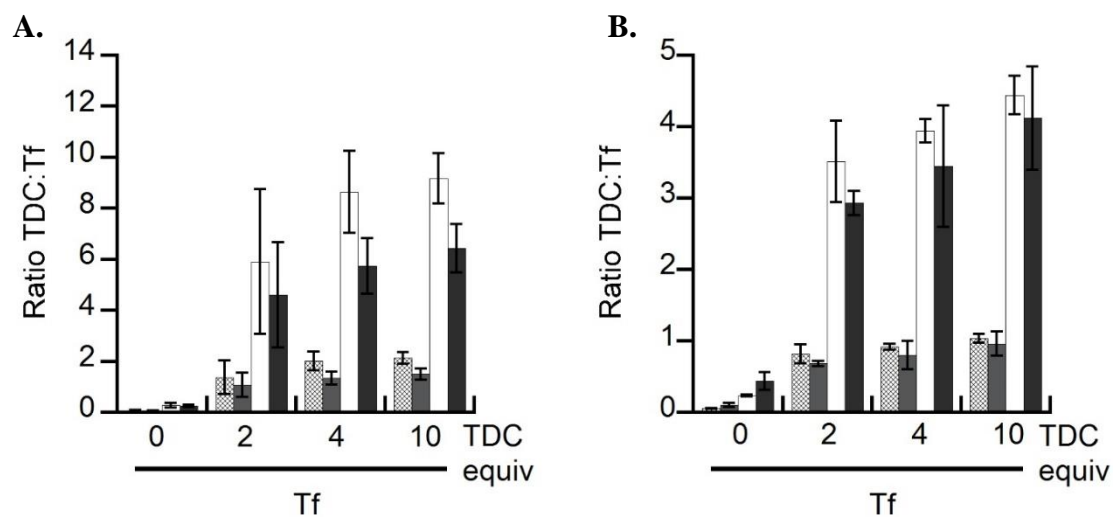


Figure A.7: Spin Dialysis UV/Vis Results with 0.89 mM bicarbonate (A.) and with 25 mM bicarbonate (B.). Striped – pre spin dialysis ( $\epsilon_{321 \text{ nm}} = 10,380 \text{ M}^{-1} \text{ cm}^{-1}$ ); light grey – Post spin dialysis ( $\epsilon_{321 \text{ nm}} = 10,380 \text{ M}^{-1} \text{ cm}^{-1}$ ); White – pre spin dialysis ( $\epsilon_{321 \text{ nm}} = 2,415 \text{ M}^{-1} \text{ cm}^{-1}$ ); Dark grey – post spin dialysis ( $\epsilon_{321 \text{ nm}} = 2,415 \text{ M}^{-1} \text{ cm}^{-1}$ ).

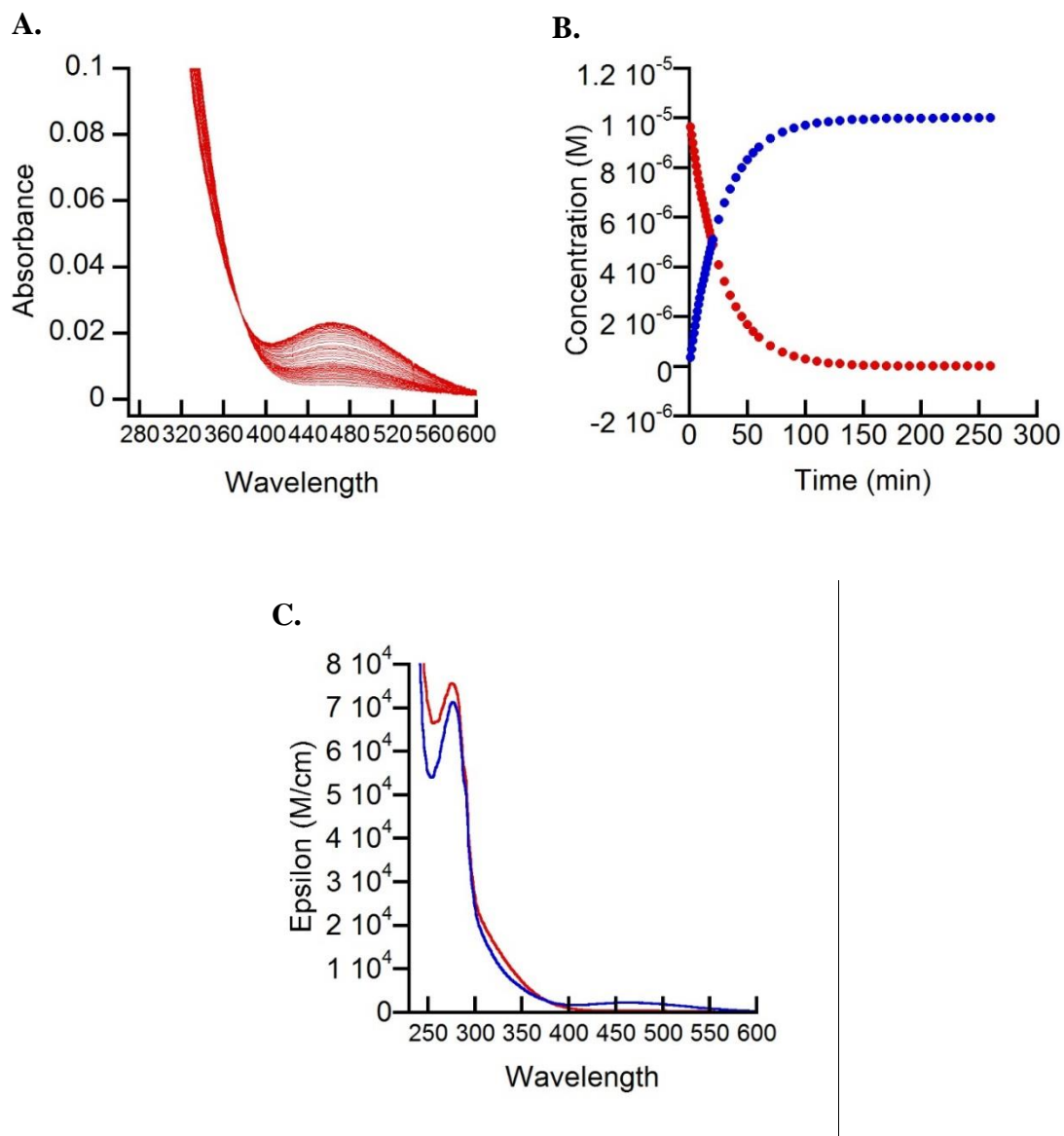


Figure A.8: Kinetic exchange of 4 equiv of TDC loaded to Tf with 10 equivalent additions of  $\text{Fe}(\text{NTA})_2$ . Fit obtained through SPECFIT/32. (A.) Series of spectra scans over 260 minutes after initial addition of  $\text{Fe}(\text{NTA})_2$  at  $t=0$  minutes. (B.) Concentration profile of the two species in respect to time. (C.) The molar extinction coefficients of each species. The red curve represents the Tf + TDC 4 equiv starting species and the blue curve represents the  $\text{Fe}_2\text{Tf}$  (+ TDC 4 equiv) species.

## APPENDIX B

### ADDITIONAL FIGURES FOR TITANIUM OXIDE AND TRANSFERRIN ASSOCIATION

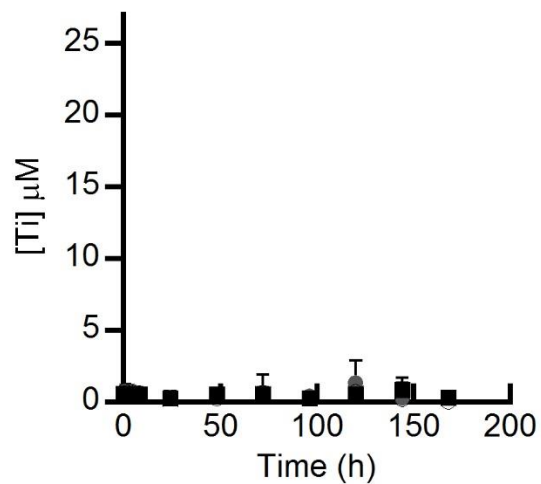


Figure B.1: ICP-OES controls in buffer: apoTf (●), filtered anatase 5 mg mL<sup>-1</sup> (■), filtered rutile 5 mg mL<sup>-1</sup> (x), filtered rutile 20 mg mL<sup>-1</sup> (○).

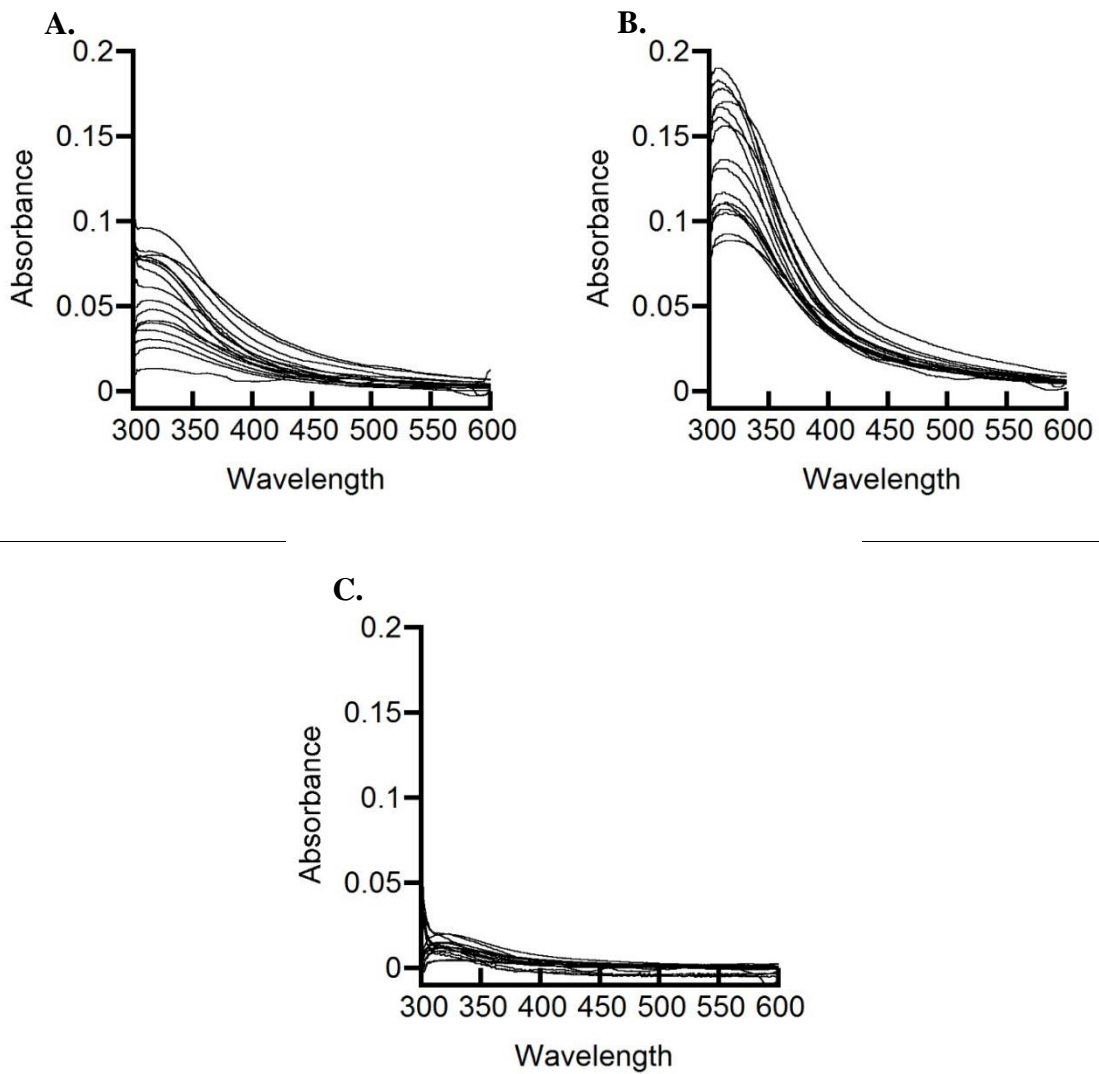


Figure B.2: UV/Vis spectrum of (A.) Tf + rutile 5 mg mL<sup>-1</sup> (apoTf subtracted); (B.) Tf + rutile 20 mg mL<sup>-1</sup> (apoTf subtracted); (C.) Tf + anatase 5 mg mL<sup>-1</sup> (apoTf subtracted).

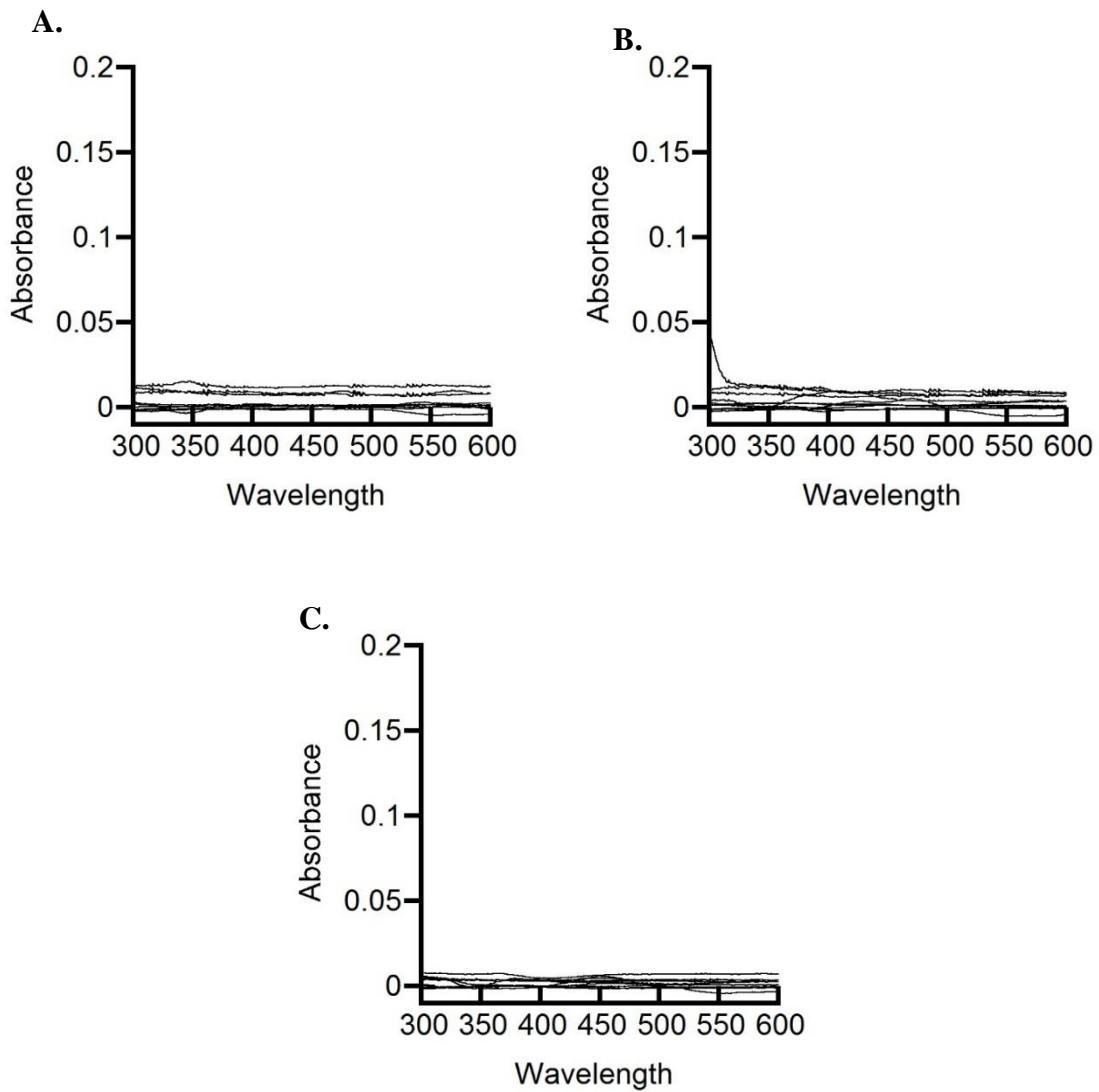


Figure B.3: UV/Vis spectrum of (A.) rutile only 5 mg mL<sup>-1</sup>; (B.) rutile only 20 mg mL<sup>-1</sup>; (C.) anatase only 5 mg mL<sup>-1</sup>.

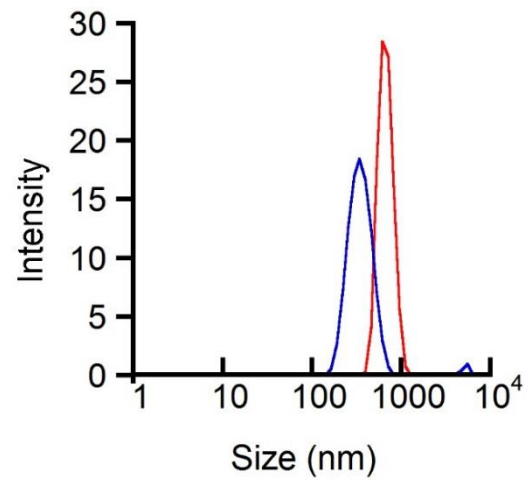


Figure B.4: DLS spectrum of (A.) anatase (—) and rutile (—) suspended in water control.

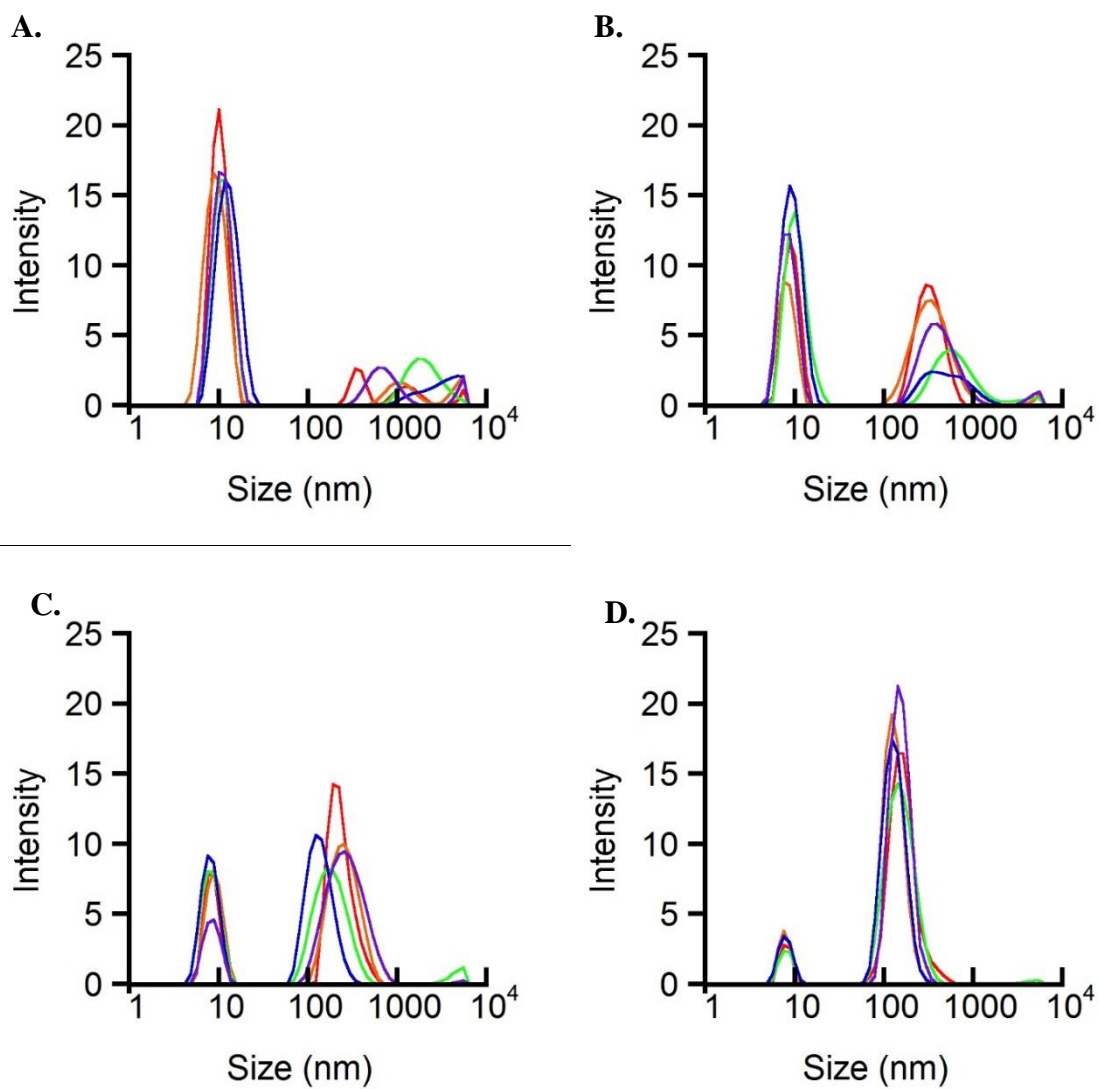


Figure B.5: DLS spectra of timepoints 0 h (—), 0.5 h (—), 1 h (—), 4 h (—), 8 h (—) (A.) apoTf; (B.) Tf + anatase 5 mg mL<sup>-1</sup>; (C.) Tf + rutile 5 mg mL<sup>-1</sup>; (D.) Tf + rutile 20 mg mL<sup>-1</sup>.

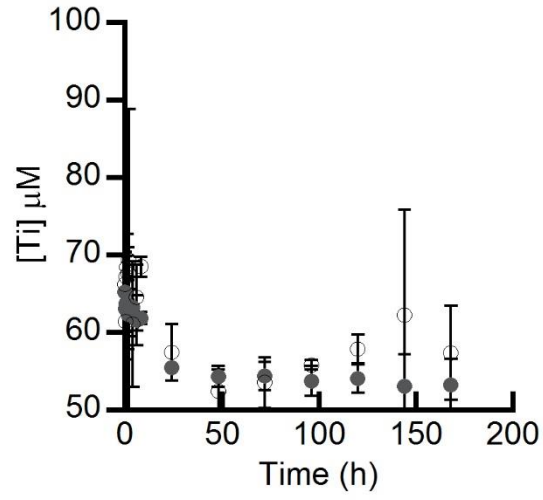


Figure B.6: ICP-OES [Fe] results for 35 µM Fe<sub>2</sub>Tf + rutile 5 mg mL<sup>-1</sup> (●) and Fe<sub>2</sub>Tf (○) over 168 h.

## APPENDIX C

### ADDITIONAL FIGURES OF DEGLYCOSYLATED TRANSFERRIN

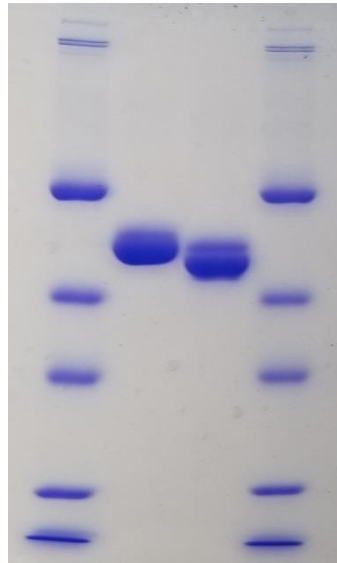


Figure C.1: SDS-PAGE gel result confirming deglycosylated transferrin. Lanes 1 and 4 containing low molecular weight ladder. Lane 2 contains apoTf. Lane 3 contains apoTf treated with PNGase F enzyme.

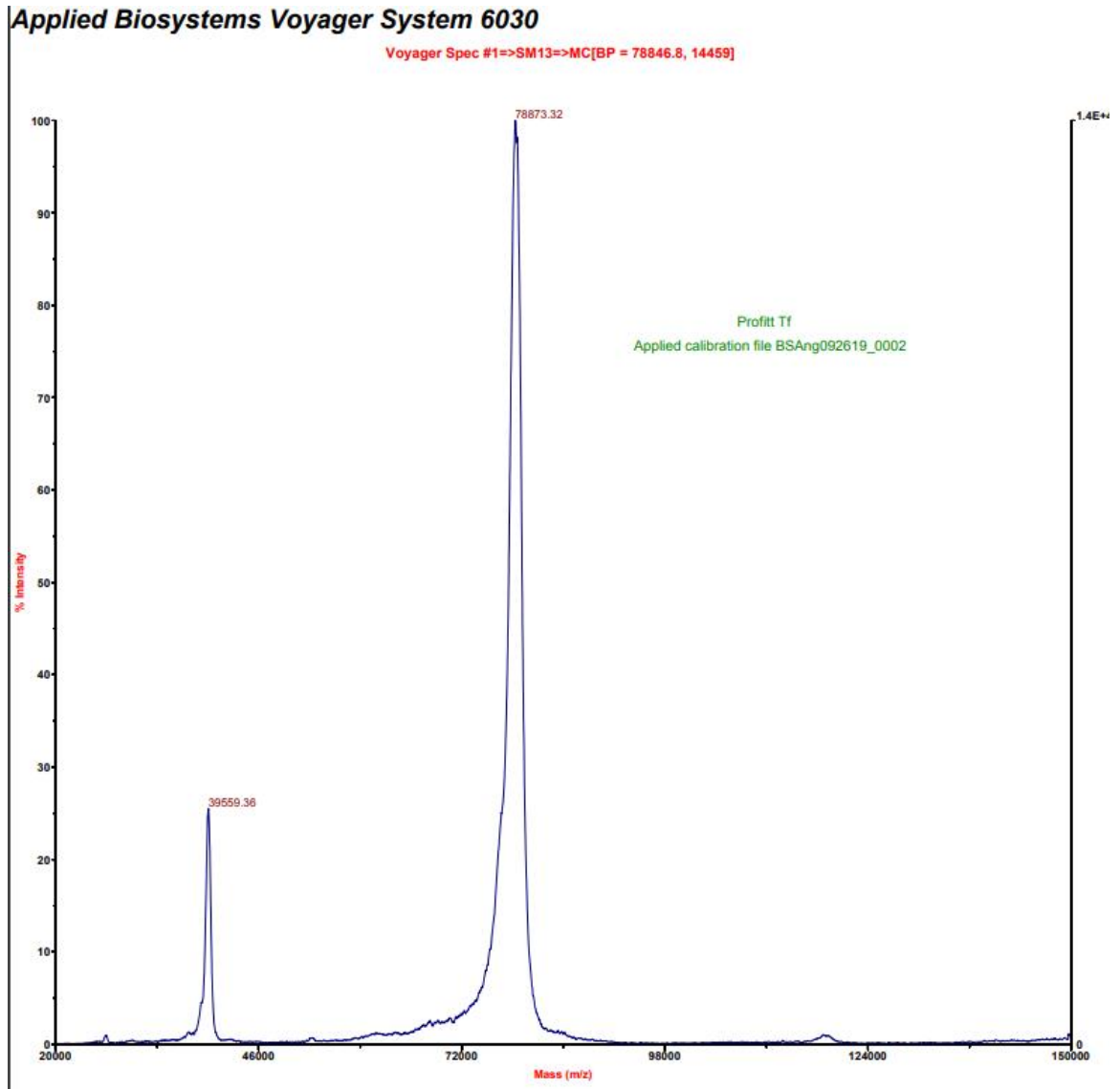


Figure C.2: MALDI-MS analysis results of apoTf in buffered solution.

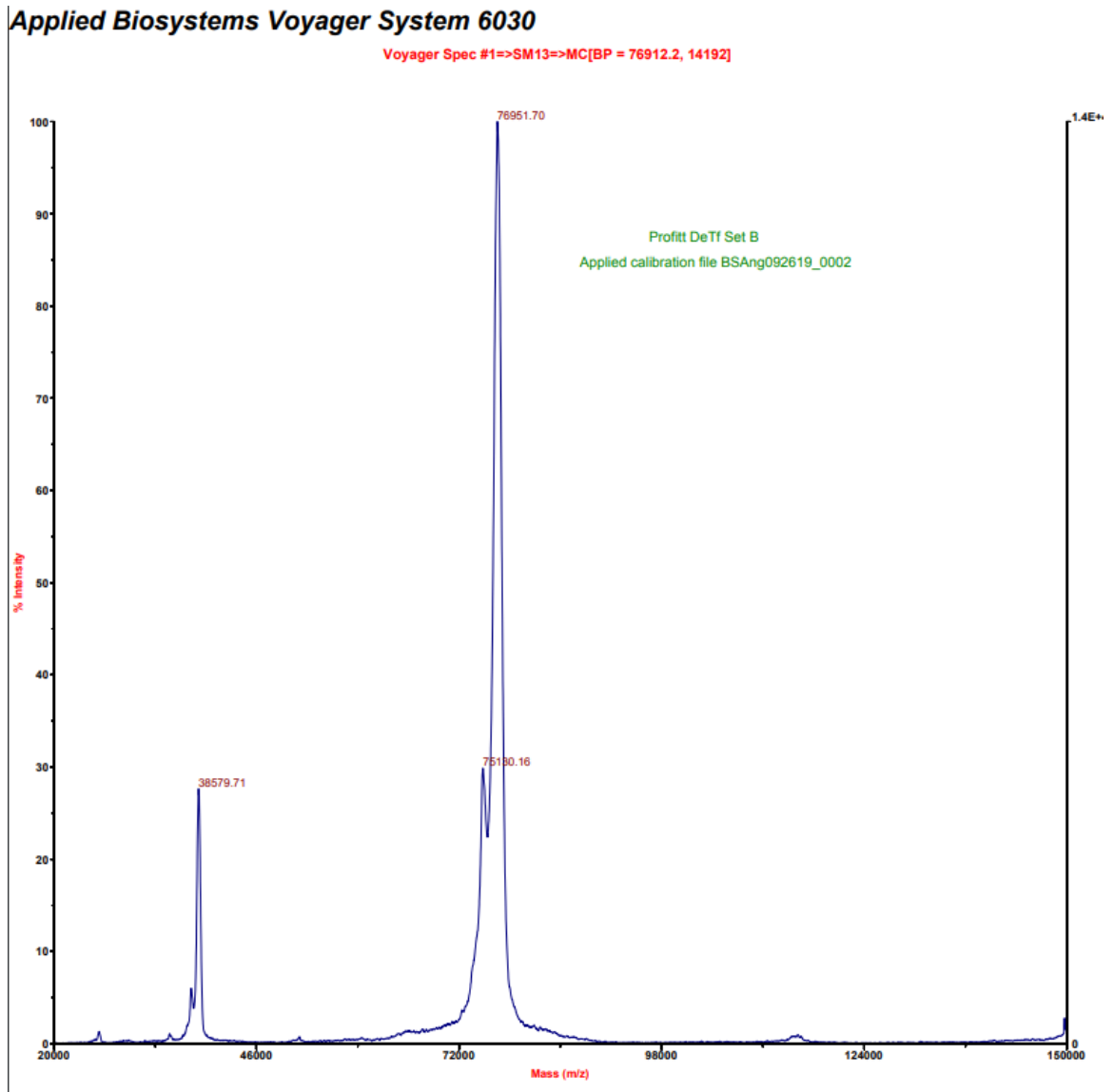


Figure C.3: MALDI-MS analysis results of deTf in buffered solution. Sample set 1 of 2.

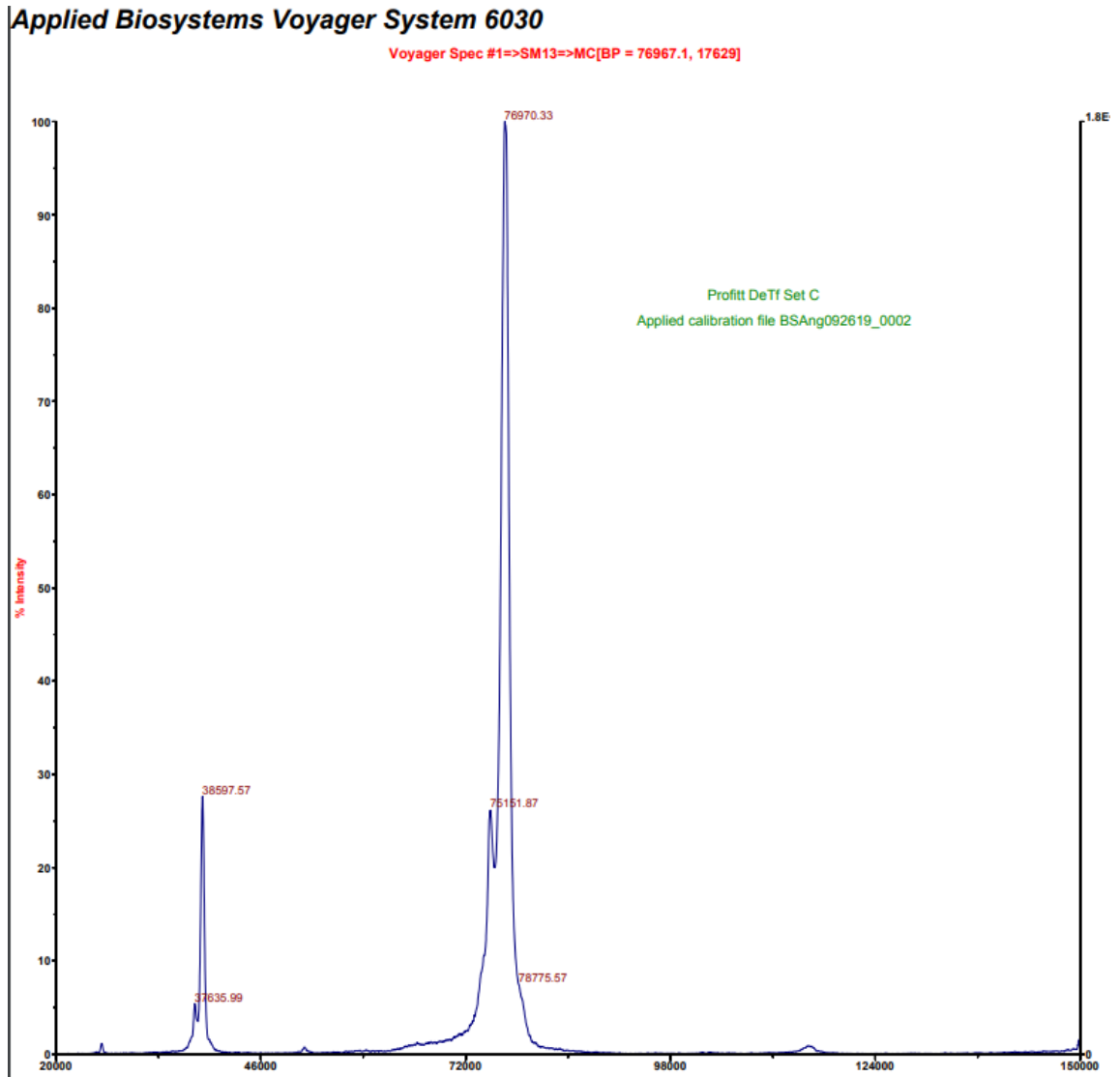


Figure C.4: MALDI-MS analysis results of deTf in buffered solution. Sample set 2 of 2.

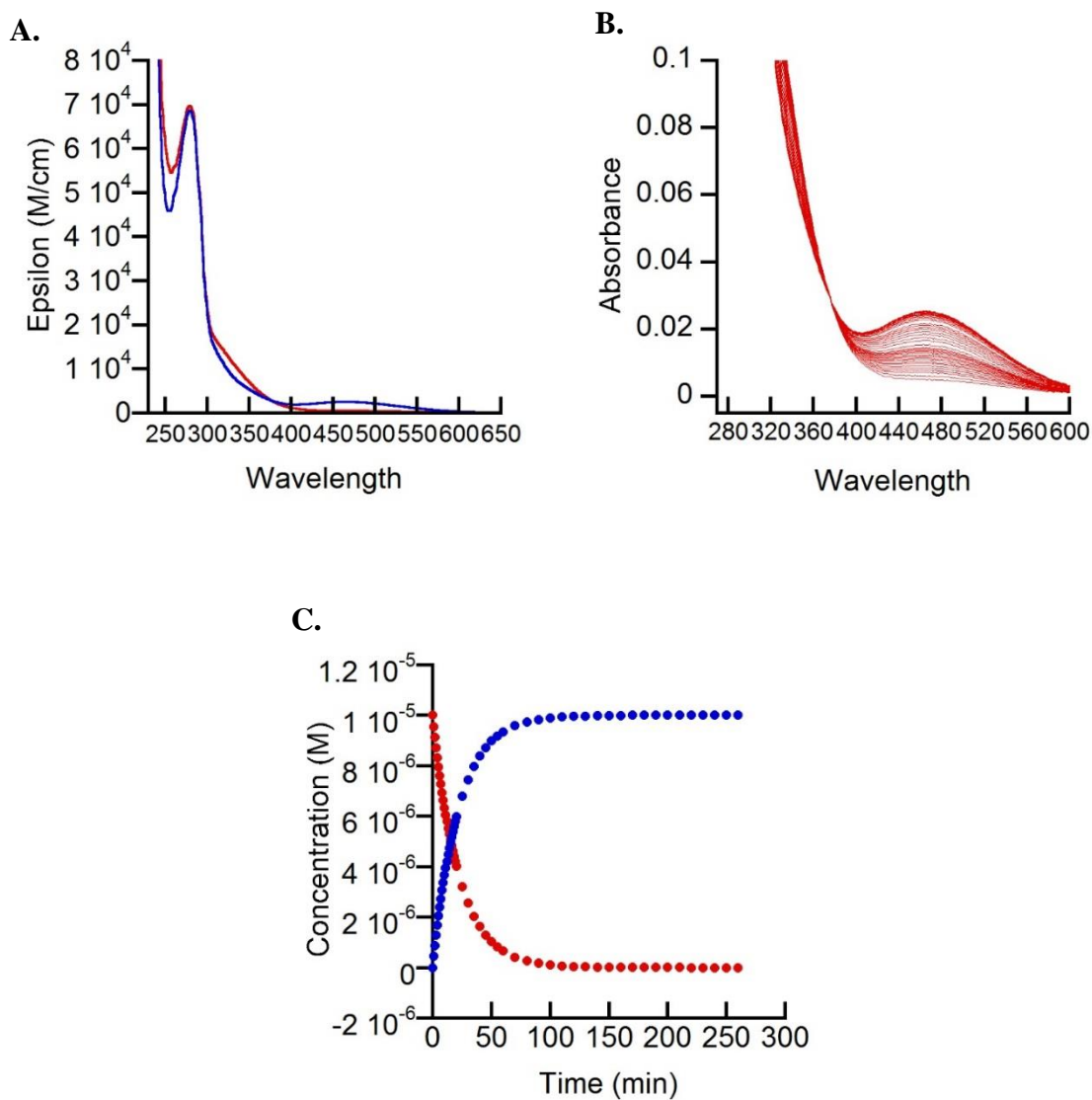


Figure C.5: Kinetic exchange of 4 equiv of TDC loaded to deTf with 10 equivalent additions of Fe(NTA)<sub>2</sub>. Fit obtained through SPECFIT/32. (A.) Series of spectra scans over 260 minutes after initial addition of Fe(NTA)<sub>2</sub> at t=0 minutes. (B.) Concentration profile of the two species in respect to time. (C.) The molar extinction coefficients of each species.

The red curve represents the deTf + TDC 4 equiv starting species and the blue curve represents the Fe<sub>2</sub>deTf (+ TDC 4 equiv) species.

## APPENDIX D

### ASSAY OF TOPOISOMERASE I INHIBITION BY TITANOCENE DICHLORIDE

The main target and focus for the mechanism of action for anticancer drug titanocene dichloride (TDC) has typically been DNA, due to TDC's similarities to cisplatin. Other primary targets for Ti(IV) complex activity have been postulated to be protein kinase C and DNA topoisomerase II.<sup>1,2</sup> Topoisomerase II (topo II) is an enzyme that controls DNA conformation and topology by making cuts to double stranded DNA.<sup>3</sup> Inhibition by metallocenes of topo II can be analyzed using agarose gel electrophoresis of a plasmid DNA, by analyzing the mobility of supercoiled DNA compared to relaxed or nicked DNA which does not run as far down the gel.<sup>4</sup> A simpler, less expensive assay using topoisomerase I was used first to practice proof of principle before moving to topo II. Topo I behaves similarly to topo II, making cuts to single stranded DNA to relax it from its supercoiled state.

Topoisomerase I isolated protein was graciously provided by John Nitiss (University of Illinois) at a concentration of 60 ng  $\mu\text{L}^{-1}$ . Reagents came from J.T. Baker (NaCl, KCl, and glycerol), Bacto (Tryptone), American Bioanalytical (agar and ampicillin), Fisher (Tris-Cl), Acros Organics (dithiothreitol), Sigma (EDTA, acetylated bovine serum albumin), Biorad (bromophenol blue), and AmericanBio (yeast extract). QIAprep Spin Miniprep kit, 1 Kb ladder, DH5 $\alpha$  cells, and pUC 19 control plasmid vector was obtained from New England Biolabs.

DH5 $\alpha$  with pUC19 E. coli cells were transformed by closely following the manufacturer protocol. Cells were spread onto plates and incubated overnight at 37°C. Overnight cell cultures were grown in 10 mL LB media with 10  $\mu$ L of 100 mg mL<sup>-1</sup> ampicillin stock added to each tube with single colonies transferred from plates. Tubes were shaken overnight at 37°C, 250 rpm. DH5 $\alpha$  pUC19 E. coli overnight cultures were pelleted and elution of plasmid DNA followed QIAprep Spin Miniprep protocol.

Procedures for the topoisomerase assay DNA gel was obtained from Nitiss et al.<sup>4</sup> Briefly, samples were prepared with 5  $\mu$ L of 5x loading dye, 2  $\mu$ L of 10x topoisomerase I reaction buffer (recipes following Nitiss et al)<sup>4</sup>, 200 ng of plasmid DNA, 30 ng of topo I enzyme, and varied equivalents of test reactant and water so final volume is equal to 20  $\mu$ L. Samples were then incubated at 37°C for 30 minutes before being loaded onto a 0.8% agarose gel and run for 2 h at 50 V. The gel was stained with an ethidium bromide solution before imaged in UV transilluminator.

Figure D.1 shows the results of analysis with additions of TDC to topo I and plasmid substrates. However, there was no positive control result seen in this analysis. The lane containing substrate alone does not show a fully supercoiled plasmid, meaning a negative result for the control. The same confusion happened in lane 3, with the buffer control, where no relaxation seems to occur, but rather a supercoiled band was present. This result could be caused by a solvent involvement in the normal enzymatic reaction. Thus, while additions up to 6x TDC to topo I show a positive result for inhibition of topoisomerase activity, more analysis is needed to confirm any buffer interaction with the normal functions of topoisomerase.

A solvent control was tested in addition to the assay in order to ensure that TDC solvent (prepared in 10%DMSO/saline 1/9 v/v) did not have any effect on the enzymatic activity. Figure D.2 shows relaxation of the plasmid under the same concentration additions of DMSO/saline as TDC studies. The relaxation of the supercoiled plasmid substrate can be seen with additions of 30 ng of topo I (Figure D.2). The results of this gel are promising for future studies under these buffer conditions, perhaps showing an inactivated enzyme during the first trial run seen in Figure D.1.

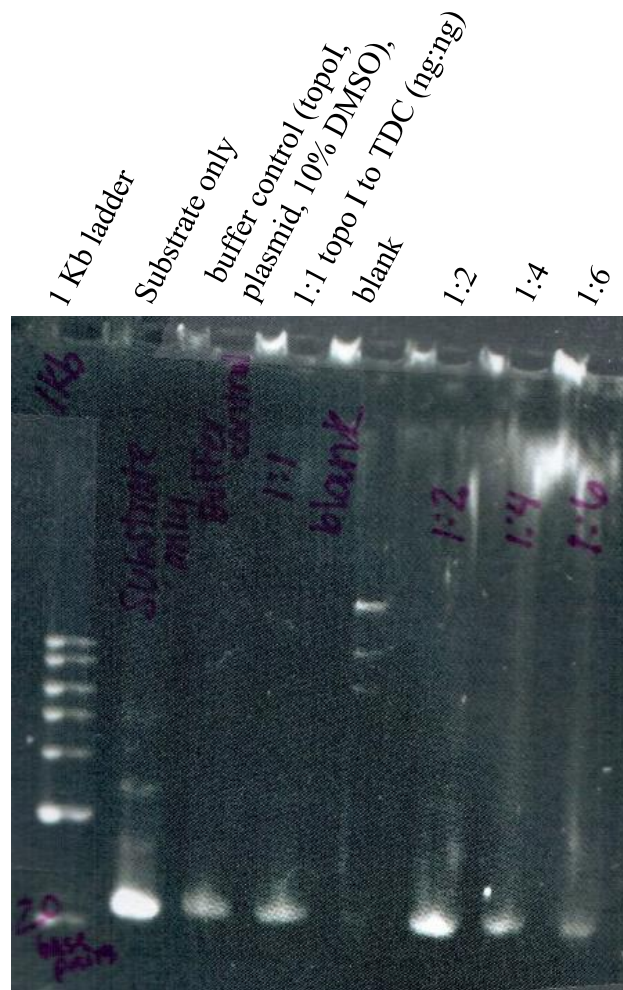


Figure D.1: Topoisomerase I assay with varied equivalents of TDC. From left to right: 1 Kb ladder, substrate only, buffer control (topoI, plasmid, 10% DMSO), 1:1 topo I to TDC (ng:ng), blank, 1:2, 1:4, 1:6 topo I to TDC (ng:ng).

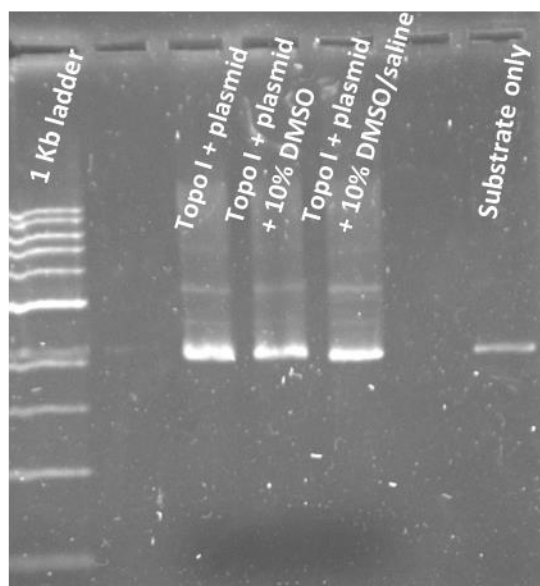


Figure D.2: Solvent control assay with topo I and plasmid relaxation with 10% DMSO and 10% DMSO/saline (1/9 v/v).

More analysis is needed to confirm the activity of TDC against the topoisomerase I enzyme. It has been shown that the preparation of TDC in 10% DMSO/saline (1/9 v/v) does not play a role in the normal enzymatic activity of topo I. Repeat analysis of topoisomerase inhibition under increased additions of TDC is needed in order to make a clear determination. Analysis of Figure D.1 outside of controls leans more towards a positive inhibition result, an interesting determination since topo I was not the primary perspective target. This result is an interesting stepping-stone before leading to the more complex topo II assay but seems to add some value and insight to the inhibitory activity of titanocene dichloride.

## References

1. Buettner, K. M.; Valentine, A. M. Bioinorganic chemistry of titanium. *Chem. Rev.* **2012**, *112* (3), 1863–1881.
2. Mokdsi, G.; Harding, M. M. Inhibition of human topoisomerase II by the antitumor metallocenes. *J. Inorg. Biochem.* **2001**, *83* (2–3), 205–209.
3. Bailly, C. DNA relaxation and cleavage assays to study topoisomerase I inhibitors. *Methods Enzymol.* **2001**, *340* (1996), 610–623.
4. Nitiss, J. L.; Soans, E.; Rogojina, A.; Seth, A.; Mishina, M. Topoisomerase assays. *Curr. Protoc. Pharmacol.* **2012**, *3.3.1-3.3*. (SUPPL.57), 1–27.